PROTON CAPTURE TO EXCITED STATES IN ^{8}BE

by

Stephen Hart Manglos

Department of Physics
Duke University

Date: 9/18/81

Approved:

N. Russell Roberson, Supervisor

A dissertation submitted in partial fulfillment of the requirements for the degree of Doctor of Philosophy in the Department of Physics in the Graduate School of Duke University

1981

ABSTRACT

(Physics)

PROTON CAPTURE TO EXCITED STATES IN ^{8}BE

by

Stephen Hart Manglos

Department of Physics
Duke University

Date: 9/18/81

Approved:

N. Russell Roberson, Supervisor

A dissertation submitted in partial fulfillment of
the requirements for the degree of Doctor
of Philosophy in the Department of
Physics in the Graduate School
of Duke University

1981

PROTON CAPTURE TO EXCITED STATES IN ^{8}BE

by

Stephen Hart Manglos

The 90° yield curve has been measured for proton capture to the region of the 2^{+} isospin-mixed pair of levels in ^{8}Be (^{7}Li(p,γ_{16})^{8}Be*) for incident proton energies from 4 to 30 MeV. The γ-rays from the capture reaction were observed for proton energies from 11.5 to 30 MeV. For E_p=4-13 MeV, the yield curve was measured by observing the decay products (two α-particles) of the isospin-mixed pair. Cross section angular distributions for ^{7}Li(p,γ_{16}) have been measured at nine energies from 12 to 30 MeV for various angles from 30° to 154°. Angular distributions of analyzing power have been measured at 13, 14, and 16 MeV proton energy for various angles from 30° to 154°. The data are compared to the predictions of a direct capture model including E1 and E2 radiation, and the model provides a good description of the data. No conclusive evidence for a giant dipole resonance built on the 16 MeV states is seen. The predictions of a direct-semidirect (DSD) model are investigated.

The 90° yield curves for ^{7}Li(p,γ_{0})^{8}Be and ^{7}Li(p,γ_{1})^{8}Be* have been measured for incident proton energies from 11.5 to 30 MeV. Cross section angular distributions for these reactions have been measured at 8 energies from 12 to 30 MeV for various angles from 30° to 154°. Angular distributions of analyzing power have been measured at 13, 14, and 16 MeV proton energy for various angles from 30° to 154°. The data are compared to the predictions of a direct capture model including E1 and E2 radiation. The model fails

significantly to predict the cross sections in the region of the observed giant dipole resonances for the two reactions. A DSD model calculation has been performed for the $^{7}Li(p,\gamma_0)$ reaction. The model provides a good description of the data.

ACKNOWLEDGEMENTS

First and foremost thanks must always be given to God, who created me, who gave me new life through His son, Jesus Christ, and who guides me by His Holy Spirit. Without Him, this work could not even have been begun.

I wish to thank Dr. N.R.Roberson for his sincere guidance, support, and assistance, and Dr. H.R.Weller for his interest in my work and for many, many useful discussions. I extend appreciation to Dr. D.R.Tilley and Dr. S.A.Wender for their interest and assistance in data collection.

Particularly heart-felt gratitude is extended to Mr. L.Ward for his indispensible assistance in data collection and for his continual spiritual support and friendship. I also wish to acknowledge Dr. M.Jensen, Mr. S.E.King, Mr. M.Wright, Miss C.Fitzpatrick, and Mr. G.Mitev for their assistance during the experiments. Additional thanks are extended to Mr. S.E.King for the use of his spectrum-fitting code.

The technical assistance of Mr. R.L.Rummel and Mr. P.Carter is greatly appreciated. Also, I wish to acknowledge Dr. F.O.Purser for his help during experiments. Special thanks are in order for Mr. S.E.Edwards for his cheerful and enthusiastic help with the computers and electronics. I wish to thank Mrs. M.Bailey for her excellent drafting work. I am grateful to Dr. E.G.Bilpuch for providing me with the research assistantship.

Many thanks are extended to my parents for their continual, loving support. Last but certainly not least, the very special love, patience, and encouragement for my wife, Carol, have been of great value to me and are greatly appreciated.

This work was supported in part by the National Science Foundation and by the United States Department of Energy.

S.H.M.

CONTENTS

List of Figures

List of Tables

PROTON CAPTURE TO EXCITED STATES IN ^{8}BE

Chapter 1 Introduction

The photonuclear reaction has been and continues to be a useful tool for investigating nuclear structure. Such a reaction is denoted here by (γ,x), where γ denotes a γ-ray incident upon a nucleus and x denotes an emitted nuclear particle. The fact that one of the channels contains a γ-ray, whose interaction with charged particles is well known theoretically, makes photonuclear reaction theories in principle more simple than other reaction theories. This simplicity can allow the extraction of more information about the particle-nucleus channel, as well as information about intermediate states (nuclear structure).

The most important nuclear structure information which has been obtained through photonuclear reactions is the systematic occurance of a large resonance in the photonuclear cross section as a function of E_x. The peak of this resonance occurs at an excitation energy of about $80/A^{1/3}$ MeV for medium and heavy nuclei and at about 20 MeV for light nuclei, and the resonance has a width from 5 to 10 MeV (Hanna, 1976). This resonance has been shown to be excited primarily by the absorption of E1 photons and is called the giant dipole resonance (GDR). The integrated photonuclear cross section in the region of the GDR is often paramatrized in terms of the percentage of the classical E1 sum rule which has been exhausted by the particular reaction studied. A sum rule is an approximate theoretical limit of the

photoabsorption cross section, integrated over energy, for a given multipolarity. The classical E1 sum rule is given by $\int\sigma\cdot dE=60\cdot NZ/A$ MeV·mb (Hayward, 1970).

In recent years, giant resonances of multipolarities other than E1 have been observed. The general requirements for a giant multipole resonance are that a localized resonance be observed in the partial photoabsorption cross section for the appropriate multipolarity, that the resonance should exhaust a significant fraction of the corresponding sum rule, and that it be located systematically with energy in many nuclei.

The capture reaction, denoted (x,γ), which is the time inverse of the photonuclear reaction, has also proved to be a very useful tool for studying giant resonances. The capture reaction has the advantage of using particle beams, which are easy to produce and manipulate, and it often allows the investigation of giant resonances which, due to target problems, can not be investigated by the photonuclear reaction. Furthermore, the measurements of angular distributions of cross section and analyzing power have provided stringent tests of various capture and giant resonance models. In some cases, the angular distributions have allowed the extraction of the T-matrix elements for the capture reaction, which can be used to further test the models and to look for strength due to multipolarities other than E1.

The GDR's that can be investigated with the photonuclear reaction are those built on the ground state of the target nucleus. Alternatively, the capture reaction, which can leave the residual nucleus in an excited state, should be a powerful tool for studying giant resonances built on excited states and for testing the Brink hypothesis (Brink, 1955), which states that a giant dipole resonance should be built on every state with some single-particle strength, regardless of its detailed nature.

In the past few years, Blatt and co-workers (Kovash et al., 1979, and Blatt et al., 1981) at Ohio State and Indiana University have studied proton capture on ^{11}B to a final state which is a highly excited unbound state, or rather, set of states, at about 19 MeV excitation energy in ^{12}C. The yield curve for this reaction, denoted $^{11}B(p,\gamma_{19})$, was measured from 23 to 60 MeV and shows pronounced peaking at about 29 MeV proton energy, which corresponds to 42 MeV excitation in ^{12}C, or about 23 MeV above the 19 MeV region. The excitation energy of 23 MeV is typical for a giant dipole resonance in light nuclei. For example, the GDR built on the ground state of ^{12}C peaks at about 23 MeV excitation energy, and the GDR built on the first excited state in ^{12}C peaks at about 22 MeV above the 4.44 MeV state. Blatt has in fact suggested that the observed peaking in the yield curve for $^{11}B(p,\gamma_{19})$ is due to a GDR built on the states formed from the stretched configuration $(d_{5/2}p_{3/2}^{-1})4^-$.

It was suggested, however, by Arnold (1979) that the capture strength might in this case be the result of direct capture only. Tsai and Londergan (1979) then performed a direct capture calculation which included effects of residual two-nucleon interactions but treated the final state as a bound state. Following this, Halderson and Philpott (1981) performed a direct capture calculation which treated the final state properly as a continuum state. They concluded that direct capture could account for the major features of the data. Therefore, a particular ambiguity exists for proton capture to the 19 MeV region in ^{12}C, since the direct calculation peaks at about 20 MeV above the 19 MeV region, which is the same energy region as might be expected for the peak of a GDR built on the stretched configuration states.

This ambiguity is removed in the case of proton capture on ^{7}Li to the region of the isospin-mixed pair of states at about 16.6 MeV in ^{8}Be, since the direct capture calculation peaks at about 10 MeV above the 16.6 MeV region.

This reaction, denoted here by $^{7}Li(p,\gamma_{16})^{8}Be^{*}$, should therefore provide a better test case both for the existence of a GDR built on highly excited states and for direct capture theory. Additionally, the direct calculation is more straightforward for $^{7}Li(p,\gamma_{16})$ than for $^{11}B(p,\gamma_{19})$, since the final states are bound to single-nucleon decay. The study of this reaction is the primary focus of this thesis. Additional investigations are reported for the two capture reactions, $^{7}Li(p,\gamma_{0})$ and $^{7}Li(p,\gamma_{1})$, and are used for comparison with the $^{7}Li(p,\gamma_{16})$ reaction.

A level diagram is shown in Fig.1 to illustrate more explicitely the processes occurring in the reaction denoted $^{7}Li(p,\gamma_{16})$. The incoming channel consists of a proton with energy E_p, incident upon the nucleus ^{7}Li, $J^{\pi}=3/2^{-}$, and the outgoing channel consists of a γ-ray plus the recoiling ^{8}Be nucleus, left in one of the excited states at E_x=16.63 and 16.92 MeV. These states incidentally decay nearly 100% into two α-particles, moving in opposite directions in the center-of-mass. This capture reaction at low energies and the isospin-mixed pair of states were studied in some detail by Marion and co-workers at the University of Maryland. They have presented evidence which indicates that the two states have mixed T=0 and T=1 isospin and are primarily single-particle plus core states, with the 16.63 MeV level being largely a ^{7}Li + proton state, and the 16.92 MeV level being largely a ^{7}Be + neutron state (Marion and Wilson, 1966). In addition, yield curves for proton capture to each state in the pair have been measured from 0.441-2.45 MeV (Sweeney and Marion, 1969), and it was seen that for off-resonance proton capture, the capture cross section to the 16.63 MeV state was roughly an order of magnitude larger than the capture cross section to the 16.92 MeV state. A model was then proposed using the shell model wave functions of Barker (1966), which gives a proton spectroscopic factor, S, of 0.470 for the 16.63 MeV state, and only

Figure 1. Level diagram for ^{8}Be. $^{7}Li + p$ shown.

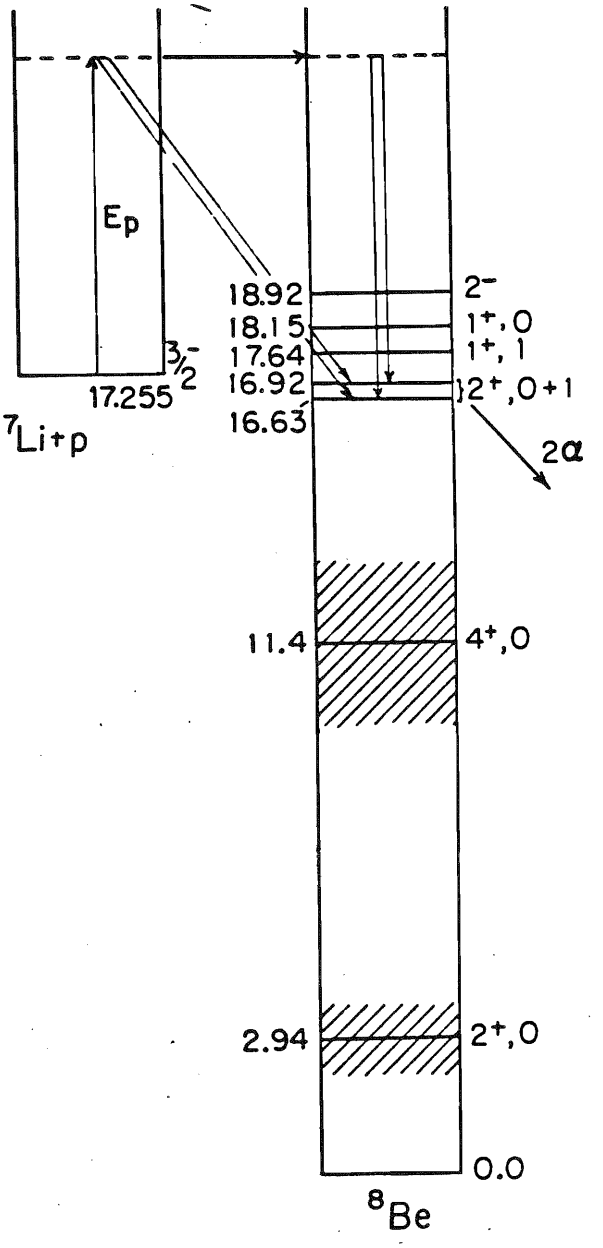
Ep
18.92
18.15
17.64
16.92
16.63
2⁻
1⁺, 0
1⁺, 1
2⁺, 0+1
2α
3/2⁻
17.255
⁷Li+p
11.4
4⁺, 0
2.94
2⁺, 0
0.0
⁸Be

0.010 for the 16.92 MeV state.

The TUNL γ-ray spectrometer does not have sufficient energy resolution to independently confirm that the 16.92 MeV state is not populated in the proton capture reaction. For the data analysis, it was assumed that both states could be populated, and the data in this thesis are quoted as measuring the capture cross sections to the region of the isospin-mixed pair.

Chapter 2 Experimental Details

A. Beam Characteristics

The data reported in this thesis were taken at Triangle Universities Nuclear Lab (TUNL). A diagram of the lab is shown in Fig.2. To accelerate beams to energies from 3 to 17 MeV, a model FN tandem Van de Graaff accelerator was used. Various ion sources provided the proton beam for injection into the tandem. The unpolarized beams for the yield curves and angular distributions were produced by one of two direct-extraction negative ion sources (DENIS I or DENIS II). The unpolarized beams were chopped and bunched before injection into the tandem, and typical repetition rates for the bunched beam were about 5 MHz, with a typical on-target pulse width of about 2 nsec. The polarized proton beams used for the analyzing power experiments were produced by the TUNL Lamb-shift polarized ion source (Clegg et al., 1970). The polarization of the beam was measured after every run by making a quench-ratio measurement (Trainor et al., 1974), using a Faraday cup located at the center of the 90-90 magnet. The polarization varied between 60% and 80% over the course of the experiment, and the typical value was about 75% and quite steady during a given run. The assumed error in the polarization as determined from the quench ratio was less than about 5%. The polarized beams were pulsed by a three-stage bunching system (Wender et al., 1980). The first stage was a linear voltage ramp of approximately 100 V peak-to-peak applied to

Figure 2. TUNL laboratory.

Cyclo-Graaff Laboratory

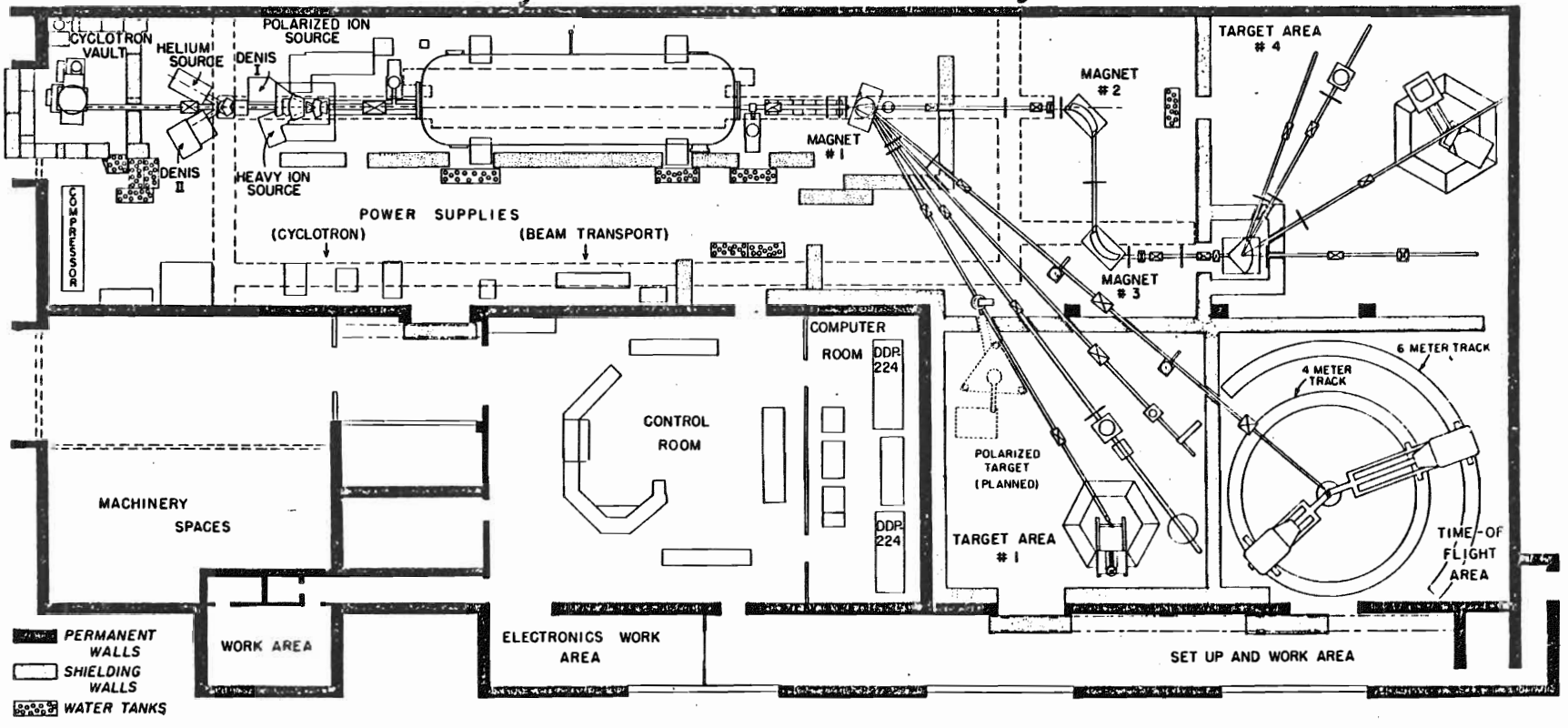

the anode of the duoplasmatron in the polarized source. Additional bunching was provided by a two-stage double-drift buncher system located before the entrance of the tandem.

Unpolarized proton beams with energies from 18-30 Mev were obtained by injecting the beam of a single-energy (15 MeV) cyclotron into the tandem (Cyclo-Graaff) (Newson et al., 1974). The normal RF structure of the cyclotron beams gave bunched protons with a 25 MHz repetition rate.

After acceleration the beams were momentum analyzed by a pair of 90° magnets. Only protons of the correct energy, as selected by the magnetic field, were allowed through the magnets. The strength of the magnetic field, and thus the energy of the beam, was determined by using a nuclear magnetic resonance fluxmeter. The beams were next steered through the 70-70 switching magnet into the 30° left beam leg in target area 4 and focused on a thin foil target placed inside an evacuated brass target chamber. This chamber was cylindrical with a 15.5 cm diameter and 8 cm height. A drawing of the capture beam leg in the target area is shown in Fig.3. The beams passing through the target were collected in the beam dump, which consisted of an insulated 6 foot pipe with a tantalum end cap. The pipe was located in a hole drilled at a 30° angle through the 1.5 feet thick concrete wall and about 4 feet into the dirt outside the wall. The current impinging on the beam dump was read, monitored, and digitized using a current integrator. Typical target currents were about 50 nA. The limiting factor on the beam current was primarily the count rate in the γ-ray spectrometer, since high count rates caused pile-up problems and high accidental coincidence rates between the NaI and the shield. A small aperture tantalum collimator of 1/16 inch thickness was used to collimate the beam just prior to the target, and the typical aperture used was a circular hole of 0.125 inches diameter. The beams were steered and focused to keep the

Figure 3. Capture beam leg.

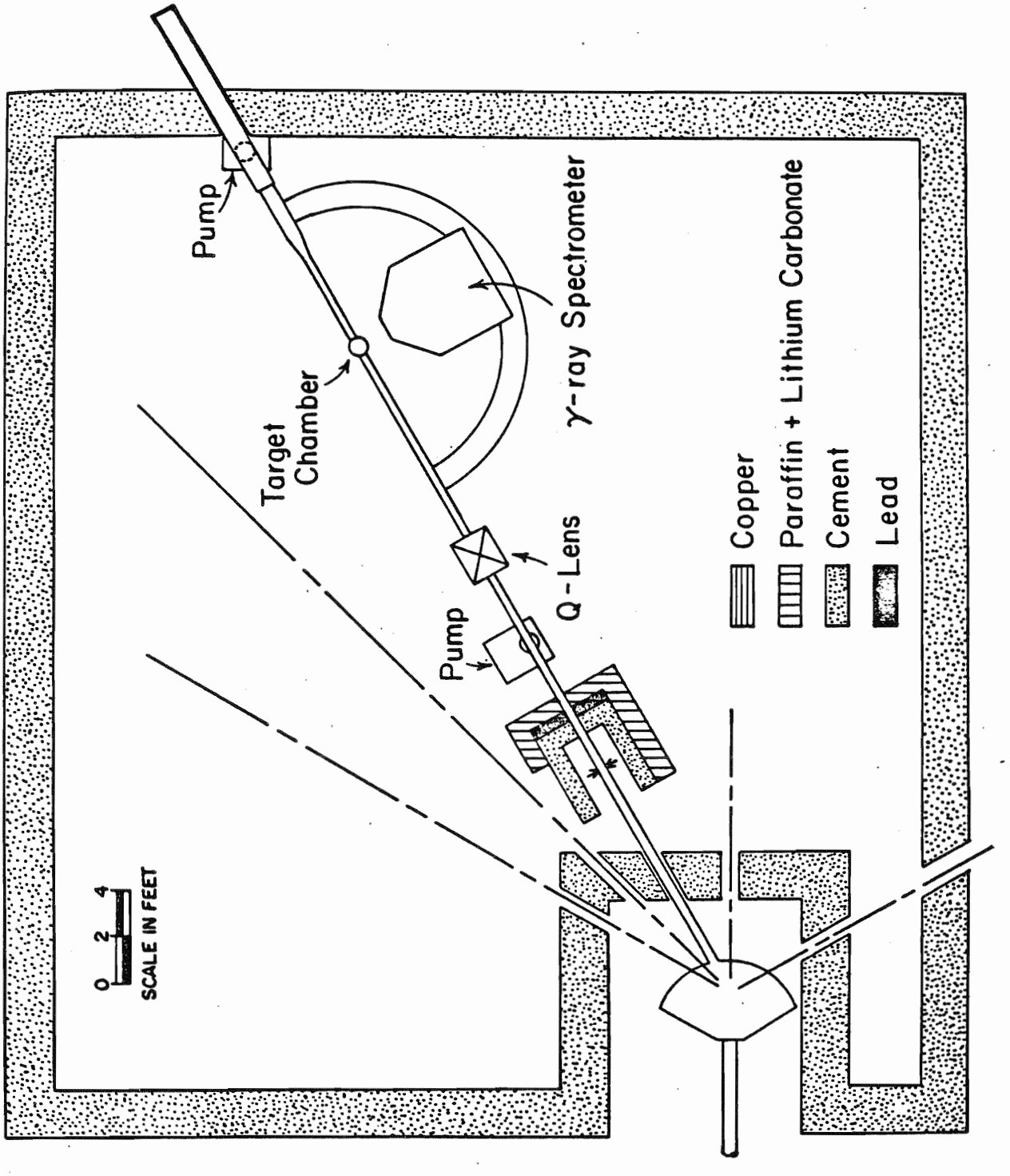
Pump
Target Chamber
γ-ray Spectrometer
Pump
Q-Lens
Copper
Paraffin + Lithium Carbonate
Cement
Lead
0 2 4
SCALE IN FEET

current on the collimator to a minimum (typically less than 1 nA).

A capacitive pick-off unit was used in the beam line to provide a timing signal from the bunched tandem beams. The unit consisted of a hollow cylinder of copper metal, as a capacitor, with a 1/16 inch wall, 1/2 inch outer diameter, and length of $2\frac{1}{2}$ inches. The signal was amplified at the beam line before being sent to the control room. For the Cyclo-Graaff experiments, a timing signal was obtained by the induction of a current in a coil of wire placed near the main RF oscillator of the cyclotron.

The 2α coincidence experiment was performed in the 52^{o} scattering chamber in target area 1. The proton beams for this experiment were momentum analyzed with the 20-70 magnet (magnet #1 in Fig.2). The beams were collimated just prior to the target using a tantalum collimator with a square aperture of dimensions 0.120 by 0.120 inches. The beams passing through the target were collected with a standard beam dump.

B. NaI Detector and Electronics

The γ-rays from the (p,γ) reactions were observed with a cylindrical 10 inch by 10 inch Bicron NaI crystal as shown in Fig.4. Six RCA-8575 photomultiplier tubes were used to collect the light from the scintillations in the crystal. The signals from the tubes were summed with a fan-in circuit and the output was clipped by a 160 nsec, 50 ohm clipping line, terminated with a 12 ohm resistor. The clipped signal, with about a 350 nsec width, was transmitted to the control room for further processing. A well-shaped NE110 plastic scintillator (Suffert et al., 1968) was positioned to cover the front and sides of the NaI and was used as an active anti-coincidence shield. The scintillations in this shield were viewed with 8 XP1031 photomultiplier tubes. The signals from the shield tubes were amplified separately, summed with a fan-in circuit, and amplified again. The output of the fan-in circuit was clipped by a 30 nsec, 50 ohm, shorted cable.

The shield and NaI were surrounded further by passive shielding, consisting of 10 cm of lead, approximately 20 cm of paraffin doped with lithium carbonate (50% lithium carbonate by weight), and a cadmium sheet across the front face. A lead collimator was used to collimate the γ-rays and was designed to just allow full illumination of the back face of the crystal by γ-rays from the target.

Using RG-8 cable to reduce attenuation, the summed signals from the NaI and shield were sent to the NaI and shield electronics set-up in the control room. A schematic diagram of these electronics is shown in Fig.5. The principle of these electronics was to send to the computer linear signals, one proportional to the γ-ray energy (E_γ) and another proportional to the time difference between the time pick-off and an event in the NaI crystal (TAC),

Figure 4. γ-ray spectrometer.

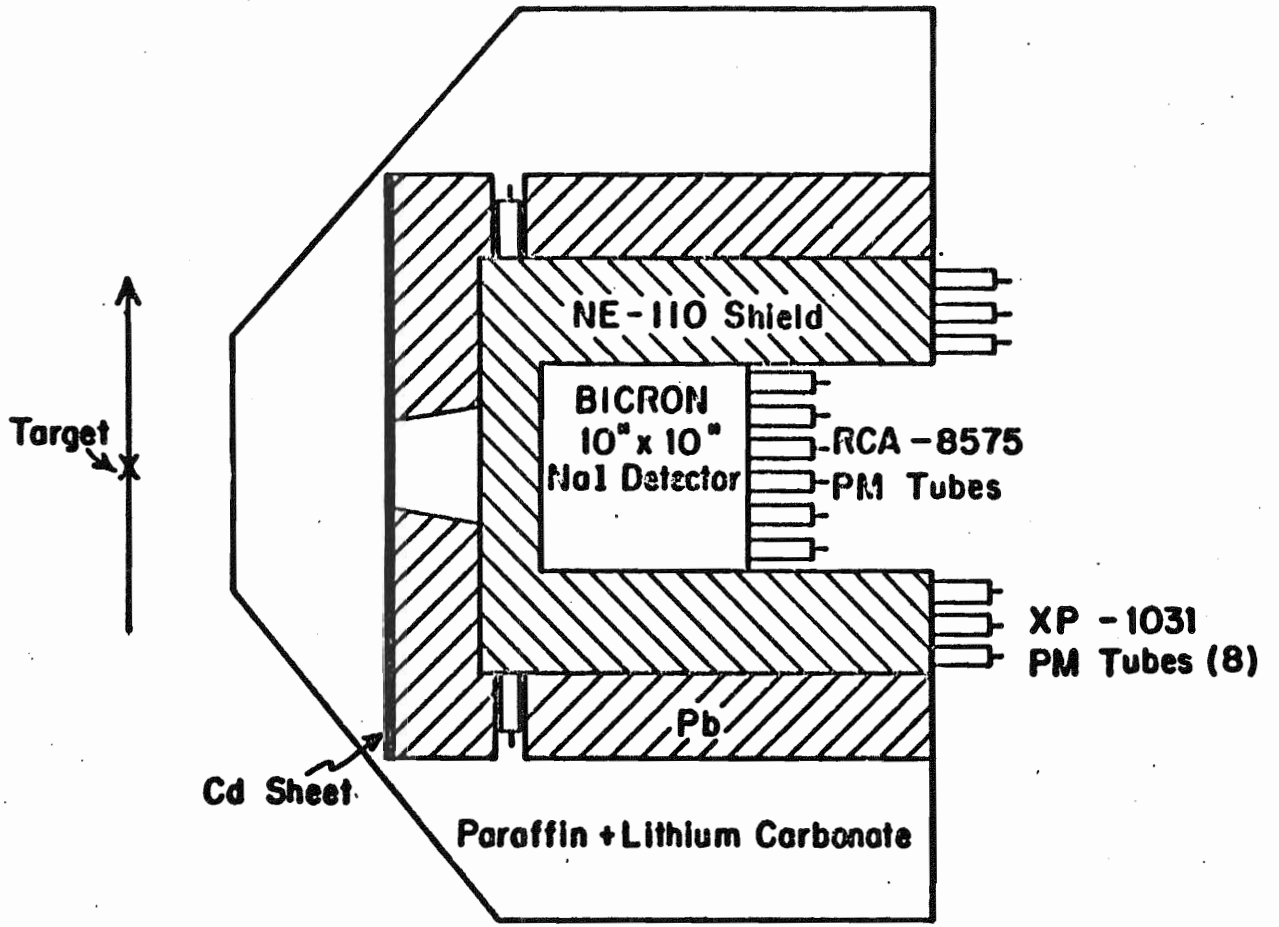
Target
NE-110 Shield
BICRON
10" x 10"
NaI Detector
RCA-8575
PM Tubes
XP-1031
PM Tubes (8)
Pb
Cd Sheet
Paraffin + Lithium Carbonate

Figure 5. NaI and Shield electronics.

NaI and SHIELD ELECTRONICS

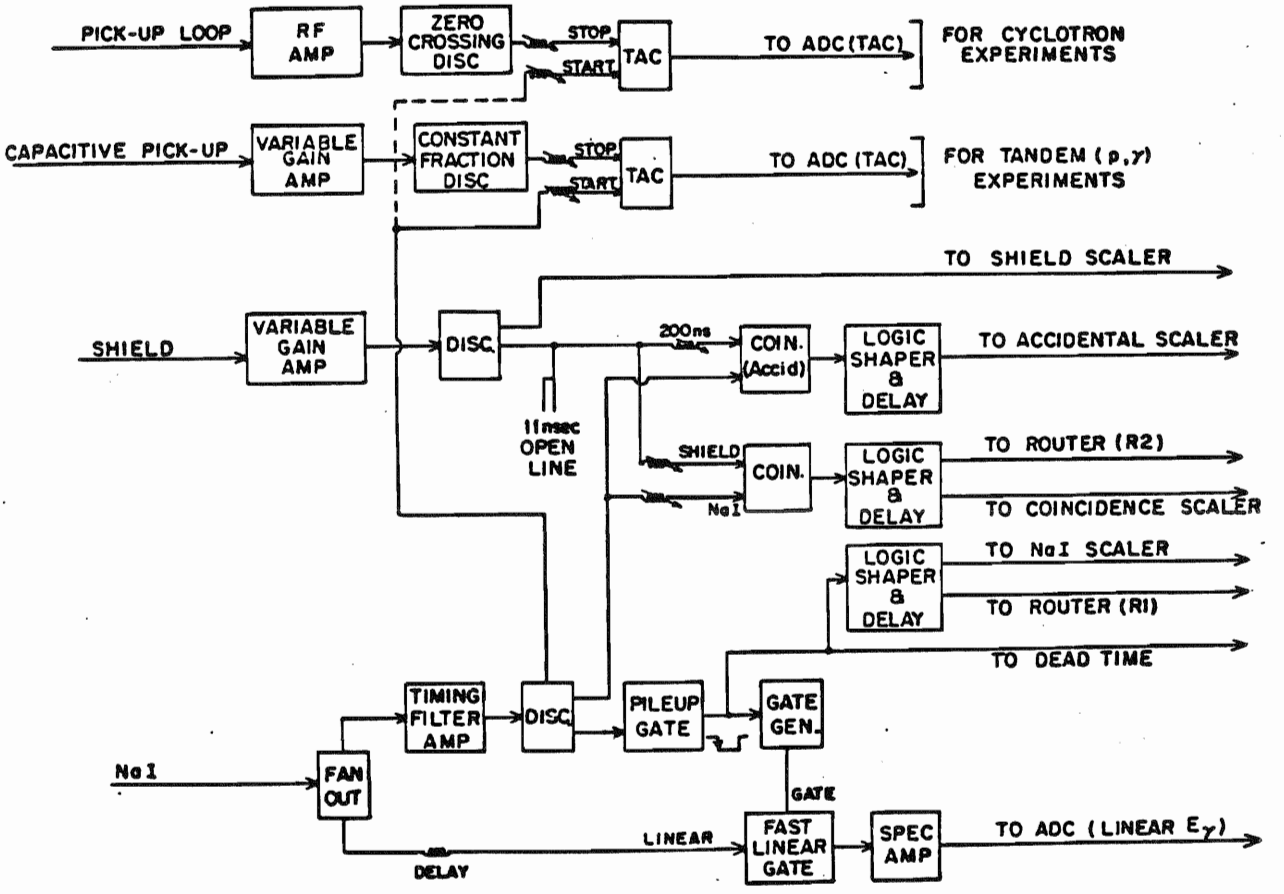

along with appropriate routing signals.

In more detail, the summed signal from the six NaI phototubes was fanned out into two signals. The first signal was sent to the linear input of a fast linear gate and then passed through a spectroscopy amplifier to give a linear signal to the ADC. The second signal from the fan-out was used to provide various logic signals. The signal was first passed through a fast amplifier to a discriminator. A gate was next used to produce a 10 μsec long signal which, by its leading edge, triggered a 400 nsec gate. This gate signal was used to open the fast linear gate for 400 nsec, allowing the 350 nsec linear signal to pass through. Thus, a signal large enough to trigger the discriminator opened the linear gate for 400 nsec and then held it closed (blocked) for 10 μsec. This 10 μsec block was implemented in an effort to reduce pile-up. The gate signal also provided a routing signal (R1) for use by the computer.

The shield electronics provided the computer with a routing pulse (R2) which indicated that the NaI linear signal had occured in coincidence with a shield signal. These routing pulses were used by the computer logic to "reject" the corresponding linear NaI signals from the γ-ray spectrum and to store them in an additional spectrum, called the "rejected spectrum" (discussed in the next section). A sample rejected event would be one in which a cosmic ray caused a simultaneous scintillation in the shield and NaI. The shield signal was amplified, sent to a fast discriminator, and after being delayed, was sent to the input of a coincidence circuit, along with a NaI logic signal. The rejection routing signal (R2) was produced if there was a coincidence. The resolving time of the coincidence circuit was about 60 nsec. The rejection efficiency was a function, in particular, of the amplifier gain setting and of the trigger level of the fast discriminator. Another

coincidence circuit was used to provide a measure of the accidental coincidence rate, which is the rate of random coincidences between the NaI and the shield pulses. This was accomplished by delaying the shield signal 200 nsec relative to the NaI signal before this coincidence circuit. The data was later corrected for the accidental counting rate.

A time-to-amplitude converter (TAC) in these electronics produced the linear signal which was proportional to the time interval between the timing signal and the NaI signal (the TAC signal). The start signal for the TAC was provided by a fast logic signal from the NaI electronics. For (p,γ) experiments using the tandem (without the cyclotron), the capacitive pick-off signal was sent to an amplifier and a discriminator before entering the stop input of the TAC. For (p,γ) experiments using the Cyclo-Graaff, the signal from the pick-up loop was sent through a RF amplifier and a zero-crossing discriminator before entering the stop input. The TAC signal produced in either case was sent to an ADC.

The pick-off signal was itself monitored to see whether or not all (or nearly all) of the beam bunches were being detected by the electronics. If any beam bunches were not detected, the associated (p,γ) data would not be stored into the proper spectrum in the computer. Additionally, if the discriminator in the pick-off circuit was set in the noise, too many bunches would be counted. The bunching system was tuned during the experiment to insure that the required number of bunches were detected. For a few cases when the beam was unstable, the number of bunches detected was counted in a scaler and used to renormalize the data upward in proportion to the percent of bunches missed by the electronics. Typically, since only 1 or 2% of the beam bunches were missed, this correction was small.

For the (p,γ) experiments, silicon surface barrier detectors were used

as target thickness monitors. These detectors were placed at 160° relative to the beam direction and were generally 2000 microns thick. The electronics consisted simply of an ORTEC model 109A preamp, connected to a spectroscopy amplifier. The particle spectra obtained from these detectors were stored in the computer, and the peak due to proton elastic scattering from ^{7}Li was used to provide a relative normalization from run to run for the (p,γ) angular distribution data.

C. On-line Computer and Computer Interface

All of the data reported in this thesis were acquired using an on-line DDP-224 computer. A locally built computer interface provided the data path and controls for the transfer of data from the analog-to-digital converters (ADC's) and routers to the computer. The important signals for data storage for the (p,γ) experiments were E_γ, TAC, R1, and R2. The linear signals E_γ and TAC were connected to ADC's, and R1 and R2 entered a two-input router. The logic of the computer system used for data taking was such that if only R1 was present, the corresponding E_γ signal was stored in the accepted data spectrum. If both R1 and R2 were present, E_γ was stored in the rejected data spectrum. The associated TAC signal was also stored, and the data taking program allowed the setting of a window on the TAC spectrum. During the experiment, the window was set around a peak corresponding to prompt γ-rays from the target. If the TAC pulse occured inside the window, the associated E_γ signal was stored in the "in-the-window" spectrum. For a TAC pulse occuring below or above the window, the E_γ signal was stored elsewhere. This time gating was used for both accepted and rejected events. The energy and TAC spectra were displayed on an oscilloscope as they were accumulated. After every run, the spectra were dumped on tape for later analysis. Sample spectra obtained are shown in the next section.

The computer also controlled and stored a number of scalers used for diagnostics. One scaler was used to count the output pulses from the current integrator, thus measuring the integrated incident beam charge for a given run. Another scaler counted this integrated charge gated by the dead time of the system, including the dead time from the 10 μsec gate and the dead time of the computer system. Other scalers counted NaI, shield, coincidence, and

accidental events as well as pulses from a real time clock. A final scaler counted the integrated charge gated by the dead time of the ADC used for the particle monitor storage.

D. NaI Spectra Data Reduction and Analysis

An accepted, in-the-window NaI spectrum for proton capture on ^{7}Li is shown in Fig.6. Also shown for comparison is the corresponding rejected, in-the-window spectrum (Fig.7), and the accepted, but below-the-window, spectrum (Fig.8). The first figure is the spectrum that was used for extracting the yields for the various ^{7}Li capture peaks labelled in the figure. The shield rejection and time-of-flight window obviously provided a great increase in the quality of the spectra. The storage of above- and below-the-window spectra allowed the monitoring of the correct setting of the TAC window. In some cases, small peaks were seen in the out-of-window spectra which corresponded to γ-rays from the reactions $^{7}Li(p,\gamma_0)$ and $^{7}Li(p,\gamma_1)$. In such cases, the γ_0 and γ_1 yields were corrected for these extra counts. For the $^{7}Li(p,\gamma_{16})$ case, no definite peaks were seen in the out-of-window spectra, so no corrections were made to the γ_{16} yield.

Shown in the next figure (Fig.9) is a plot of the same Li spectrum, labelling ^{7}Li capture lines and possible contaminants and including the results of a multiple peak fitting program called MULFIT (S.E.King, 1980). The program MULFIT fitted simultaneously the peaks in the spectra to a standard γ-ray line shape obtained from $^{3}H(p,\gamma)$ spectra taken at TUNL with the same NaI spectrometer. Three variable parameters were used in the fit for each peak: the peak height, the peak centroid, and the peak width. For spectra taken at different angles but the same energy, the ^{7}Li peak widths were held fixed. Since the first excited state of ^{8}Be has a non-negligible width (Γ=1.5 MeV), the γ_1 peak was fit with the standard line shape, convoluted with a Lorentzian line shape. Using MULFIT, the yields for $^{7}Li(p,\gamma_0)$, $^{7}Li(p,\gamma_1)$, and $^{7}Li(p,\gamma_{16})$ were extracted from the spectra for

Figure 6. $^{7}Li(p,\gamma)$ spectrum. Used thick Li metal target. Shown are capture to ground state of ^{8}Be (γ_0), capture to first excited state (γ_1), and capture to isospin-mixed pair (γ_{16}).

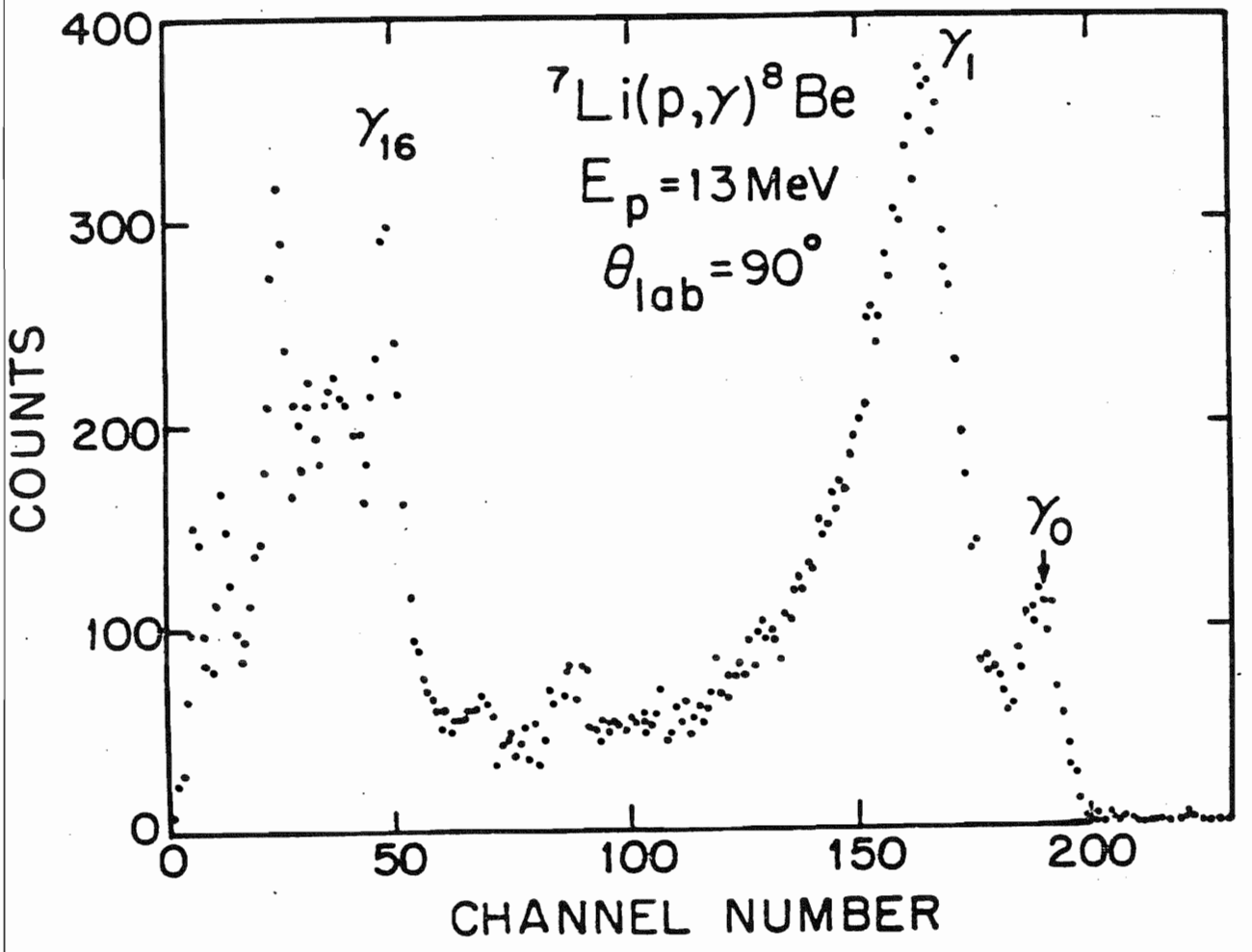
400
300
200
100
0
COUNTS
0
50
100
150
200
CHANNEL NUMBER
γ_{16}
γ_1
γ_0
$^7Li(p,\gamma)^8Be$
$E_p = 13\,MeV$
$\theta_{lab} = 90°$

Figure 7. $^{7}Li(p,\gamma)$ rejected, in-the-window spectrum.

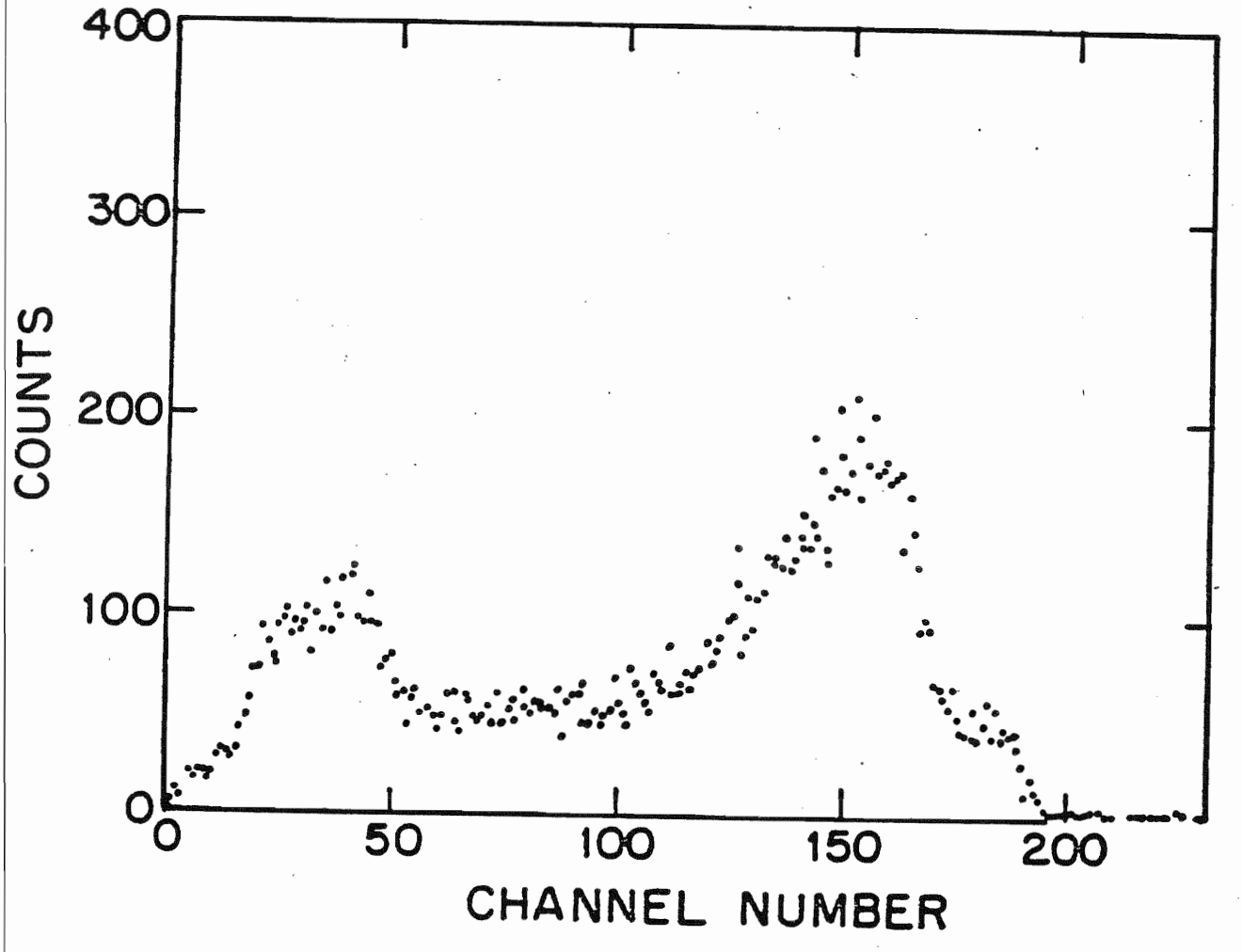
400
300
200
100
0
COUNTS
0
50
100
150
200
CHANNEL NUMBER

Figure 8. $^{7}Li(p,\gamma)$ accepted, below-the-window spectrum.

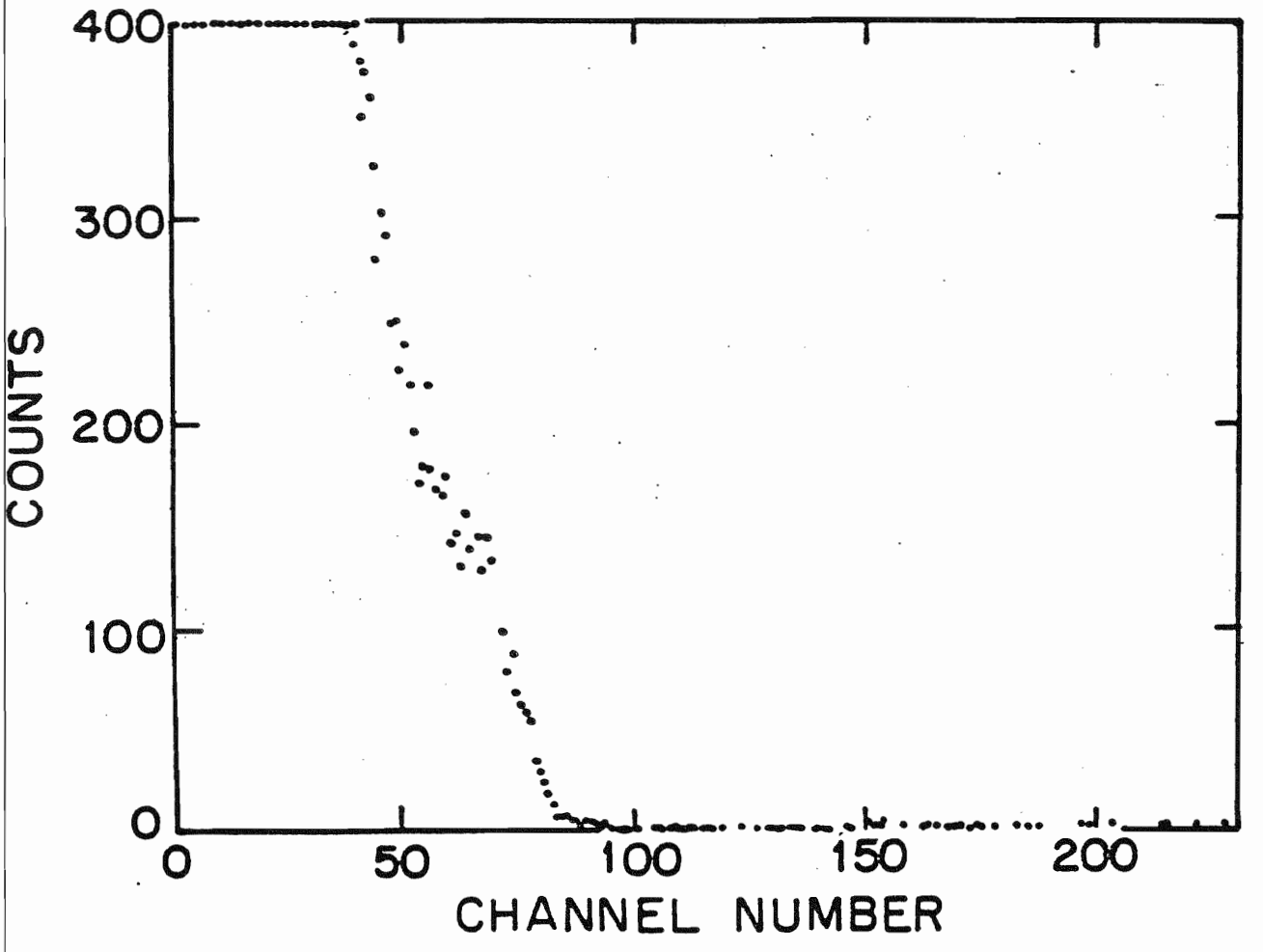
400
300
200
100
0
COUNTS
0
50
100
150
200
CHANNEL NUMBER

Figure 9. $^{7}Li(p,\gamma)$ spectrum with line-shape fitting. Shown are $^{7}Li(p,\gamma_0)$, $^{7}Li(p,\gamma_1)$, and $^{7}Li(p,\gamma_{16})$ and the predicted positions of various contaminant capture lines

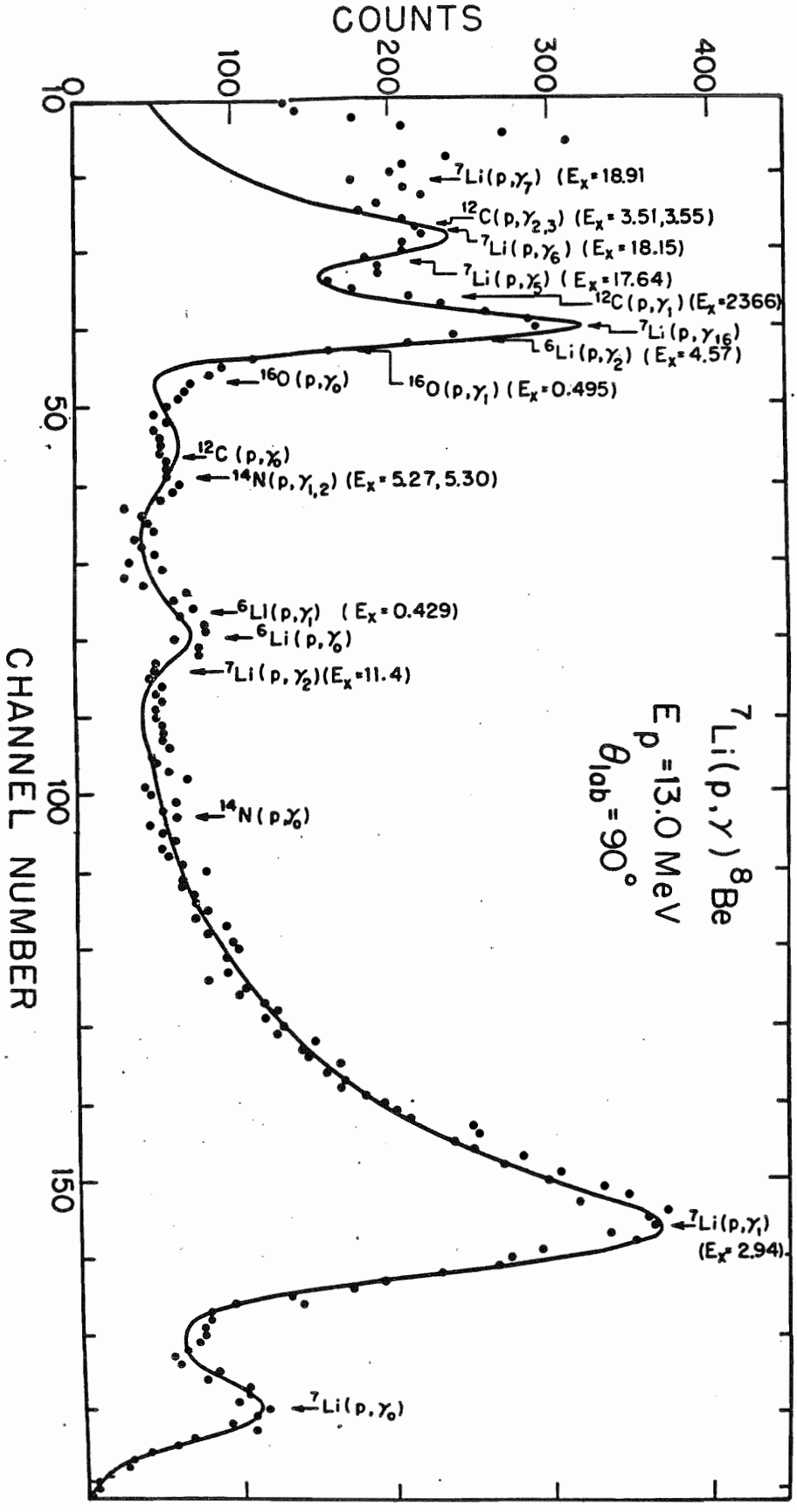
COUNTS
0
100
200
300
400
CHANNEL NUMBER
0
50
100
150
$^{7}Li(p,\gamma_7)$ (E_x=18.91
$^{12}C(p,\gamma_{2,3})$ (E_x=3.51,3.55)
$^{7}Li(p,\gamma_6)$ (E_x=18.15)
$^{7}Li(p,\gamma_5)$ (E_x=17.64)
$^{12}C(p,\gamma_1)$ (E_x=2366)
$^{7}Li(p,\gamma_{16})$
$^{6}Li(p,\gamma_2)$ (E_x=4.57)
$^{16}O(p,\gamma_0)$
$^{16}O(p,\gamma_1)$ (E_x=0.495)
$^{12}C(p,\gamma_0)$
$^{14}N(p,\gamma_{1,2})$ (E_x=5.27,5.30)
$^{6}Li(p,\gamma_1)$ (E_x=0.429)
$^{6}Li(p,\gamma_0)$
$^{7}Li(p,\gamma_2)$(E_x=11.4)
$^{14}N(p,\gamma_0)$
$^{7}Li(p,\gamma_1)$
(E_x=2.94)
$^{7}Li(p,\gamma_0)$
$^{7}Li(p,\gamma)^{8}Be$
E_p=13.0 MeV
θ_{lab}=90°

further analysis. Other observed peaks in the spectra were fit only to help construct the background under the γ_{16} peak, which was due largely to the tails of higher energy peaks. Most of the data analysis described above was performed with the TUNL VAX 11/780 computer.

Absolute cross sections for the data were determined in part from the absolute efficiency of the NaI spectrometer for detecting γ-rays. This efficiency was determined for 15 MeV γ-rays by measuring the $^{12}C(p,\gamma)$ thick target yield curve over the 15.07 MeV resonance in ^{13}N and comparing to a previous measurement of the number of γ-rays per proton (Marrs et al., 1975). Measurements of the accept-reject ratio for the full energy γ-rays and the shielding attenuation as a function of energy were used to extrapolate this efficiency to other energies (Weller and Roberson, 1981). The ratio of the full energy γ-rays (accepts-plus-rejects) divided by the total response of the NaI (accepts and rejects integrated down to zero energy) is essectially constant as a function of energy (Hayward), so it was not necessary to include this term in the extrapolation to other energies.

E. 2α Coincidence Experiment, Detector Set-up, and Electronics

As discussed earlier, the final state in the $^{7}Li(p,\gamma_{16})^{8}Be^{*}$ reaction is actually a pair of isospin-mixed states in ^{8}Be. These states decay almost 100% (more than 99%) (Ajzenberg-Selove, 1979) into two α-particles. A pictorial representation of the reaction is shown in Fig.10. An alternate measurement of the cross section for $^{7}Li(p,\gamma_{16})$ was provided by the 2α coincidence experiment, which detected the two decay α-particles in coincidence. Since the isospin-mixed pair does decay nearly 100% into 2 α-particles, and since the capture process involving a single γ-transition to these states is the only likely way of populating these states, the total cross section (σ_T) measured in the 2α reaction should be equal to the total cross section measured in the $^{7}Li(p,\gamma_{16})$ reaction. Since measurements of (p,γ_{16}) angular distributions for E_p=13-30 MeV indicate that the γ-transitions are predominantly E1, the angular distribution of α-particles should be expandable in terms of Legendre polynomials of orders zero and two only (Sweeney and Marion, 1969). That is: $\sigma(\theta)=A_0P_0(\cos(\theta))+A_2P_2(\cos(\theta))$. It was decided in our experiment to measure the α-particles at the zero of P_2, thus providing a direct measure of A_0 and σ_T ($\sigma_T=4\pi\cdot A_0$).

The detectors used in the 2α coincidence experiment were silicon surface barrier detectors. Two sets of two detectors were used for the experiment, one set placed at a forward angle (at the zero of $P_2(\cos(\theta))$ in the center-of-mass system) and the other set placed at the predicted backward angle for the coincident α-particle. (A kinematics program was written, called DEKIN, to calculate the expected angles and energies for the coincident α-particles.) Each set consisted of a front detector and a back detector. The front detector was selected to be thick enough to stop the α-particles from the

Figure 10. Classical picture of $^{7}Li(p,\gamma_{16})^{8}Be^{*} \longrightarrow 2\alpha$.

$^{7}Li(p,\gamma_{16})^{8}Be^{*} \longrightarrow 2\alpha$

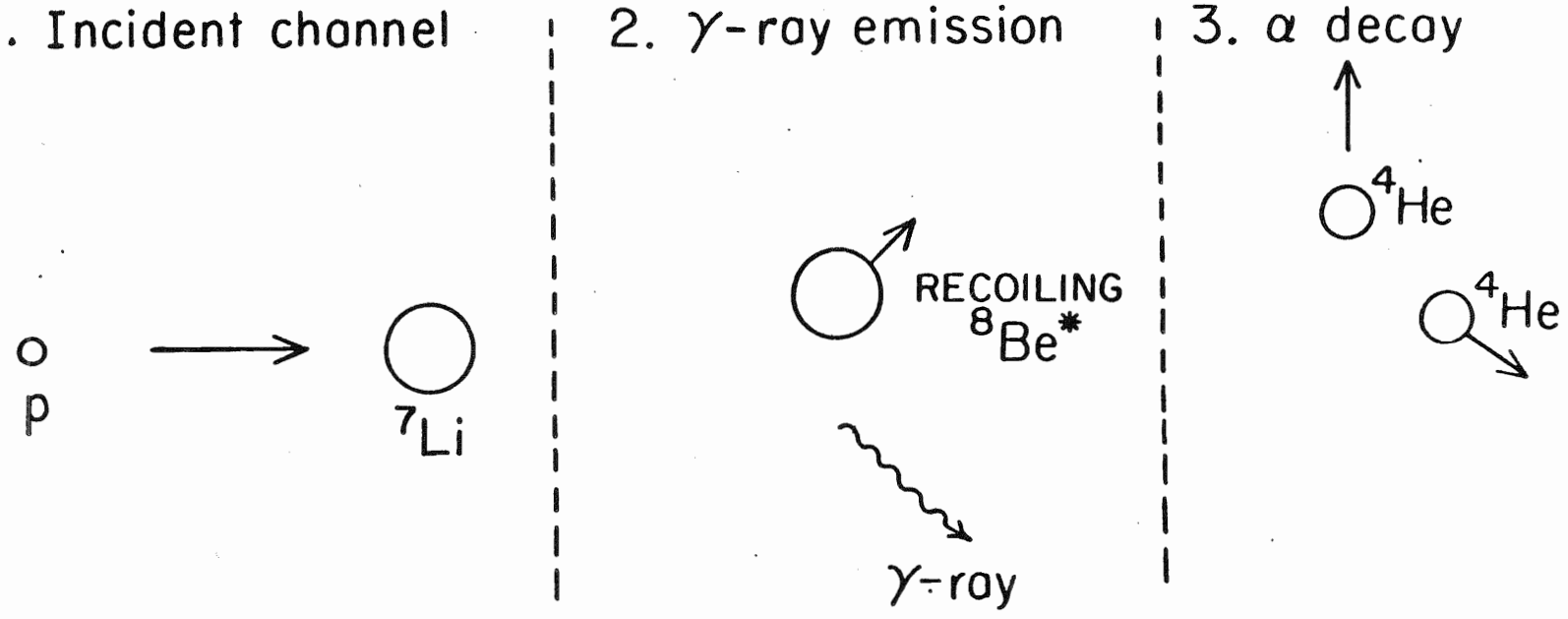

decay of the isospin-mixed pair but thin enough to let higher energy α's and most protons pass through. The back detector of each set was 2000 microns thick and was operated in anti-coincidence with the front detector.

The electronics for the 2α experiment are shown in Fig.11. The thin, front detectors are labelled "E", and the thicker back detectors are labelled "V" for "veto". Fast preamps (ORTEC models 142A or 142B) were used for all four detectors. The electronics for sets 1 and 2 were identical. Set 1 was placed at the forward angle and set 2 was placed at the backward angle. The energy output from the E preamp was passed through a spectroscopy amplifier to produce a linear signal, called E_1 or E_2, which was sent to an ADC at the computer interface. Timing single channel analyzers were used as discriminators to create logic signals from both front and back detectors. These logic signals were fed to an overlap coincidence operated in the anti-coincidence mode such that an output was obtained only if an E signal was present without a V signal. The T outputs from the two E preamps were amplified and fed to two fast discriminators, which produced the start and stop signal for a combination time-to-amplitude converter and single-channel analyzer (TAC/SCA). The TAC output was a linear function of the time difference between the arrival of a particle in the forward detector (1) and the backward detector (2). This timing signal helped decrease background in the energy spectra (as discussed in more detail in the following section). The SCA-out signal from the TAC/SCA was a logic signal which occured if the TAC signal was within the limits of the SCA window. This signal was run in coincidence with the output of the two other coincidence circuits to provide a gate signal allowing the E_1, E_2, and TAC pulses to be stored by the ADC's. The logic of the coincidences was such that, to obtain the gate signal, there must have been simultaneously a pulse in detector E_1 but not in V_1, a pulse in

Figure 11. 2α coincidence experiment electronics. The detectors labelled 1 were placed at the forward angle and the detectors labelled 2 were placed at the backward angle.

2α COINCIDENCE ELECTRONICS

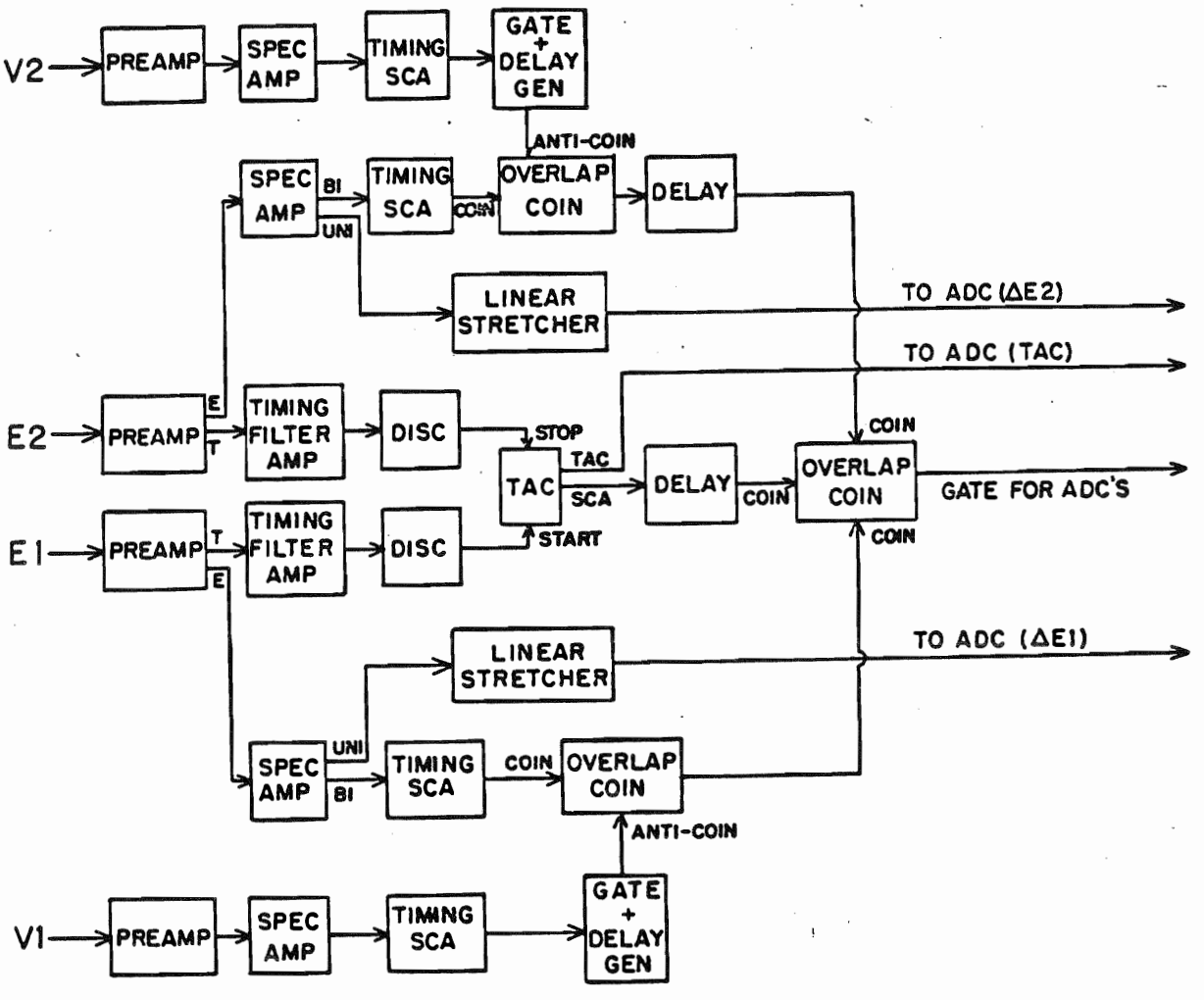

E_2 but not in V_2, and a timing signal within the range of the SCA on the TAC. The spectra observed are discussed in detail in the following section.

F. 2α Spectra and Analysis

The two energy signals (E_1 and E_2) and the TAC signal produced by the electronics, gated as described in the previous section, were stored in the computer and dumped on tape in "event mode" for later analysis. The analysis program, using the TUNL off-line DDP-224 computer, generated two gated spectra, in addition to the normal ungated energy and TAC spectra. One gated spectrum was the TAC spectrum gated with windows on E_1 and E_2, called the "energy-gated TAC". The second spectrum was a summed E_1 plus E_2 spectrum gated by a window in the TAC spectrum and a window on E_2. The windows on these spectra were set as described below.

For a given incident beam energy, DEKIN was used to calculate the predicted energies of the α-particles from the 16.6 MeV region at the specified detector angles, and during the experiment each detector was energy calibrated using an ^{241}Am α-particle source and a pulser. In the analysis, windows corresponding to the predicted energies were set on E_1 and E_2 to obtain the energy-gated TAC spectrum. A gated TAC spectrum for 10 Mev incident protons is shown in Fig.12. The region in the gated TAC spectra corresponding to coincidences between the α-particles had consistently a double-peaked nature, as seen in the figure, which was unexpected. This was believed to be due to a time jitter in the electronics, but since the background in the spectra was small, the final yield should not have been affected. Next an E_1+E_2 summed spectrum was obtained, gated by a window placed in the TAC spectrum surrounding the peak determined by the energy-gated TAC, and by a window placed in the E_2 spectrum surrounding the predicted α-particle energy. Gated and ungated summed spectra are shown in Fig.13. The gated spectrum shows a well-defined peak near the correct energy as predicted by the

Figure 12. Gated TAC spectrum for 2α coincidence experiment.

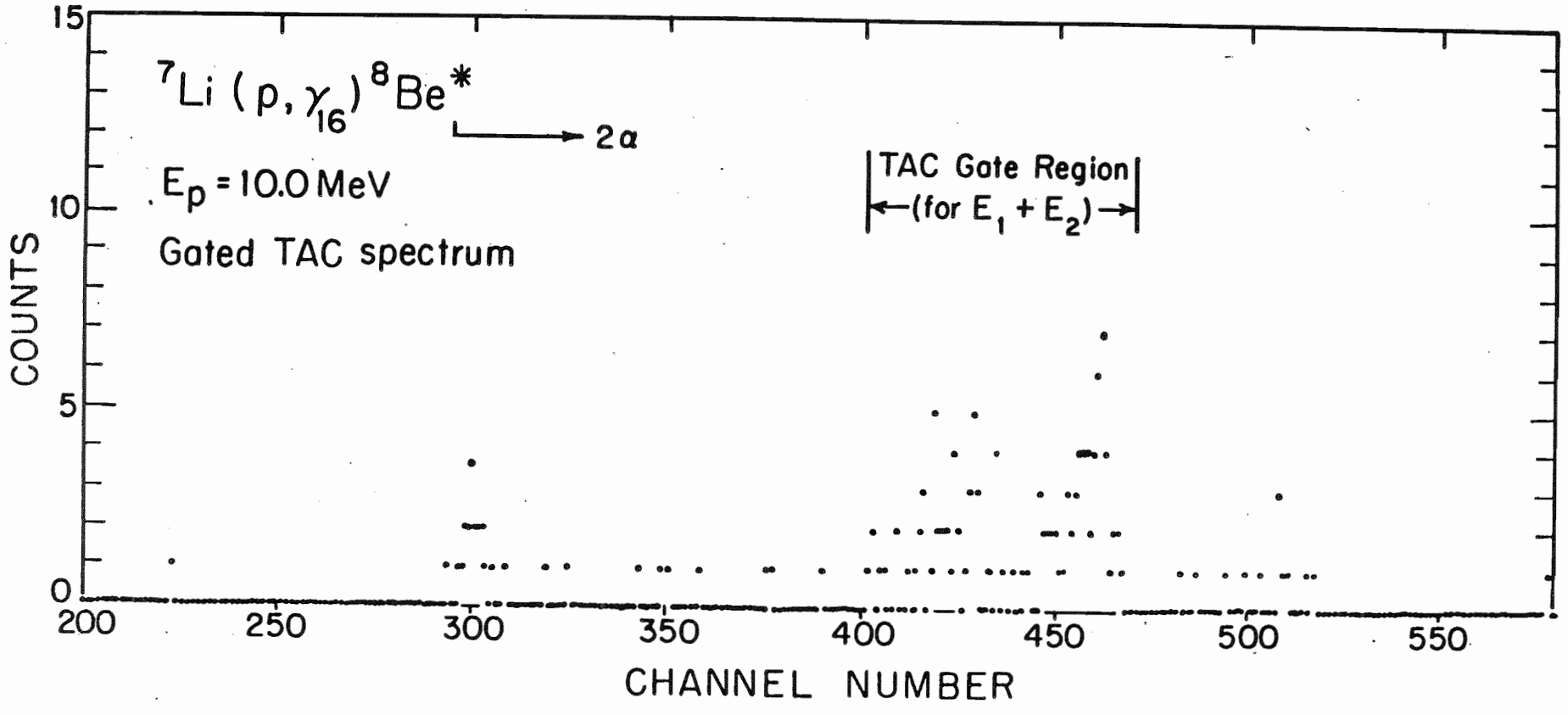
$^{7}Li\,(p,\gamma_{16})\,^{8}Be^{*}$
$\longrightarrow 2\alpha$
$E_p = 10.0$ MeV
Gated TAC spectrum
TAC Gate Region
(for $E_1 + E_2$)
COUNTS
CHANNEL NUMBER
0
5
10
15
200
250
300
350
400
450
500
550

Figure 13. Gated and ungated E_1+E_2 spectra for 2α coincidence experiment.

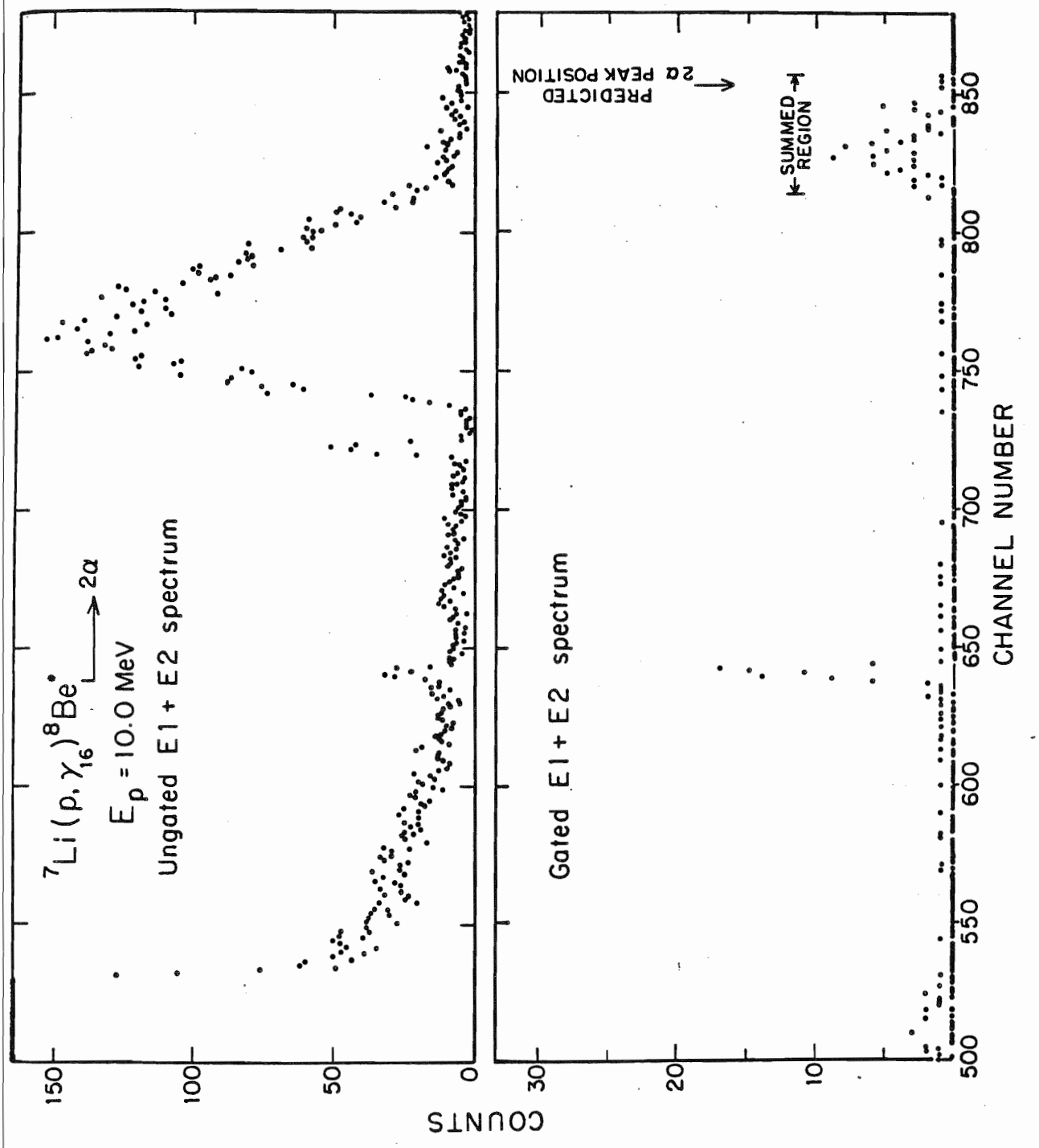
$^{7}Li(p,\gamma_{16})^{8}Be^{*}$ → 2α
E_p = 10.0 MeV
Ungated E1 + E2 spectrum
Gated E1 + E2 spectrum
PREDICTED 2α PEAK POSITION
SUMMED REGION
COUNTS
CHANNEL NUMBER
150
100
50
0
30
20
10
500
550
600
650
700
750
800
850

kinematics calculation. This peak was summed to obtain the yield for the $^{7}Li(p,\gamma_{16})^{8}Be^{*} \longrightarrow 2\alpha$ reaction. Clearly the gating requirements were necessary in this experiment, due to the high background count rate relative to the proper 2α coincidences.

Further analysis, performed with various gating windows, indicated that the windows in the initial analysis were properly set to detect the full number of coincidences in the data.

A potential problem that was checked involved the efficiency for detecting the second α-particle in coincidence with the first. Since the capture γ-ray is not detected in this experiment, the excited ^{8}Be nucleus recoils in an unspecified direction after the proton capture and before decay into two α-particles. Thus, depending on the direction of recoil, the α-particles can come out at different lab angles for the same center-of-mass angle. In the experiment, the forward detector was tightly collimated, with a circular hole subtending an angle of 1.5°. Calculations were performed which estimated that the backward angle detector should subtend at least an angle of about 5.5°, both in and out of the reaction plane, to observe all of the possible α-particles in coincidence with those in the forward detector. In the experiment, a circular collimator subtending 8.1° was used for the backward detector. Although this was believed to be sufficient, an experimental check was made by observing the number of 2α coincidences from the 16.6 Mev region as a function of the back angle, keeping the forward angle fixed. These experiments indicated that indeed the collimator size was adequate. They also indicated that the calculated angles for the two α-particles were correct.

G. Targets

The targets used for the $^{7}Li(p,\gamma)$ experiments were thick, 10–20 mg/cm^2, foils of natural lithium, which were obtained by pressing lithium metal. After pressing, the foils were mounted on target rings and stored in mineral oil. Care was taken to reduce surface contamination of the targets, and they were not stored longer than a day in mineral oil before being used. When used, the targets were washed with pentane to remove the mineral oil and quickly pumped under vacuum in the target chamber. Speed was important to reduce oxidation of the lithium. These targets were too thick to measure with α-particles from an ^{241}Am source, so cross sections were determined from thin targets or by comparing TUNL data to published data. The details of the absolute cross section determination and errors involved are discussed in Chapt.3.

Thin LiF targets were used for the 2α coincidence experiment and also for the absolute cross section measurements of the $^{7}Li(p,\gamma_0)$ reaction. These targets were prepared by evaporation of natural LiF onto thin (20 μg/cm^2) aluminum foils mounted on target rings. The thicknesses of these targets were measured by comparing to the (p,p_0) data of Gleyvod *et al.* (1965) and were typically about 250 μg/cm^2, implying a ^{7}Li thickness of about 70 μg/cm^2. These results were in agreement to within 10% of those determined from the energy loss of 5.477 MeV α-particles from an ^{241}Am source. The targets were fairly strong, and it was not necessary to store them under vacuum.

Chapter 3 $^{7}Li(p,\gamma_{16})^{8}Be^{*}$ Experimental Results

A. Absolute Cross Section

Before discussing the determination of the absolute cross section for the $^{7}Li(p,\gamma_{16})$ reaction, it is necessary to consider the effects of possible sources of background under the γ_{16} peak. The effects of $^{12}C(p,\gamma_{1})$, $^{16}O(p,\gamma_{0}+\gamma_{1})$, and $^{6}Li(p,\gamma_{2})$ (see Fig.9 in Chapt.2) are discussed in the following paragraphs.

Carbon was clearly present in the target, since fixed energy γ-rays were seen with energies of 15.11 and 12.71 MeV, which were presumedly produced by the $^{12}C(p,p'\gamma)$ reaction. In addition, the particle monitor spectra showed a peak which was determined using kinematics to be due to protons elastically scattered from ^{12}C. These two reactions provided an estimate of the amount of carbon present by comparison with published $(p,p'\gamma)$ and (p,p_{0}) data. For the (p,p_{0}) case, the cross section data of Peele (1957) predicted a ^{12}C target thickness (for a typical case) of about 300 $\mu g/cm^{2}$. (In comparison, the ^{7}Li target thickness was between 10 and 20 mg/cm^{2}). The absolute yields of γ-rays from both the 15.11 and 12.71 MeV states were difficult to determine precisely due to the large background in the γ-ray spectra at these energies. It was possible, however, to obtain an estimated yield from the 12.71 MeV state, and a comparison to the cross section data of Berghofer *et al.* (1976) indicated that the ^{12}C thickness in the targets was about 500 $\mu g/cm^{2}$. In the following

analysis, the value of about 500 $\mu g/cm^2$ was used as a rough upper limit.

The cross section for the reaction $^{12}C(p,\gamma_1)$ has been reported in the literature only for small energy ranges. The reported 90^o cross section is about 1 $\mu b/sr$ for 3-9 MeV protons (Johnson, 1974), has a peak value of about 1.5 $\mu b/sr$ at 22 MeV, in the region of the GDR, and is much smaller(less than 1/2 $\mu b/sr$) off the GDR. (Berghofer *et al.*, 1976) The cross section is difficult to measure in the energy region of E_p=10-20 MeV, due to the 15.11 and 12.71 MeV lines and the small cross section. Using a cross section of 1 $\mu b/sr$, and a ^{12}C thickness of 500 $\mu g/cm^2$, the $^{12}C(p,\gamma_1)$ yield was predicted to be about 4% of the $^{7}Li(p,\gamma_{16})$ yield for protons in the tandem energy region. This should be considered as a rough upper limit on the effects of $^{12}C(p,\gamma_1)$. No correction was made to the data, but the estimate of 4% is included in the overall error in the (p,γ_{16}) cross section.

The particle monitor spectra indicated that ^{16}O was also present in the target. A comparison of the proton elastic scattering yield from ^{16}O to known cross section data (Skwiersky *et al.*, 1974) gave, typically, an ^{16}O thickness of about 70 $\mu g/cm^2$. Using this target thickness and the capture data of Harakeh *et al.* (1975), it was predicted that the $^{16}O(p,\gamma_0+\gamma_1)$ yield was about 1% of the $^{7}Li(p,\gamma_{16})$ yield (for 16 MeV protons). This small effect was neglected in the analysis.

Since the targets were made of natural Li (7.5% ^{6}Li), ^{6}Li was known to be present. However, capture of protons by ^{6}Li leading to the second excited state of ^{7}Be has not been reported in the literature. For low energy protons, the yield for this reaction has been found to be less than 4% of the total yield of capture γ-rays to the ground and first excited states (Baskin and Carlson, 1955). It seems therefore quite likely that the effect of $^{6}Li(p,\gamma_2)$ should be small.

The resolution (width) of the γ_{16} peak could not be precisely determined from the spectra and was estimated by the measured γ-ray resolutions from the $^{14}N(p,\gamma)$ reaction (Wender et al., 1981) and by the beam energy spread due to target thickness. On the basis of these estimates, a resolution of 7.0% (FWHM) was used in the peak fitting routine for the γ_{16} peak. This resolution provided a good fit to the γ_{16} peak as shown in Fig.9 in Chapt.2. However, since varying the width in the fitting procedure could cause changes in the yield without significantly changing the quality of the fit, an error of $\pm$15% was included in the estimate of the error on the absolute cross section.

Although a large part of the background under the γ_{16} peak was due to the tails of higher energy peaks and therefore could be accounted for reliably by the fitting program, there may have been additional background due, for example, to pile-up and improper beam alignment. Initial experiments showed that it was possible to produce a large additional background under the γ_{16} peak by letting the beam impinge upon objects in the beam line, such as the target rings or the pick-off unit. Efforts were therefore made to keep this background as small as possible. The error in the absolute cross section introduced by this effect was estimated to be less than about 20%.

The $^{7}Li(p,\gamma_{16})$ absolute cross section was determined at 13 MeV from the ratio of its yield to the $^{7}Li(p,\gamma_{0})$ yield and by knowing the $^{7}Li(p,\gamma_{0})$ absolute cross section (measured with a thin LiF target as discussed in Chapt.4). The cross section determined in this manner was 0.613 μb/sr at 90^{o} for E_p=13 MeV. Using the measured angular distribution results at 13 MeV (Sec.C of this chapter), a total cross section of 7.10 μb was obtained. The absolute error on this cross section is about +20%, -30%, including the errors discussed in the previous paragraphs and the error from the $^{7}Li(p,\gamma_{0})$ absolute cross section determination (+15%).

An alternate measurement of the $^{7}Li(p,\gamma_{16})$ absolute cross section was provided by the 2α coincidence experiment, as described in Chapt.2. The value of σ_T for (p,γ_{16}) at 13 MeV as determined by this experiment was 4.60 μb with an absolute error of ±16%. This uncertainty was determined from the statistical error (±11%), the estimated error in the target thickness (±10%), and the estimated error in the detector solid angle (±5%). This cross section is 0.65 times the cross section obtained from the (p,γ_{16}) experiment, and the difference is just barely within the quoted errors. The two cross sections at 13 MeV were averaged, and a value of σ_T=5.85 μb was obtained. The absolute error on the average value, considering the previous discussion, should then be about 40%.

B. Yield Curve Data

The 90° yield curve for the reaction $^{7}Li(p,\gamma_{16})^{8}Be^{*}$ is shown in Fig.14 from 4 to 30 MeV. The closed dots represent the γ-ray data, taken with the NaI spectrometer. The absolute differential cross sections were obtained by normalizing the yield curve to the 90° cross section at 13 MeV, which was obtained from the averaged total cross section (5.85 μb as discussed in the previous section) by using the measured value of a_2. (Since a_4 is quite small and somewhat uncertain, it was not used to obtain this 90° cross section). The error bars are statistical only. The curve is the result of a direct capture calculation to be discussed in chapt.5. Gaps in the yield curve (at about 15 MeV and about 17.5 MeV) were regions where the presence of various (p,p'γ) lines made it impossible to extract the yield for the γ_{16} peak. Some identified sources for the various (p,p'γ) lines were decays from the 15.11 MeV and 12.71 MeV states to the ground state of ^{12}C. The lowest (p,γ) data point was at 11.5 MeV, since below that energy the γ_{16} peak could not be extracted, again due to the presence of various (p,p'γ) lines in the spectra.

The (p,γ) yield curve is very smooth throughout the region measured. The regions of apparent structure, such as the 3 points from 11.5 to 12.5 MeV, and the points from 18.5 to 20 MeV, may be due to small uncertainties in the data analysis procedure. In particular, for the 11.5-12.5 MeV region, there was some suggestion of a contaminant peak in the γ-ray spectra very near to the γ_{16} peak, and these points should therefore be considered somewhat unreliable.

A yield curve for σ_T was obtained from the 2α experiment for E_p=4 to 13 MeV. The 90° γ-ray cross sections were calculated from the measured σ_T using the predicted values of a_2 from the E1-E2 direct capture calculation (chapt.5). (The angular distribution data for E_p=13-30 MeV indicate that the

Figure 14. 90^{o} yield curve for $^{7}Li(p,\gamma_{16})$. Error bars represent the statistical errors associated with the data points. The solid curve is the result of the direct capture calculation.

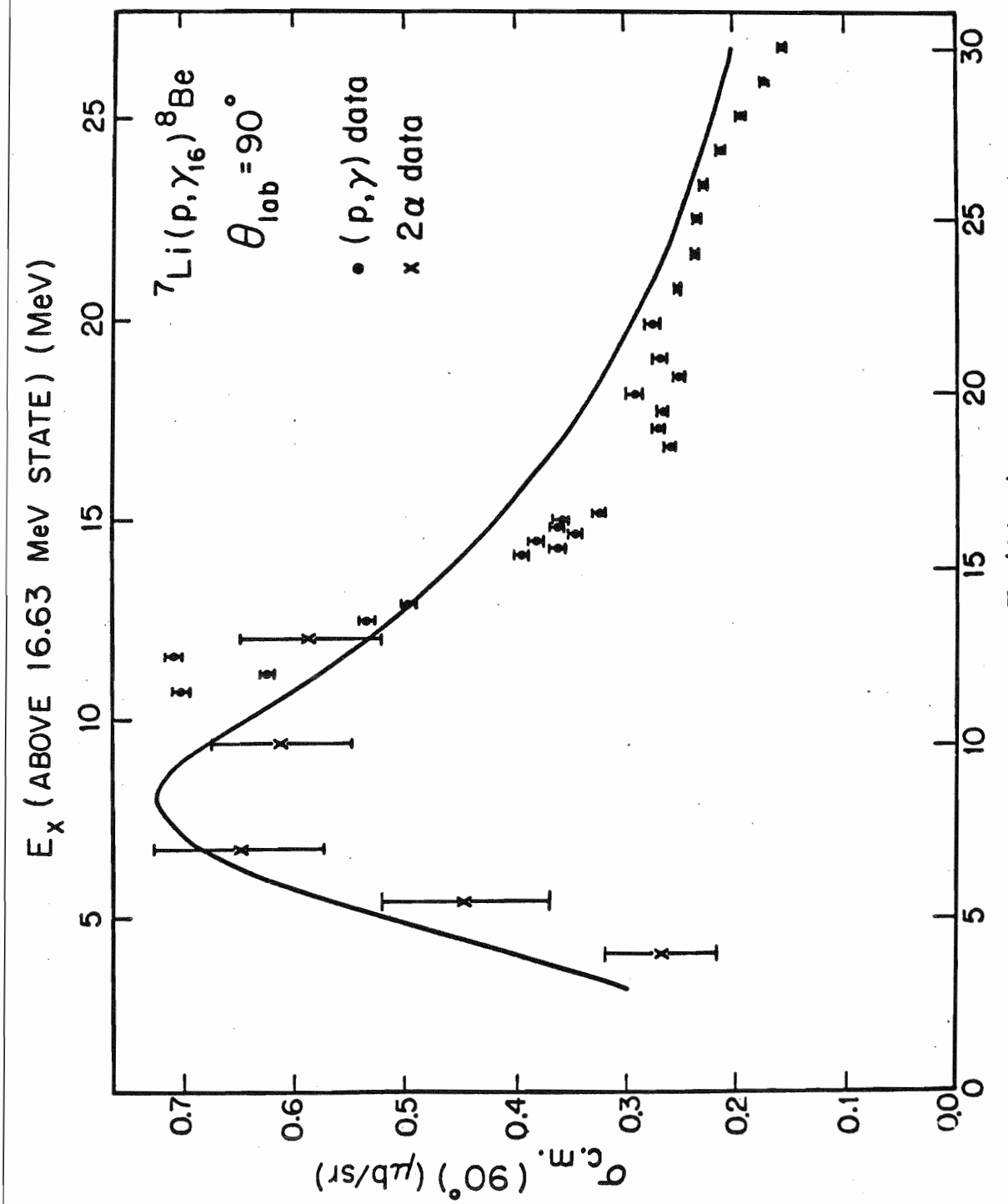
$^7Li(p,\gamma_{16})^8Be$
$\theta_{lab} = 90°$
• (p,γ) data
× 2α data
E_x (ABOVE 16.63 MeV STATE) (MeV)
E_p (MeV)
$\sigma_{c.m.}$ (90°) (μb/sr)
0.0
0.1
0.2
0.3
0.4
0.5
0.6
0.7
0
5
10
15
20
25
30

direct model is quite reliable). The results were normalized to the averaged cross section at 13 MeV and are shown with statistical error bars as the X's in the figure. The yield curve shows a broad resonance-like shape, peaking at about 25 MeV excitation energy in ^{8}Be which is about 8 MeV above the final states near 17 MeV. This energy is not, however, where a giant dipole resonance would be expected, which is typically at about 20 MeV above the final state in light nuclei (see, for example, the discussion of $^{7}Li(p,\gamma_0)$ and $^{7}Li(p,\gamma_1)$ in Chapt.4).

A yield curve for $\sigma_T(p,\gamma_{16})$ (the angle integrated total cross section) was obtained from the (p,γ_{16}) 90^{o} yield curve from 11.5 to 30 MeV by using the measured a_2 values (Sec. C of this chapter), which were assumed to vary smoothly with energy. These values of σ_T, combined with those measured in the 2α experiment, were detailed balanced to obtain $\sigma_T(\gamma,p)$. The integrated yield obtained was $\int\sigma_T(\gamma,p)\cdot dE$ = 10.3 MeV·mb. This is about 9% of the classical E1 sum rule, which is 60 NZ/A = 120 MeV·mb for ^{8}Be.

C. Angular Distributions of Cross Section and Analyzing Power

Angular distributions of cross section for the $^{7}Li(p,\gamma_{16})$ reaction were measured at seven angles from 30° to 154° for 8 energies between 12 and 30 MeV. In addition, the 14 MeV angular distribution was measured at 13 angles from 30° to 154°. The measured angular distributions are shown in Fig.15. The error bars are statistical only.

The angular distributions of cross section were fit to the orthogonal basis of Legendre polynomials $P_k(\cos(\theta))$ according to:

$$\sigma(\theta) = A_0[1+\sum_{k=1}^{4} a_k P_k(\cos(\theta))].$$

A fitting procedure was used which minimized the value of χ^2, which is defined as:

$$\chi^2 = \sum \frac{(\sigma(\theta)-\sigma_{fit}(\theta))^2}{\Delta(\sigma)^2},$$

where $\sigma(\theta)$ is the experimental cross section, $\sigma_{fit}(\theta)$ is the value of the fit, and $\Delta(\sigma)$ is the uncertainty in the experimental cross section. The fits obtained are shown as the solid curves in the angular distribution figures. The values of a_k obtained, and the values of χ^2 for the fits, are reported in Table I. The fact that χ^2 is often greater than 1 suggests that errors other than statistical are present in the data. The true error bars on the cross sections can be estimated by multiplying by $\sqrt{\chi^2}$. The data at 22 MeV have been fit only through a_3, since they were not of sufficient quality to obtain a reliable a_4.

A plot as a function of energy of the experimental a_k's is shown in Fig.16. The error bars here are again statistical only. The curve represents the results of the direct capture calculations to be discussed in Chapt.5.

Angular distributions of analyzing power have been measured at 13, 14, and 16 MeV. The data at 13 and 14 MeV were taken at 7 angles each, while 13

Figure 15. Cross section angular distributions for $^{7}Li(p,\gamma_{16})$. Error bars represent the statistical errors associated with the data points. The solid curves are the result of the Legendre polynomial fits.

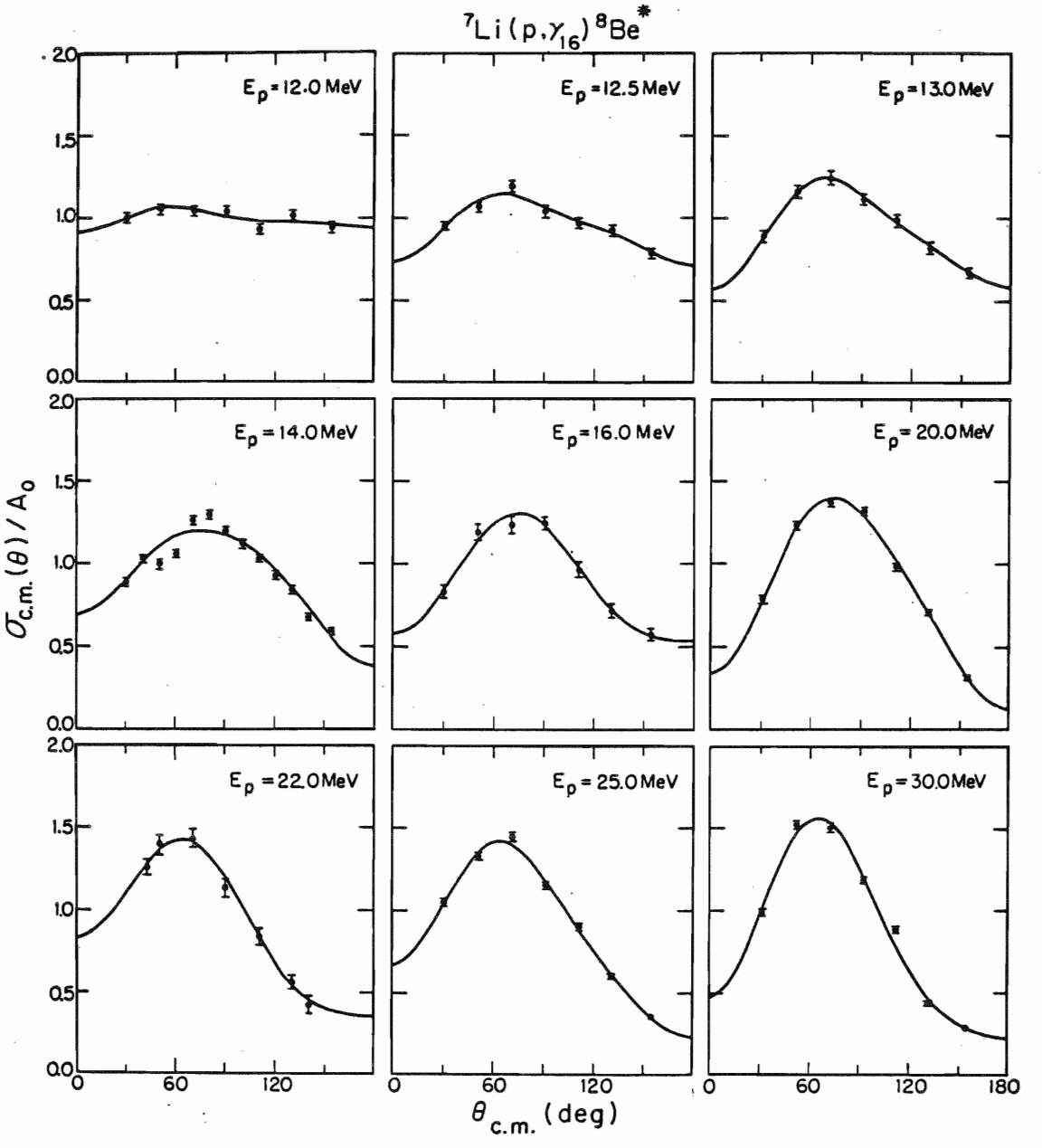
$^{7}Li(p,\gamma_{16})^{8}Be^{*}$
E_p = 12.0 MeV
E_p = 12.5 MeV
E_p = 13.0 MeV
E_p = 14.0 MeV
E_p = 16.0 MeV
E_p = 20.0 MeV
E_p = 22.0 MeV
E_p = 25.0 MeV
E_p = 30.0 MeV
$\sigma_{c.m.}(\theta) / A_o$
$\theta_{c.m.}$ (deg)
0.0
0.5
1.0
1.5
2.0
0
60
120
180

Table I. $^{7}Li(p,\gamma_{16})$ a_k Coefficients

E_p	a_1	a_2	a_3	a_4	χ^2
12.0	0.042±.18	-0.035±.25	-0.050±.32	-0.043±.41	3.02
12.5	0.109±.18	-0.196±.25	-0.096±.33	-0.075±.42	2.91
13.0	0.169±.20	-0.335±.28	-0.174±.39	-0.087±.46	0.68
14.0	0.170±.08	-0.394±.13	-0.015±.17	-0.072±.19	7.59
16.0	0.218±.25	-0.462±.34	-0.200±.49	0.017±.57	2.18
20.0	0.293±.10	-0.677±.14	-0.185±.21	-0.094±.25	4.07
22.0	0.503±.47	-0.412±.63	-0.268±.99	----------	0.67
25.0	0.451±.10	-0.466±.15	-0.235±.22	-0.087±.24	5.54
30.0	0.542±.10	-0.564±.15	-0.422±.22	-0.085±.22	28.16

Figure 16. a_k coefficients from the Legendre polynomial fits for $^7Li(p,\gamma_{16})$. The error bars represent the statistical errors. The solid curves are the result of the direct capture calculation.

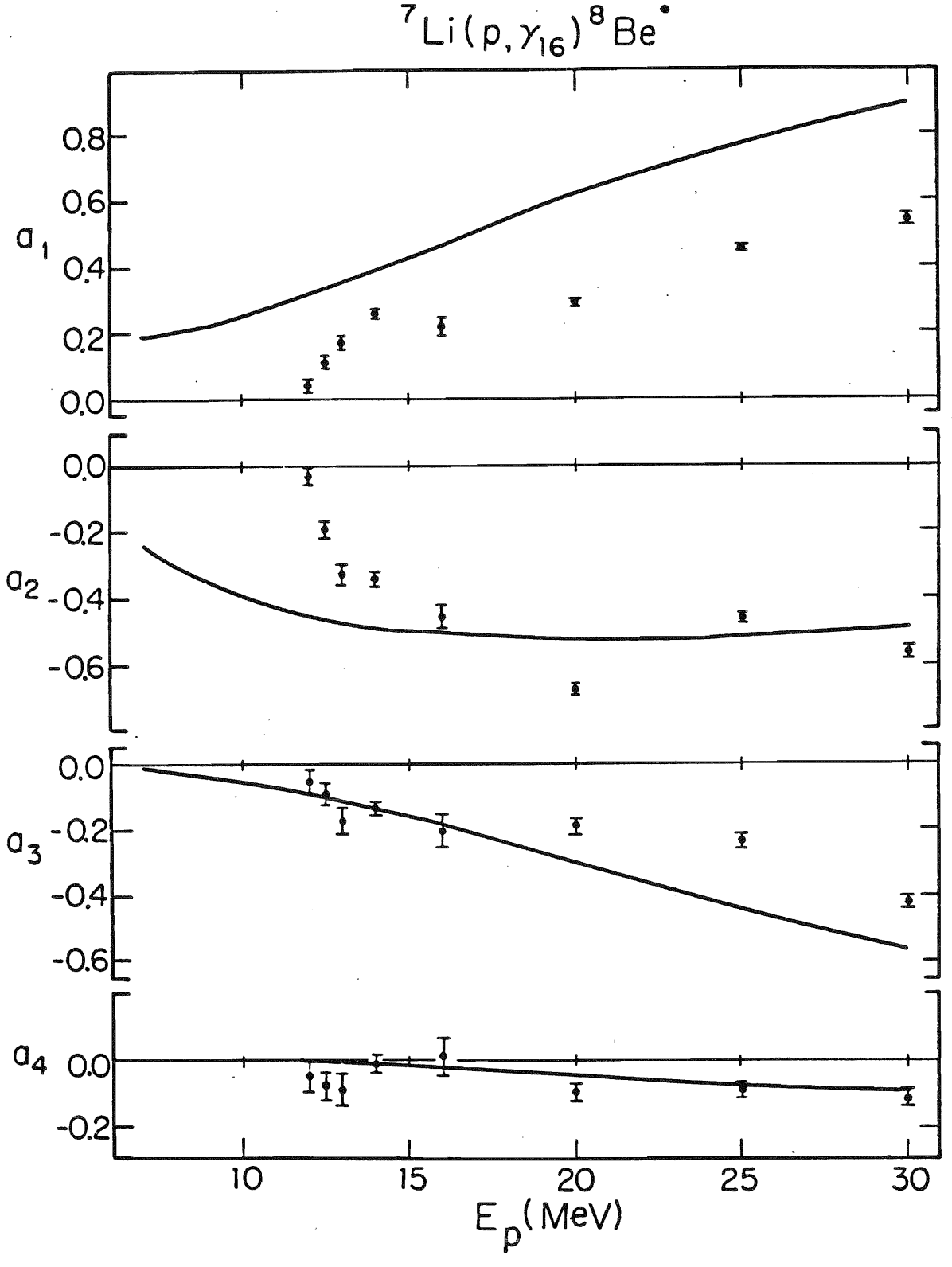
$^7Li(p,\gamma_{16})^8Be^*$
a_1
0.8
0.6
0.4
0.2
0.0
a_2
0.0
-0.2
-0.4
-0.6
a_3
0.0
-0.2
-0.4
-0.6
a_4
0.0
-0.2
10
15
20
25
30
E_p(MeV)

angles were measured at 16 MeV. The analyzing power, A(θ), is equal to:

$$\frac{1}{P}\cdot\frac{N_+-N_-}{N_++N_-},$$

where N_+ denotes the number of counts with the beam spin "up", and N_- denotes the number of counts with the spin "down", and P denotes the beam polarization. The analyzing power data have been fit to the expression:

$$\sigma(\theta)A(\theta) = A_0\sum b_k P_k^1(\cos(\theta)),$$

where $P_k^1(\cos(\theta))$ is an associated Legendre polynomial of order k. The measured angular distributions of analyzing power along with the fits are shown in Fig.17, and the values of b_k obtained from the fits are given in Table II. The error bars quoted are statistical only.

The effects of the contaminants (discussed earlier in this section) on the analyzing power data can be shown to be small. For example, the reaction $^{12}C(p,\gamma_1)$ would produce an error in the asymmetry for $^{7}Li(p,\gamma_{16})$ of no greater than 0.01 assuming a rather large asymmetry in $^{12}C(p,\gamma_1)$ of 0.4.

Figure 17. Analyzing power angular distributions for $^{7}Li(p,\gamma_{16})$. The error bars represent the statistical errors. The solid curves are the result of the associated Legendre polynomial fits. The dashed curves are the result of the direct capture calculation.

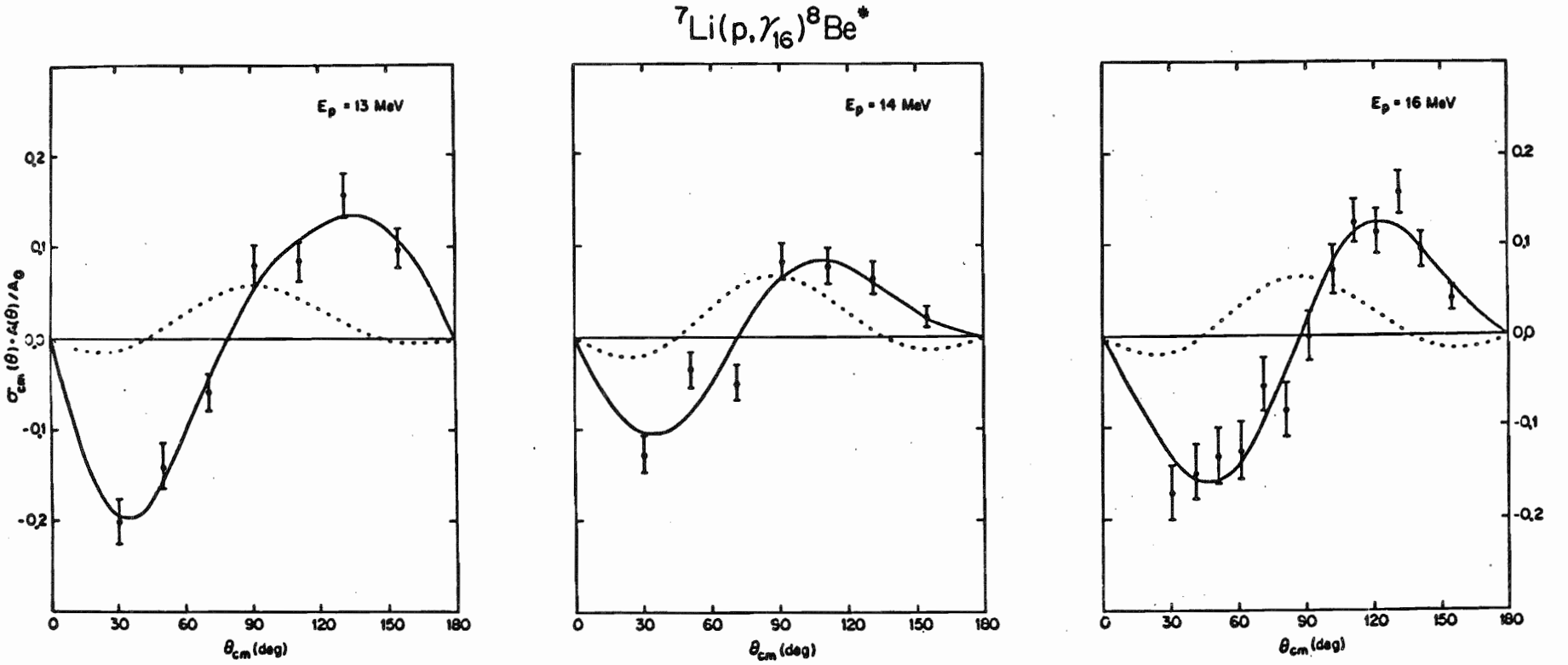
$^7Li(p,\gamma_{16})^8Be^*$
E_p = 13 MeV
E_p = 14 MeV
E_p = 16 MeV
$\sigma_{cm}(\theta) \cdot A(\theta) / A_0$
θ_{cm} (deg)
0,2
0,1
0,0
-0,1
-0,2
0
30
60
90
120
150
180

Table II. $^{7}Li(p,\gamma_{16})$ b_k Coefficients

E_p	b_1	b_2	b_3	b_4	χ^2
13.0	0.016±.011	−0.100±.008	−0.022±.006	−0.011±.005	1.64
14.0	0.026±.010	−0.049±.006	−0.025±.005	−0.001±.004	4.18
16.0	−0.003±.009	−0.093±.006	−0.013±.005	0.009±.005	1.35

Chapter 4 $^{7}Li(p,\gamma_0)$ and $^{7}Li(p,\gamma_1)$ Experimental Results

A. Yield Curves

The 90^{o} yield curve for $^{7}Li(p,\gamma_0)$ has been measured at energies from 11.5 to 30 MeV using a thick Li metal target. The data obtained are shown in Fig.18. The absolute cross sections for the TUNL data were determined by normalizing to a measurement using a LiF target of known thickness. (This thickness was determined as discussed in Chapt.2). Due to the presence of the flourine, only the capture yield to the ground state of ^{8}Be(ie:$^{7}Li(p,\gamma_0)$) was measured. The measurement gave the absolute $^{7}Li(p,\gamma_0)$ cross section at E_p=12 MeV, to an estimated accuracy of $\pm$15%. This accuracy was determined from the error associated with the efficiency of the detector ($\pm$10%), the estimated error in the target thickness ($\pm$10%), and the statistical error for the γ_0 peak ($\pm$6%). The solid curve in the figure is a smoothed representation of the Stanford data as taken from a plot in the paper (Fisher *et al.*, 1976) (and should therefore be considered only an approximation to the data). There has been no relative normalization of the data sets in the figure, and in the region of overlap, the absolute cross sections of the two data sets are in good agreement. The dashed curve and the dotted-and-dashed curve shown in the figure are the results of direct capture calculations (described in chapt.5). The yield curve shows the broad concentration of strength typical of a GDR. In this case, the concentration of strength peaks at about 22 MeV excitation

Figure 18. 90^{o} yield curve for $^{7}Li(p,\gamma_{0})$. Error bars represent the statistical errors associated with the data points. For those points shown without error bars, the error was smaller than the size of the dot. The solid curve is a representation of the Stanford data. The dashed and dotted-and-dashed curves are the result of direct capture calculations which are discussed in Chapter 5, Section D.

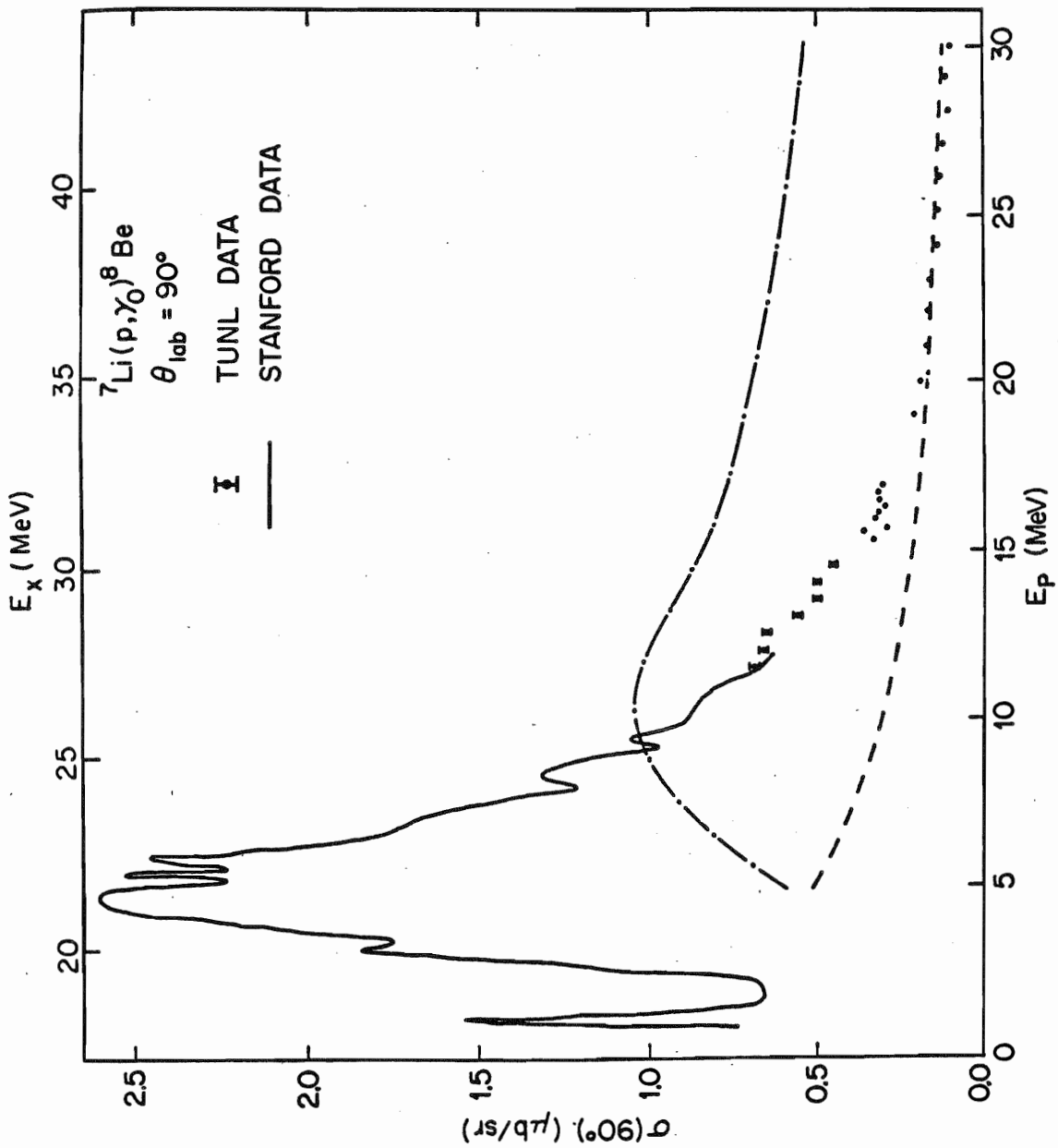
$^7Li(p,\gamma_0)^8Be$
$\theta_{lab} = 90°$
TUNL DATA
STANFORD DATA
E_x (MeV)
E_p (MeV)
$\sigma(90°)$ (μb/sr)
0.0
0.5
1.0
1.5
2.0
2.5
0
5
10
15
20
25
30
35
40

energy in ^{8}Be (about 5.5 MeV proton energy). Additionally, it should be noted that there is some suggestion of structure in the yield curves, which is also characteristic of a GDR. The total cross section has been summed over energy according to $\int\sigma_T(\gamma,p)\cdot dE_\gamma$ for comparison with the dipole sum rule for ^{8}Be, where $\sigma_T(\gamma,p)$ is the total (γ,p) cross section and was obtained from the (p,γ) data using detailed balance. The total (p,γ) cross section as a function of energy was obtained from the Stanford data for E_p=2-11 MeV, and from the TUNL 90° yield curve, using measured values of a_2 (discussed in the following section) for energies from 11.5-30 MeV. The value obtained for the sum was 16.5 MeV-mb which is 13.8% of the classical sum rule prediction of 120 MeV-mb.

The 90° yield curve for proton capture to the first excited state of ^{8}Be (^{7}Li(p,γ_1)) is shown in Fig.19. The absolute cross section for this yield curve was obtained from the ratio of the γ_1 to the γ_0 yield, using the γ_0 cross section measured with the LiF target. Because of the finite width of the first excited state, it was necessary in forming this ratio to integrate the entire line shape down to zero energy. The effect of the NaI detector efficiency, which is different for γ_1 than for γ_0 since E_γ is different, was included in the cross section determination. The γ_1 cross section at 90° for E_p=12 MeV determined in this manner was 3.58 mb/sr. The absolute uncertainty in this value includes the uncertainty in the γ_0 cross section ($\pm$15%) and the uncertainty in the ratio of γ_1 to γ_0 ($\pm$10%) giving a total uncertainty of $\pm$18%. The solid curve in Fig.19 is again a smoothed representation of the Stanford data (Fisher *et al.*, 1976). In this case, however, the Stanford data has been normalized down (multiplied by 0.610) to give agreement with our data at 11.5 MeV. This disagreement between the two data sets, which is greater than the predicted errors, was investigated by using MULFIT to fit the spectrum at 3.25 MeV reported in the Stanford paper. The results of MULFIT

Figure 19. 90^{o} yield curve for $^{7}Li(p,\gamma_{1})$. Error bars represent the statistical errors associated with the data points. The solid curve is a representation of the Stanford data multiplied by 0.61. The dashed and dotted-and-dashed curves are the result of direct capture calculations which are discussed in Chapter 5, Section D.

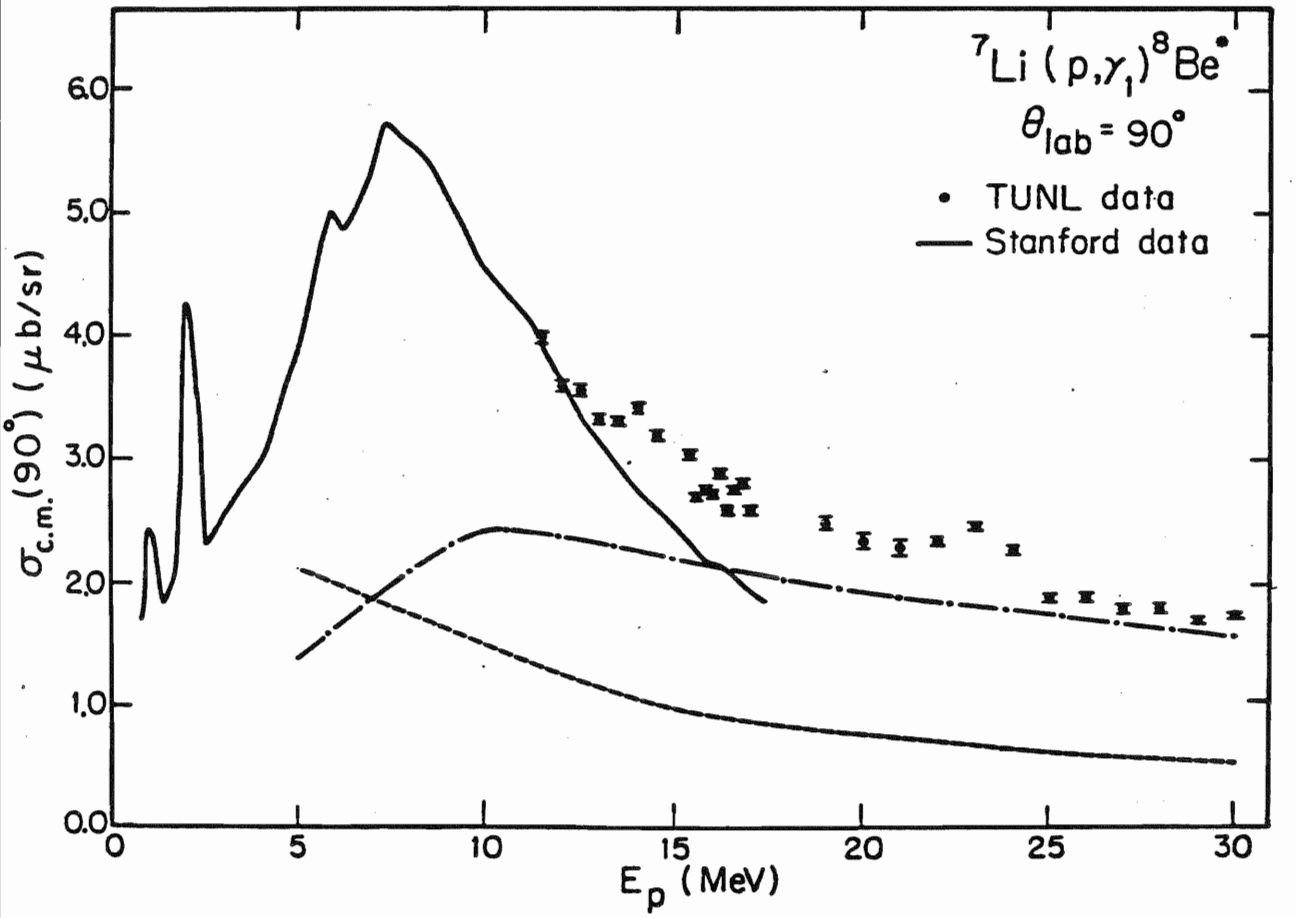
$^7Li\,(p,\gamma_1)^8Be^*$
$\theta_{lab} = 90°$
• TUNL data
— Stanford data
$\sigma_{c.m.}(90°)$ (μb/sr)
6.0
5.0
4.0
3.0
2.0
1.0
0.0
0
5
10
15
20
25
30
E_p (MeV)

gave a ratio of the sums of γ_0 to γ_1 of 0.50, while the Stanford paper reports a ratio of 0.44. These numbers agree to within 12%, and it was concluded that MULFIT and the Stanford peak fitting program are in close agreement. The discrepancy between the TUNL data and the Stanford data for the (p,γ_1) reaction has not been resolved.

As before, the dashed curve and dotted-and-dashed curve in the figure are the results of direct capture calculations.

The data show the giant dipole resonance built on the first excited state of ^{8}Be, which peaks at about 7.5 MeV proton energy, which is about 24 MeV excitation energy, or about 21 MeV above the first excited state. The peak has thus been shifted upward relative to the γ_0 GDR by approximately the energy of the first excited state (2.94 MeV). The integrated cross section obtained for comparison with the sum rule was found to be 17.3 MeV-mb, using the normalized value of the Stanford data for E_p=2-11.5 MeV and the TUNL data for E_p=11.5-30 MeV. This value is 14.4% of the sum rule, 120 MeV-mb, which is very nearly the same as that exhausted in the case of the ground state GDR.

B. Angular Distributions of Cross Section and Analyzing Power

Angular distributions of cross section for both $^{7}Li(p,\gamma_0)$ and $^{7}Li(p,\gamma_1)$ have been measured at seven angles and at eight energies from 12-30 MeV and fitted with Legendre polynomials. Angular distributions of analyzing power for the two reactions have been measured at seven angles for 13 and 14 MeV and at thirteen angles for 16 MeV. These data were fit to associated Legendre polynomials.

The angular distributions of cross section for $^{7}Li(p,\gamma_0)$, with the Legendre polynomial fits, are shown in Fig.20. The a_k's extracted in the fits are shown in Fig.21 and listed in Table III along with the values of χ^2 obtained in the fits. The dashed curve and the dotted-and-dashed curve shown are again the results of direct capture calculations. The error bars given are statistical only. Since χ^2 for the Legendre polynomial fits is in general bigger than one it is apparent that there was some small additional uncertainty in the data (perhaps due to the peak fitting procedure). The exceptionally large χ^2 at E_p=25 MeV may indicate the presence of some problem in the data at this energy. Nonetheless, the values of a_k obtained at 25 MeV seem quite reasonable when compared with the other energies (see figure), and indeed the entire data set shows a very smooth behavior as a function of energy.

Fisher *et al.* (1976) at Stanford have measured a_k coefficients for $^{7}Li(p,\gamma_0)$ in small energy steps from 2 to 16 MeV protons. A smoothed representation of their results is shown in Fig. 21 as the solid curves. A comparison of the TUNL data with the Stanford results shows good overall agreement in a_1 (positive and slowly rising from 12-16 MeV), good agreement in a_4 (essentially zero), and reasonable agreement in a_3 (negative). There is,

Figure 20. Cross section angular distributions for $^{7}Li(p,\gamma_0)$. Error bars represent the statistical errors associated with the data points. The solid curves are the result of the Legendre polynomial fits.

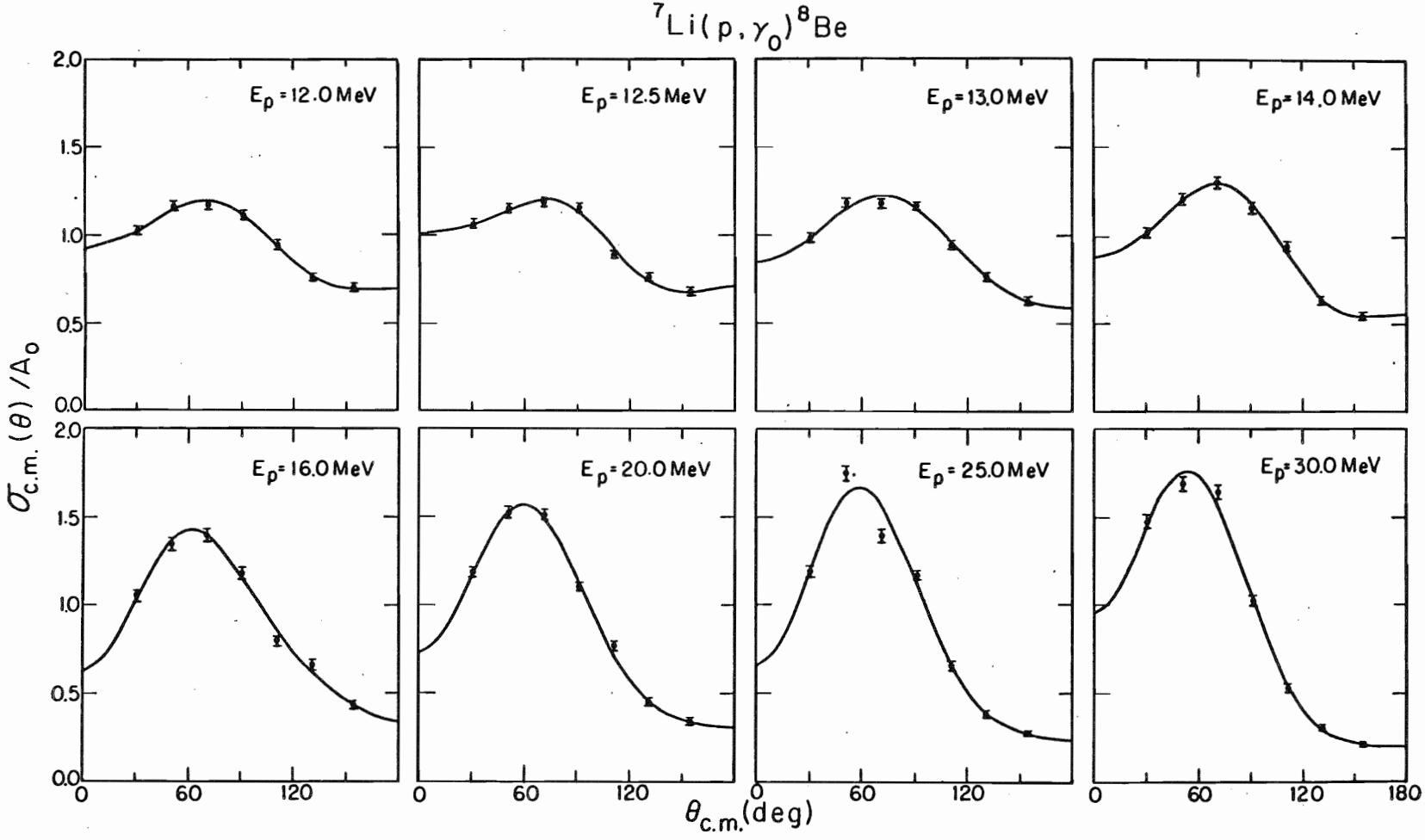
$^{7}Li(p,\gamma_0)^{8}Be$
E_p = 12.0 MeV
E_p = 12.5 MeV
E_p = 13.0 MeV
E_p = 14.0 MeV
E_p = 16.0 MeV
E_p = 20.0 MeV
E_p = 25.0 MeV
E_p = 30.0 MeV
$\sigma_{c.m.}(\theta)/A_0$
$\theta_{c.m.}$(deg)
0.0
0.5
1.0
1.5
2.0
0
60
120
180

Figure 21. a_k coefficients from the Legendre polynomial fits for $^7Li(p,\gamma_0)$. The error bars represent the statistical errors. The solid line is an approximate representation of the Stanford data (Fisher et al., 1970). The dashed and dotted-and-dashed curves are the result of direct capture calculations which are discussed in Chapter 5, Section D.

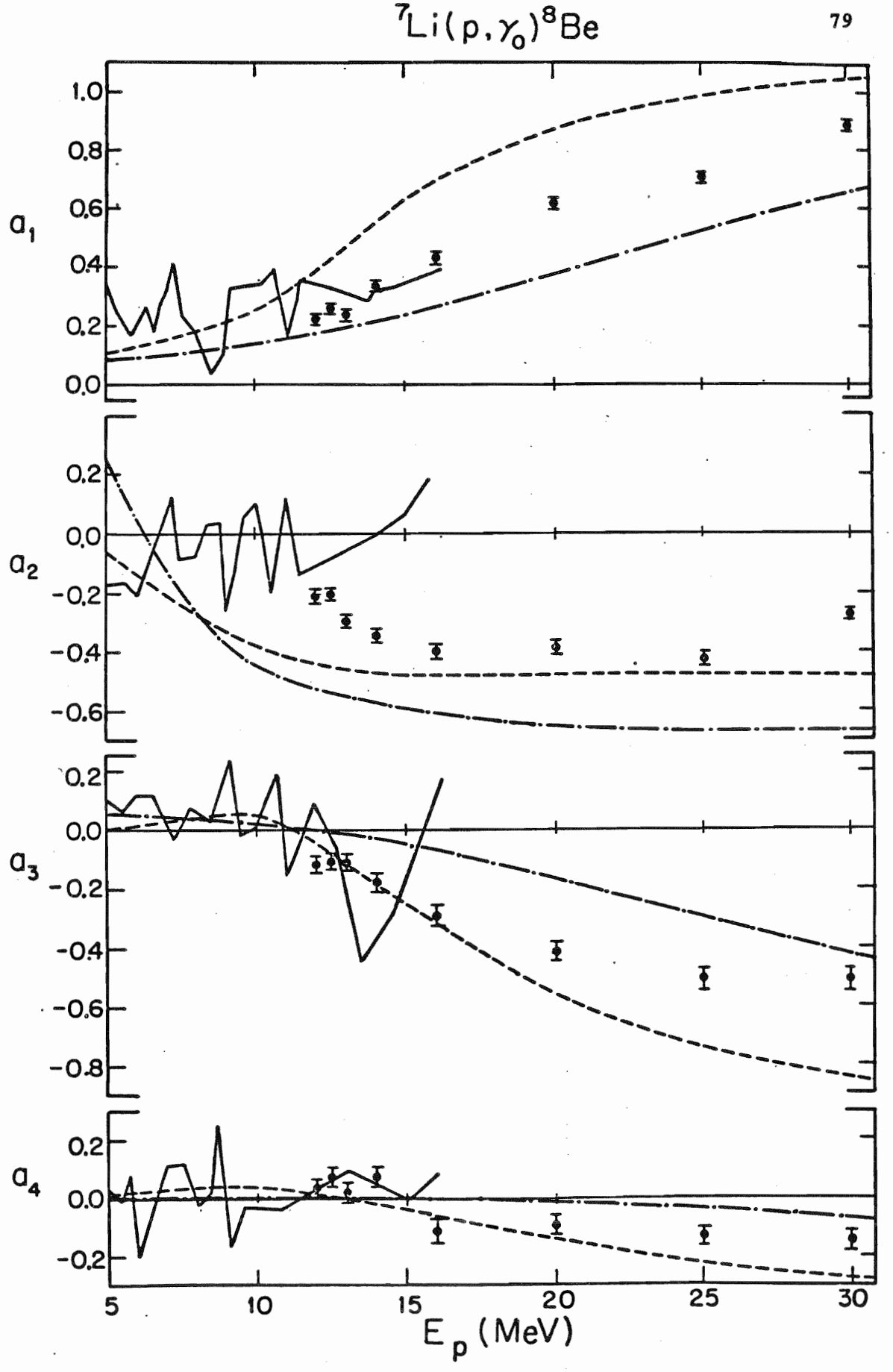
$^7Li(p,\gamma_0)^8Be$
a_1
a_2
a_3
a_4
1.0
0.8
0.6
0.4
0.2
0.0
-0.2
-0.4
-0.6
-0.8
5
10
15
20
25
30
E_p (MeV)

Table III. $^{7}Li(p,\gamma_0)$ a_k Coefficients

E_p	a_1	a_2	a_3	a_4	χ^2
12.0	0.229±.013	-0.217±.019	-0.117±.025	0.036±.031	1.28
12.5	0.260±.014	-0.211±.020	-0.107±.026	0.073±.033	2.73
13.0	0.241±.014	-0.302±.019	-0.111±.027	0.021±.032	2.74
14.0	0.337±.015	-0.350±.022	-0.177±.030	0.075±.036	1.72
16.0	0.434±.017	-0.403±.025	-0.291±.035	-0.109±.043	4.12
20.0	0.624±.012	-0.385±.019	-0.413±.028	-0.091±.030	3.22
25.0	0.711±.014	-0.423±.022	-0.505±.033	-0.130±.034	19.10
30.0	0.893±.014	-0.274±.025	-0.512±.035	-0.144±.033	4.33

however, less agreement in a_2. The Stanford data report a nearly constant a_2 with an average value of about −0.05 up to 16 MeV. The TUNL data clearly show a negatively increasing a_2 of −0.2 to −0.4.

The analyzing power data for $^7Li(p,\gamma_0)$ are shown in Fig.22 along with the results of the fits to the associated Legendre polynomials. The values of b_k obtained from the fits are shown in Table IV. The fits were of good quality as indicated by the low values of χ^2.

The angular distributions of cross section for $^7Li(p,\gamma_1)$ are shown in Fig.23, along with the Legendre polynomial fits. The a_k's extracted are shown in Fig.24 and listed in Table V. The dashed curve and the dotted-and-dashed curve are again the result of direct capture calculations. The error bars on the data are statistical only, and the variances in χ^2 indicate that in some cases the error bars should have been somewhat larger. Note that at E_p=25 MeV, χ^2 is large, as was true for the γ_0 case. The a_k's, however, show a fairly smooth energy dependence.

Fisher *et al.* (1976) at Stanford have also measured a_k's from 2–16 MeV, and in the region of overlap (12–16 MeV), there is quite good agreement with the TUNL data. The solid curves in the figure are a smoothed representation of their results.

The analyzing power angular distributions for $^7Li(p,\gamma_1)$ along with the associated Legendre polynomial fits are shown in Fig.25, and the b_k's obtained are listed in Table VI. The fits appear to be of good quality and the b_k's obtained are all quite small.

Figure 22. Analyzing power angular distributions for $^{7}Li(p,\gamma_0)$. The error bars represent the statistical errors. The solid curves are the result of the associated Legendre polynomial fits. The dashed and dotted-and-dashed curves are the result of direct capture calculations which are discussed in Chapter 5, Section D.

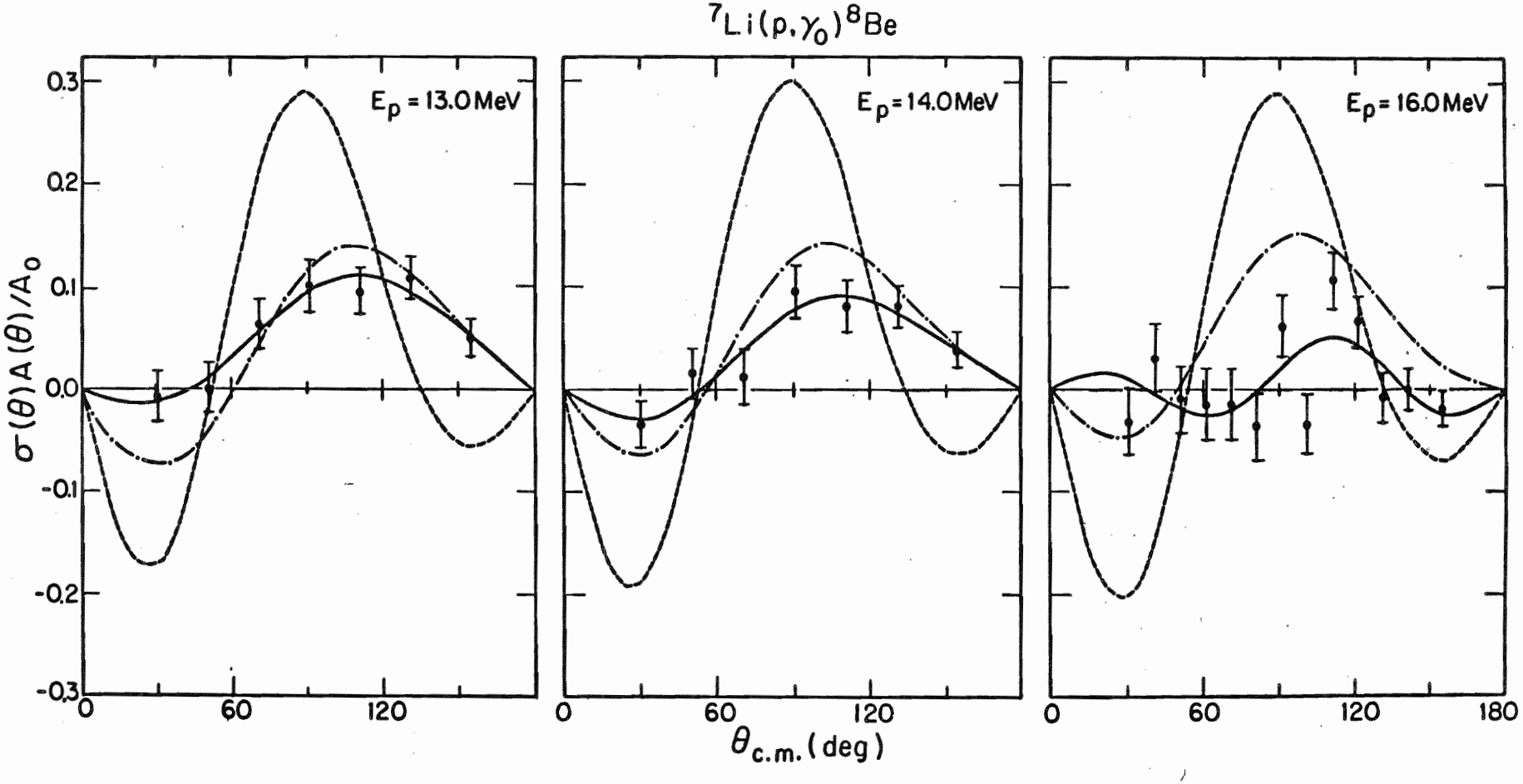
$^7Li(p,\gamma_0)^8Be$
E_p = 13.0 MeV
E_p = 14.0 MeV
E_p = 16.0 MeV
$\sigma(\theta)A(\theta)/A_0$
$\theta_{c.m.}$ (deg)
0.3
0.2
0.1
0.0
-0.1
-0.2
-0.3
0
60
120
180

Table IV. $^{7}Li(p,\gamma_0)$ b_k Coefficients

E_p	b_1	b_2	b_3	b_4	χ^2
13.0	0.082±.011	−0.029±.008	−0.008±.006	0.000±.005	0.41
14.0	0.061±.012	−0.029±.008	−0.011±.006	0.000±.005	0.85
16.0	0.012±.011	−0.014±.007	−0.005±.006	0.013±.005	2.22

Figure 23. Cross section angular distributions for $^{7}Li(p,\gamma_1)$. The error bars represent the statistical errors associated with the data points. The solid curves are the result of the Legendre polynomial fits.

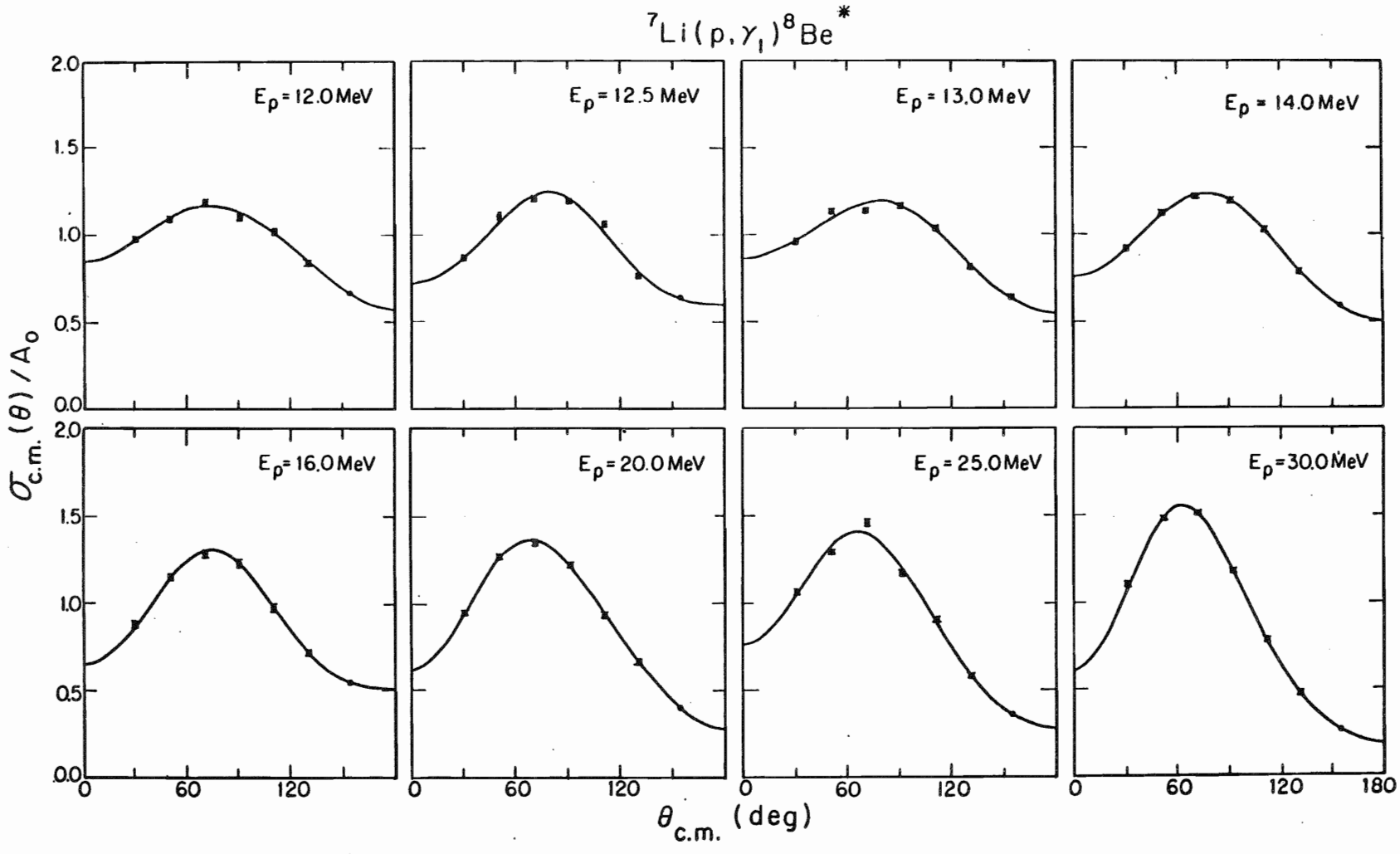
$^{7}Li(p,\gamma_1)^{8}Be^{*}$
E_p = 12.0 MeV
E_p = 12.5 MeV
E_p = 13.0 MeV
E_p = 14.0 MeV
E_p = 16.0 MeV
E_p = 20.0 MeV
E_p = 25.0 MeV
E_p = 30.0 MeV
$\sigma_{c.m.}(\theta) / A_o$
$\theta_{c.m.}$ (deg)
0.0
0.5
1.0
1.5
2.0
0
60
120
180

Figure 24. a_k coefficients from the Legendre polynomial fits for $^7Li(p,\gamma_1)$. The error bars represent the statistical errors. The dashed and dotted-and-dashed curves are the result of the direct capture calculations which are discussed in Chapter 5, Section D.

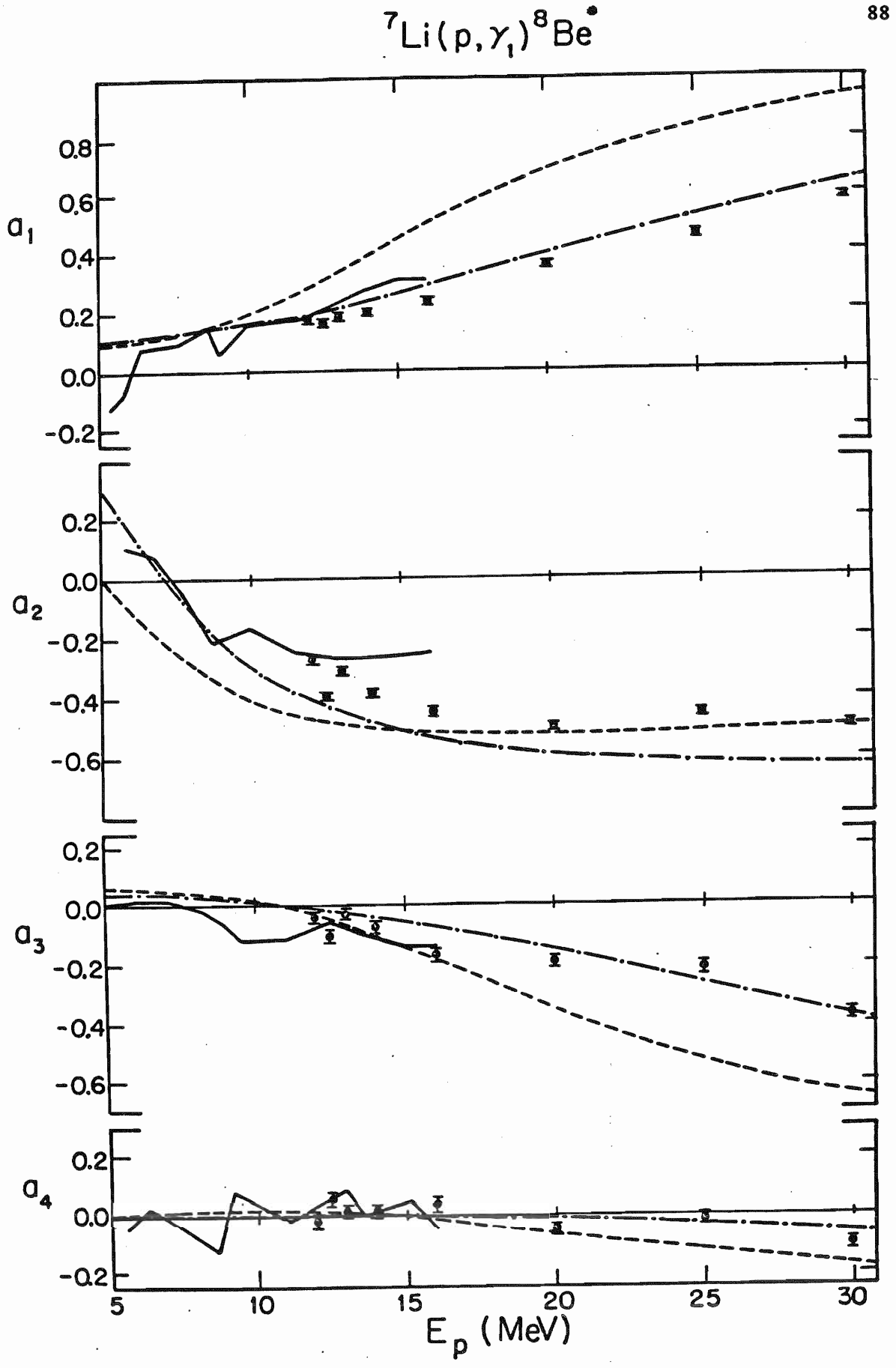
$^7Li(p,\gamma_1)^8Be^*$
a_1
a_2
a_3
a_4
0.8
0.6
0.4
0.2
0.0
-0.2
-0.4
-0.6
5
10
15
20
25
30
E_p (MeV)

Table V. $^{7}Li(p,\gamma_1)$ a_k Coefficients

E_p	a_1	a_2	a_3	a_4	χ^2
12.0	0.173±.008	-0.274±.012	-0.041±.016	-0.021±.020	2.68
12.5	0.165±.008	-0.395±.012	-0.104±.016	0.053±.020	10.91
13.0	0.183±.008	-0.312±.011	-0.031±.016	0.013±.019	7.91
14.0	0.201±.009	-0.384±.012	-0.074±.017	0.012±.022	0.74
16.0	0.238±.009	-0.449±.014	-0.169±.019	0.034±.024	0.21
20.0	0.358±.006	-0.500±.008	-0.193±.012	-0.052±.014	1.24
25.0	0.458±.007	-0.459±.011	-0.217±.016	-0.022±.017	16.50
30.0	0.588±.006	-0.504±.010	-0.377±.015	-0.099±.015	0.30

Figure 25. Analyzing power angular distributions for $^{7}Li(p,\gamma_1)$. The error bars represent the statistical errors. The solid curves are the result of the associated Legendre polynomial fits. The dashed and dotted-and-dashed curves are the result of the direct capture calculations which are discussed in Chapter 5, Section D.

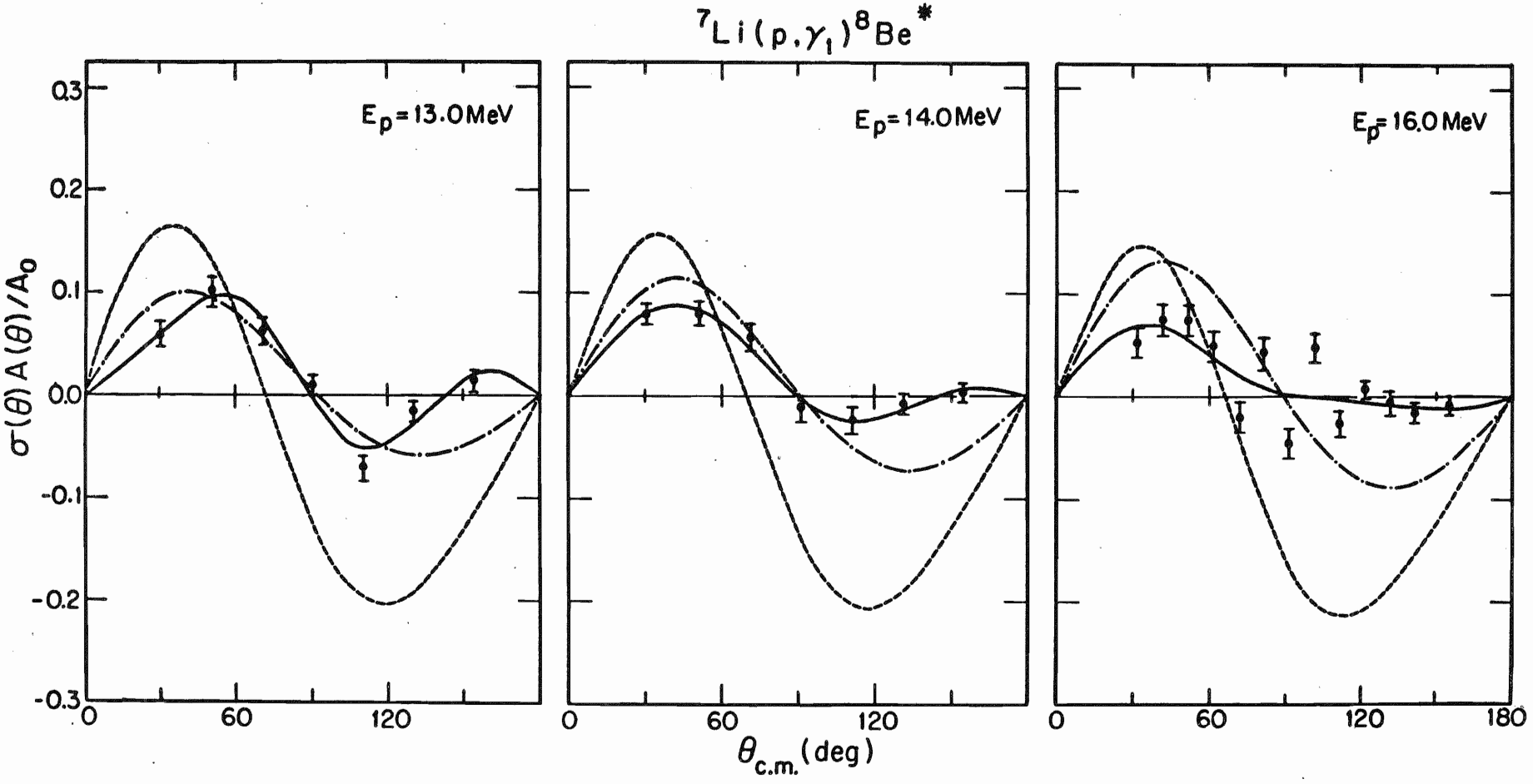
$^{7}Li(p,\gamma_1)^{8}Be^{*}$
E_p=13.0MeV
E_p=14.0MeV
E_p=16.0MeV
$\sigma(\theta)A(\theta)/A_0$
$\theta_{c.m.}$(deg)
0.3
0.2
0.1
0.0
-0.1
-0.2
-0.3
0
60
120
180

Table VI. $^{7}Li(p,\gamma_1)$ b_k Coefficients

E_p	b_1	b_2	b_3	b_4	χ^2
13.0	0.021±.006	0.041±.004	0.013±.003	−0.013±.003	2.50
14.0	0.023±.006	0.033±.004	0.015±.003	−0.002±.003	0.57
16.0	0.018±.005	0.021±.003	0.010±.003	0.005±.002	4.67

Chapter 5 Direct and Semidirect Calculations

A. Introduction

The details and results of our direct and semidirect model calculations are discussed in this chapter. This section gives a brief introduction to the direct and direct-semidirect capture models and discusses the applicabilty of these models.

The direct capture model has been discussed extensively in the literature (see, for example, Lane (1959)). In this model, an incident nucleon moves in the potential of the target nucleus and then radiates a photon while falling directly into the final state. No intermediate, or compound nuclear, state is formed in this "one-step" process. The final state consists of a core plus single-particle state, where the single-particle is the incoming particle, in addition to the emitted (free) γ-ray. The core is identical to the target. The T-matrix element computed in actual direct calculations is written $\langle u_b | d^L | \chi \rangle$, where u_b represents the radial wave function of the captured particle in the field of the core (the final state), χ represents the wave function of the initial continuum state of the particle in the field of target, and d^L is the radial part of the electro-magnetic transition operator. where L is the multipolarity of the radiation.

Direct capture calculations have been compared with experimental capture data for various cases (Cvelbar and Whetstone, 1972, Weller and Roberson,

1980, and Rolfs, 1973). For low-energy (<2 MeV) incident nucleons, interesting work was done by Rolfs (1973), who performed calculations which assumed that the capture data could be described as contributions from compound nuclear states interfering with the smoothly varying direct capture background. In fact, one of the main characteristics of direct capture is such a smooth variance as a function of energy. The result obtained by Rolfs shows remarkable agreement between the direct capture calculations and the "background" cross sections between the low energy resonances.

At higher energies (up to 20 MeV) however, the situation changes dramatically. Here it is found that the direct cross section is often much smaller that the capture data and does not predict the observed structure in the yield curves (Brown, 1964). The data in fact show large and broad resonant effects, which have been successfully described as giant multipole resonances. In particular, the giant dipole resonance (GDR) is seen in most capture reactions leading to the ground state and occurs at an excitation energy in the compound nucleus of about $80/A^{1/3}$ MeV in heavy nuclei and about 20 MeV in light nuclei (Hayward, 1970). In the region of the GDR, the cross sections calculated for direct E1 capture are typically a factor of about 5-10 less than the data. At energies above the resonance, direct capture should again describe the general trend of the data.

Since the early capture work showed that a direct-only capture model was unable to predict the capture data in the region of the GDR, the semidirect model (Brown, 1964, and Clement et al., 1965) was suggested to describe the effects of the GDR and has since been expanded to allow for the possibility of other giant resonances.

In the semidirect model, a nucleon is incident upon a target nucleus, which is able to oscillate in various collective modes. The particle is then

inelastically scattered (or "captured") into a bound single-particle state, simultaneously exciting a collective oscillation in the nucleus (typically the GDR). This collective state can then decay either by re-emission of the incident nucleon (which accounts for almost all of the decay width) or by γ-ray decay (which is enhanced due to the collective nature of the compound state). The model, then, is designed to calculate the cross section for the capture process, with a nucleon entering the nucleus and a γ-ray emitted from the collective state. The term "semidirect" arises from the fact that, although the lifetime of collective excitation, as determined from the width according to h/Γ, is much larger than the time for a direct process, it is much less than that of a typical compound nuclear state. This short lifetime implies that the decay process occurs, with emission of a γ-ray, before the excitation can mix into the surrounding compound nuclear states (Brown, 1964).

Actual capture calculations first compute T-matrix elements, and in the direct-semidirect (DSD) model, the semidirect term is added to the direct capture matrix element. The DSD matrix element is thus given by:

$$\langle u_b | d^L | \chi \rangle + \frac{1}{E-E_R+i\Gamma/2} \langle u_b | h^L(r) | \chi \rangle,$$

where E_R and Γ give the resonance energy and width (determined generally by experiment) of the giant resonance to be calculated. The form factor, denoted by $h^L(r)$, is the radial part of the nucleon-nucleus interaction which excites the collective excitation (Weller and Roberson, 1980). Various expressions have been suggested for this form factor (Brown, 1964, Clement et al., 1965, and Potokar, 1973).

B. Direct Capture Model Calculations

Since the purpose of this disertation is to investigate the existence of giant resonances built on highly excited states, the experimental data will be first compared with direct capture calculations. Any discrepancies in this comparison should indicate the need for including the semidirect (collective) term in the calculations.

Direct calculations have been performed in this investigation using the fortran code RADCAP (Cotanch, 1978). (The actual code used was a version modified by Mitev (1980) to include the exact electromagnetic transition operator). The details of the theory used in the code, the parameters used, and the conversion of the results of the code to cross sections are described in the following paragraphs.

The incident channel (proton plus ^{7}Li target in this case) was described in the program by the wave function (χ) of an continuum proton moving in the optical potential of ^{7}Li. The potential used (listed in Table VII) was the global energy-dependant fit to (p,p) data for light nuclei (A<17) obtained by Watson *et al.* (1969). This global potential does not necessarily give the "best fit" to the scattering data for ^{7}Li at every energy, but since our direct capture calculations need to be valid for 3 to 30 MeV incident protons, it was desirable to use a slowly-varying (with energy) optical potential. This potential does provide a reasonable fit to the available (p,p) data, although the published data for ^{7}Li(p,p) is scanty. Therefore, the optical potential used was believed to be reasonable, but the parameters should be considered somewhat uncertain (or adjustable).

The final state in the capture process is generally assumed to be a bound state, although calculations can be made for capture reactions in which

Table VII. Watson Optical Potential

$$V_R = 60.0 + 0.4(Z/A^{1/3}) + 27.0[(N-Z)/A] - 0.3E_{cm}$$

$$V_{so} = 5.5$$

$$r_R = r_I = r_{so} = r_c = 1.15 - 0.001E_{cm}$$

$$a_R = a_{so} = 0.57, \quad a_I = 0.5$$

$$W_s = W_s(E) + 10.0(N-Z)/A$$

where: $W_s(E) = 0.64E_{cm}$ for $E_{cm} < 13.8$ MeV

$9.60 \text{ MeV} - 0.06E_{cm}$ for $E_{cm} \geq 13.8$ MeV

$$W_V = 0.0$$

the final state is a continuum state (Halderson and Philpott, 1981). The bound final state in our calculation was described by the wave function (u_b) for a bound proton in a Woods-Saxon well. The shape parameters (r,a) used for the real and spin-orbit wells were obtained from Watson's potential, but the real potential strength, V_0, was adjusted by the program to give the experimental binding energy of the single-particle.

The electromagnetic operators, d^L, used in the calculations were exact (not the long-wavelength approximation) and are given by:

$$d^L = \frac{(2L+1)!!}{(L+1)k_\gamma^L}\left\{j_L(k_\gamma r) - k_\gamma r \cdot j_{L+1}(k_\gamma r)\right\}$$

(Eisenberg and Greiner, 1970). In the long-wavelength approximation, $kr \ll 1$, the EL operator is simply given by "r^L".

After calculation of the wave functions as a function of r, the radial matrix element $\langle u_b | d^L | \chi \rangle$ was calculated by numerical integration. The integration was done from r=0 to r=40 fm, with a step size of 0.15 fm. At 40 fm the bound state wave function has become sufficiently small to be neglected.

The following notation was used for the calculations. The capture reaction is denoted by a(x,γ)c, where a is the total angular momentum of the target nucleus, x is the spin of the incident particle, and c is the total angular momentum of the final state. In addition, b denotes the spin of the γ-emitting (intermediate) state. Other definitions that will be used are L, which is the multipolarity of the γ radiation, ℓ_a and j_a, which are, respectively, the orbital and total angular momentum of the particle in the incident channel, and ℓ and j, which are, respectively, the orbital and total angular momentum of the single-particle in the final state. I_c is defined as the Clebsch-Gordan coefficient connecting the isospins:
$I_c = C(T_a T_{az}, 1/2\ t_z | T_c T_{cz})$, where T_a, T_{az} are the total isospin and z-projection

for the target a, T_c, T_{cz} are the total isospin and z-projection for the final state c, and t_z is the z-projection of the isospin for the incident nucleon.

In our calculations as performed by RADCAP, the target spin is assumed to be zero, and therefore the final state angular momentum c is just the single particle angular momentum j. The T-matrix elements for target spin zero are calculated from the radial matrix elements from RADCAP according to:

$$T_G = i^{\ell_a - \ell - L} C(j\ 1/2\ L\ 0, j_a\ 1/2) \left(\frac{CNORM}{2j_a+1}\right)^{1/2} e_L \langle u_b | d^L | \chi \rangle,$$

where e_L is the recoil effective charge for the given multipolarity (Hayward,1970). The effective charge for electric multipoles is given in general as $e_L = (A_2^L Z_1 + (-1)^L Z_2 A_1^L)/(A_1+A_2)^L$ (Buck and Pilt, 1977), where 1 refers to the projectile and 2 refers to the target. The factor CNORM is calculated by RADCAP and is defined as: $4\pi \cdot \frac{197.3289}{137.036} \cdot \frac{k_\nu}{E_a k_a} \cdot \frac{2j+1}{2x+1} \cdot B_L^2$, where $B_L^2 = \frac{L+1}{(2L+1)L} \frac{k_f^{2L}}{((2L-1)!!)^2}$.

For the equations for a_k, b_k, and σ_T which follow we have assumed that the capture process depends on the core only in providing the average potential and on the final state parentage to the target core plus a single nucleon. Therefore, the true equations (target spin a) are simple factors times the target spin zero equations. It is possible, then, to write the target spin "a" total cross section in terms of the T-matrix elements for target spin zero (T_G) as: $\sigma_T = 4\pi A_0 = \sum_j I_c^2 S_j \cdot \frac{\hat{c}^2}{\hat{a}^2 \hat{j}^2} \sum_{j_a} \hat{j}_a^2 |T_G|^2$, where $\hat{x} = (2x+1)^{1/2}$ and a and c are the true target and final state spins. S_j is the spectroscopic factor describing the final single-particle state. The a_k and b_k coefficients for target spin a are calculated from:

$$a_k = \frac{\sum_j I_c^2 S_j \frac{1}{\hat{j}^2} \bar{A}_k}{\sum_j I_c^2 S_j \frac{1}{\hat{j}^2} \sum_{j_a} \frac{\hat{j}^2}{\hat{c}^2} |T_G|^2}$$

and

$$b_k = \frac{\sum_j I_c^2 S_j \frac{1}{\hat{j}^2} \bar{B}_k}{\sum_j I_c^2 S_j \frac{1}{\hat{j}^2} \sum_{j_a} \frac{\hat{j}^2}{\hat{x}^2} |T_G|^2} .$$

In the j-j coupling scheme (used in this thesis), where $\ell_a + s = j_a$ and $j_a + a = b$, $\bar{A}_k$ and $\bar{B}_k$ are calculated from $T_G(\ell_a, j_a)$ using the expressions:

$$\bar{A}_k = \sum_{tt'} (-1)^{a-c+1-x+k+j-j'} \hat{j}\,\hat{j}'\hat{\ell}\,\hat{\ell}'\hat{L}\,\hat{L}'\hat{b}^2 2^{\hat{}},2$$

$$C(\ell\ 0\ \ell'0,k\ 0) \cdot W(\ell\ j\ \ell' j', x\ k) \cdot [\ ] \cdot C(L\ 1\ L'-1,k\ 0) \cdot W(j\ b\ j'b', a\ k)$$

$$W(L\ b\ L'b', c\ k) \cdot \mathrm{Re}(T_G T'^{*}_G)$$

and

$$\bar{B}_k = \frac{3\sqrt{x}\,\hat{x}\hat{k}}{[(x+1)k(k+1)]}$$

$$\sum (-1)^{a-c+1+\ell'-j'} \hat{j}\,\hat{j}'\hat{\ell}\,\hat{\ell}'\hat{L}\,\hat{L}'\hat{b}^2 2^{\hat{}},2$$

$$C(\ell\ 0\ \ell'0,k\ 0) \cdot [\ ] \cdot C(L\ 1\ L'-1,k\ 0) \cdot W(j\ b\ j'b', a\ k) \cdot W(L\ b\ L'b', c\ k)$$

$$X(\ell\ x\ j, \ell' x\ j', k\ 1\ k) \cdot \mathrm{Re}(iT_G T'^{*}_G),$$

where $[\ ] = \frac{1}{2}[1+(-1)^{L+p+L'+p'+k}]$, and p equals the mode of the γ radiation (ie, p=1 for electric, p=0 for magnetic). (See Weller and Roberson (1980) for more discussion). The sum over t and t' means over $pp'LL'bb'\ell\ell'j$ and j'. It should be noted that since the T_G are the target spin zero matrix elements, $\bar{A}_k$ and $\bar{B}_k$ must also be calculated using a=0 and c=j.

C. Comparison with $^{7}Li(p,\gamma_{16})$ Data

A direct capture calculation, as described in the previous section, has been performed for the reaction $^{7}Li(p,\gamma_{16})$ for comparison with the experimental data. The target in this case is ^{7}Li, which has $J^{\pi}=3/2^{-}$, the incident particle is a proton, and the final states are the two 2^{+} isospin-mixed levels in ^{8}Be. As discussed earlier in this thesis, the reported values (Sweeney and Marion, 1969) for the proton spectroscopic factors for these states are S=0.470 for the 16.63 MeV level and S=0.010 for the 16.92 MeV level. These values are consistent with experimental evidence which indicates that the 16.63 MeV state is predominantly a single proton plus ^{7}Li core, while the 16.92 MeV state is predominantly a single neutron plus ^{8}Be core (Marion and Wilson, 1966). Thus, the 16.92 MeV state should not be excited in the direct capture process, since the direct cross section is directly proportional to S. The very small effect of this state has therefore been neglected in our calculations. The 16.63 MeV state is a mixture of T=0 and T=1 isospin and $p_{1/2}$ and $p_{3/2}$ single-particle states. Using the equations given by Marion and co-workers, we have calculated the separate spectroscopic factors for the $p_{3/2}$ and $p_{1/2}$ states. Equation 19 in Marion *et al.* (1967) gives: $|16.63\rangle=0.772|T=0\rangle + 0.636|T=1\rangle$, and from Table III in Sweeney and Marion (1969) we have the coefficients of fractional parentage (cfp_{j}) for j=1/2 or 3/2, and T=0 or T=1. Therefore,

$$cfp_{3/2}=0.772(0.4316)+0.636(0.4864)=0.6425, \text{ and}$$

$$cfp_{1/2}=0.772(0.2003)+0.636(0.1319)=0.2385.$$

The spectroscopic factors used in our direct capture calculations are given by $S=n\cdot cfp^{2}$, where n is the number of available nucleons. In ^{8}Be, n is 4, so we have finally, $S_{1/2}=0.228$ and $S_{3/2}=1.651$. These values were compared with the

calculations of Cohen and Kurath (1967), and it was seen that the cfp's were in quite good agreement. These values of S therefore seem reliable, but may be subject to some uncertainty, since they have not been determined experimentally.

For the target spin zero calculation as performed by RADCAP, the reaction is described as a $1/2^+$ projectile incident upon a 0^+ core, going to a final state which is partly $p_{3/2}$ $(3/2^-)$ and partly $p_{1/2}$ $(1/2^-)$. For our calculation, direct capture involving both E1 and E2 radiation has been considered. The allowed E1 and E2 capture matrix elements can be determined by examining the angular momentum and parity changes. Since we used the j-j coupling scheme, the contributing matrix elements can be labeled by the ℓ_a and j_a for the projectile and by the multipolarity of the outgoing radiation (L). The notation used for the amplitude of the matrix element was $\ell_{a_j}(L)$ and the phase $\phi_{\ell_{a_{j_a}}}$. Since E1 radiation has J=1 and must change the parity, the appropriate E1 capture matrix elements are: $s_{1/2}$, $d_{3/2}$, and $d_{5/2}$ for the $p_{3/2}$ component of the final state, and $s_{1/2}$ and $d_{3/2}$ for the $p_{1/2}$ component. Since E2 radiation has J=2 and must not change the parity, the E2 capture matrix elements are: $p_{1/2}$, $p_{3/2}$, $f_{5/2}$, and $f_{7/2}$ for the $p_{3/2}$ component, and $p_{3/2}$ and $f_{5/2}$ for the $p_{1/2}$ component.

The equations for $\bar{A}_k$ and $\bar{B}_k$ obtained are then, for the $p_{3/2}$ component (assuming only E1 and E2 radiation):

$$\begin{aligned}
\bar{A}_1 = {} & 1.732\ s_{1/2}(E1)p_{1/2}(E2)\cos(\phi_{p_{1/2}} - \phi_{s_{1/2}}) \\
& + 2.449\ s_{1/2}(E1)p_{3/2}(E2)\cos(\phi_{p_{3/2}} - \phi_{s_{1/2}}) \\
& - 1.095\ d_{3/2}(E1)p_{1/2}(E2)\cos(\phi_{p_{1/2}} - \phi_{d_{3/2}}) \\
& + 1.239\ d_{3/2}(E1)p_{3/2}(E2)\cos(\phi_{p_{3/2}} - \phi_{d_{3/2}}) \\
& + 5.217\ d_{3/2}(E1)f_{5/2}(E2)\cos(\phi_{f_{5/2}} - \phi_{d_{3/2}}) \\
& - 1.138\ d_{5/2}(E1)p_{3/2}(E2)\cos(\phi_{p_{3/2}} - \phi_{d_{5/2}})
\end{aligned}$$

$$+ 0.9128\ d_{5/2}(E1)f_{5/2}(E2)\cos(\phi_{f_{5/2}} - \phi_{d_{5/2}})$$
$$+ 8.606\ d_{5/2}(E1)f_{7/2}(E2)\cos(\phi_{f_{7/2}} - \phi_{d_{5/2}})$$

$$\bar{A}_2 = 0.6325\ s_{1/2}(E1)d_{3/2}(E1)\cos(\phi_{d_{3/2}} - \phi_{s_{1/2}})$$
$$+ 2.324\ s_{1/2}(E1)d_{5/2}(E1)\cos(\phi_{d_{5/2}} - \phi_{s_{1/2}})$$
$$+ 0.800\ d^2_{3/2}(E1)$$
$$- 1.470\ d_{3/2}(E1)d_{5/2}(E1)\cos(\phi_{d_{5/2}} - \phi_{d_{3/2}})$$
$$- 1.200\ d^2_{5/2}(E1)$$
$$- 1.134\ p_{1/2}(E2)f_{5/2}(E2)\cos(\phi_{f_{5/2}} - \phi_{p_{1/2}})$$
$$+ 1.145\ p_{3/2}(E2)f_{5/2}(E2)\cos(\phi_{f_{5/2}} - \phi_{p_{3/2}})$$
$$- 1.296\ p_{3/2}(E2)f_{7/2}(E2)\cos(\phi_{f_{7/2}} - \phi_{p_{3/2}})$$
$$+ 0.6122\ f^2_{5/2}(E2)$$
$$+ 1.039\ f_{5/2}(E2)f_{7/2}(E2)\cos(\phi_{f_{7/2}} - \phi_{f_{5/2}})$$
$$+ 2.041\ f^2_{7/2}(E2)$$

$$\bar{A}_3 = 1.309\ s_{1/2}(E1)f_{5/2}(E2)\cos(\phi_{f_{5/2}} - \phi_{s_{1/2}})$$
$$+ 3.703\ s_{1/2}(E1)f_{7/2}(E2)\cos(\phi_{f_{7/2}} - \phi_{s_{1/2}})$$
$$+ 1.859\ d_{3/2}(E1)p_{3/2}(E2)\cos(\phi_{p_{3/2}} - \phi_{d_{3/2}})$$
$$+ 2.650\ d_{3/2}(E1)f_{5/2}(E2)\cos(\phi_{f_{5/2}} - \phi_{d_{3/2}})$$
$$- 2.342\ d_{3/2}(E1)f_{7/2}(E2)\cos(\phi_{f_{7/2}} - \phi_{d_{3/2}})$$
$$+ 2.683\ d_{5/2}(E1)p_{1/2}(E2)\cos(\phi_{p_{1/2}} - \phi_{d_{5/2}})$$
$$+ 3.036\ d_{5/2}(E1)p_{3/2}(E2)\cos(\phi_{p_{3/2}} - \phi_{d_{5/2}})$$
$$- 2.434\ d_{5/2}(E1)f_{5/2}(E2)\cos(\phi_{f_{5/2}} - \phi_{d_{5/2}})$$
$$- 2.869\ d_{5/2}(E1)f_{7/2}(E2)\cos(\phi_{f_{7/2}} - \phi_{d_{5/2}})$$

$$\bar{A}_4 = 4.276\ p_{1/2}(E2)f_{7/2}(E2)\cos(\phi_{f_{7/2}} - \phi_{p_{1/2}})$$
$$+ 3.665\ p_{3/2}(E2)f_{5/2}(E2)\cos(\phi_{f_{5/2}} - \phi_{p_{3/2}})$$

$$+ 4.320\ p_{3/2}(E2)f_{7/2}(E2)\cos(\phi_{f_{7/2}} - \phi_{p_{3/2}})$$
$$+ 1.959\ f^2_{5/2}(E2)$$
$$- 3.463\ f_{5/2}(E2)f_{7/2}(E2)\cos(\phi_{f_{7/2}} - \phi_{f_{5/2}})$$
$$- 1.469\ f^2_{7/2}(E2)$$

$$\bar{B}_1 = 1.732\ s_{1/2}(E1)p_{1/2}(E2)\sin(\phi_{p_{1/2}} - \phi_{s_{1/2}})$$
$$- 1.225\ s_{1/2}(E1)p_{3/2}(E2)\sin(\phi_{p_{3/2}} - \phi_{s_{1/2}})$$
$$+ 0.5477\ d_{3/2}(E1)p_{1/2}(E2)\sin(\phi_{p_{1/2}} - \phi_{d_{3/2}})$$
$$- 2.479\ d_{3/2}(E1)p_{3/2}(E2)\sin(\phi_{p_{3/2}} - \phi_{d_{3/2}})$$
$$+ 2.608\ d_{3/2}(E1)f_{5/2}(E2)\sin(\phi_{f_{5/2}} - \phi_{d_{3/2}})$$
$$- 0.5692\ d_{5/2}(E1)p_{3/2}(E2)\sin(\phi_{p_{3/2}} - \phi_{d_{5/2}})$$
$$+ 2.738\ d_{5/2}(E1)f_{5/2}(E2)\sin(\phi_{f_{5/2}} - \phi_{d_{5/2}})$$
$$- 4.303\ d_{5/2}(E1)f_{7/2}(E2)\sin(\phi_{f_{7/2}} - \phi_{d_{5/2}})$$

$$\bar{B}_2 = 0.3162\ s_{1/2}(E1)d_{3/2}(E1)\sin(\phi_{d_{3/2}} - \phi_{s_{1/2}})$$
$$- 0.7746\ s_{1/2}(E1)d_{5/2}(E1)\sin(\phi_{d_{5/2}} - \phi_{s_{1/2}})$$
$$+ 1.225\ d_{3/2}(E1)d_{5/2}(E1)\sin(\phi_{d_{5/2}} - \phi_{d_{3/2}})$$
$$- 0.7071\ p_{1/2}(E2)p_{3/2}(E2)\sin(\phi_{p_{3/2}} - \phi_{p_{1/2}})$$
$$- 0.3780\ p_{1/2}(E2)f_{5/2}(E2)\sin(\phi_{f_{5/2}} - \phi_{p_{1/2}})$$
$$+ 0.9545\ p_{3/2}(E2)f_{5/2}(E2)\sin(\phi_{f_{5/2}} - \phi_{p_{3/2}})$$
$$+ 0.4320\ p_{3/2}(E2)f_{7/2}(E2)\sin(\phi_{f_{7/2}} - \phi_{p_{3/2}})$$
$$- 1.212\ f_{5/2}(E2)f_{7/2}(E2)\sin(\phi_{f_{7/2}} - \phi_{f_{5/2}})$$

$$\bar{B}_3 = 0.4364\ s_{1/2}(E1)f_{5/2}(E2)\sin(\phi_{f_{5/2}} - \phi_{s_{1/2}})$$
$$- 0.9258\ s_{1/2}(E1)f_{7/2}(E2)\sin(\phi_{f_{7/2}} - \phi_{s_{1/2}})$$
$$- 0.6197\ d_{3/2}(E1)p_{3/2}(E2)\sin(\phi_{p_{3/2}} - \phi_{d_{3/2}})$$
$$+ 0.2208\ d_{3/2}(E1)f_{5/2}(E2)\sin(\phi_{f_{5/2}} - \phi_{d_{3/2}})$$

$$+ 1.171\ d_{3/2}(E1)f_{7/2}(E2)\sin(\phi_{f_{7/2}} - \phi_{d_{3/2}})$$
$$+ 0.8944\ d_{5/2}(E1)p_{1/2}(E2)\sin(\phi_{p_{1/2}} - \phi_{d_{5/2}})$$
$$+ 0.2530\ d_{5/2}(E1)p_{3/2}(E2)\sin(\phi_{p_{3/2}} - \phi_{d_{5/2}})$$
$$- 1.217\ d_{5/2}(E1)f_{5/2}(E2)\sin(\phi_{f_{5/2}} - \phi_{d_{5/2}})$$
$$+ 0.2390\ f_{5/2}(E2)f_{7/2}(E2)\sin(\phi_{f_{7/2}} - \phi_{f_{5/2}})$$

$$\bar{B}_4 = - 1.069\ p_{1/2}(E2)f_{7/2}(E2)\sin(\phi_{f_{7/2}} - \phi_{p_{1/2}})$$
$$+ 0.9163\ p_{3/2}(E2)f_{5/2}(E2)\sin(\phi_{f_{5/2}} - \phi_{p_{3/2}})$$
$$- 0.4320\ p_{3/2}(E2)f_{7/2}(E2)\sin(\phi_{f_{7/2}} - \phi_{p_{3/2}})$$
$$+ 1.212\ f_{5/2}(E2)f_{7/2}(E2)\sin(\phi_{f_{7/2}} - \phi_{f_{5/2}})$$

For the $p_{1/2}$ component:

$$\bar{A}_1 = 3.464\ s_{1/2}(E1)p_{3/2}(E2)\cos(\phi_{p_{3/2}} - \phi_{s_{1/2}})$$
$$+ 0.6928\ d_{3/2}(E1)p_{3/2}(E2)\cos(\phi_{p_{3/2}} - \phi_{d_{3/2}})$$
$$+ 6.235\ d_{3/2}(E1)f_{5/2}(E2)\cos(\phi_{f_{5/2}} - \phi_{d_{3/2}})$$

$$\bar{A}_2 = - 2.000\ s_{1/2}(E1)d_{3/2}(E1)\cos(\phi_{d_{3/2}} - \phi_{s_{1/2}})$$
$$- 1.000\ d^2_{3/2}(E1)$$
$$+ 1.000\ p^2_{3/2}(E2)$$
$$+ 0.8571\ p_{3/2}(E2)f_{5/2}(E2)\cos(\phi_{f_{5/2}} - \phi_{p_{3/2}})$$
$$+ 1.714\ f^2_{5/2}(E2)$$

$$\bar{A}_3 = - 3.464\ s_{1/2}(E1)f_{5/2}(E2)\cos(\phi_{f_{5/2}} - \phi_{s_{1/2}})$$
$$- 4.157\ d_{3/2}(E1)p_{3/2}(E2)\cos(\phi_{d_{3/2}} - \phi_{p_{3/2}})$$
$$- 2.771\ d_{3/2}(E1)f_{5/2}(E2)\cos(\phi_{f_{5/2}} - \phi_{d_{3/2}})$$

$$\bar{A}_4 = -\,6.857\; p_{3/2}(E2) f_{5/2}(E2) \cos(\phi_{f_{5/2}} - \phi_{p_{3/2}}) - 1.714\; f^2_{5/2}(E2)$$

$$\bar{B}_1 = -\,1.732\; s_{1/2}(E1) p_{3/2}(E2) \sin(\phi_{p_{3/2}} - \phi_{s_{1/2}}) - 1.386\; d_{3/2}(E1) p_{3/2}(E2) \sin(\phi_{p_{3/2}} - \phi_{d_{3/2}}) + 3.118\; d_{3/2}(E1) f_{5/2}(E2) \sin(\phi_{f_{5/2}} - \phi_{d_{3/2}})$$

$$\bar{B}_2 = -\,1.000\; s_{1/2}(E1) d_{3/2}(E1) \sin(\phi_{d_{3/2}} - \phi_{s_{1/2}}) + 0.7143\; p_{3/2}(E2) f_{5/2}(E2) \sin(\phi_{f_{5/2}} - \phi_{p_{3/2}})$$

$$\bar{B}_3 = -\,1.155\; s_{1/2}(E1) f_{5/2}(E2) \sin(\phi_{f_{5/2}} - \phi_{s_{1/2}}) + 1.386\; d_{3/2}(E1) p_{3/2}(E2) \sin(\phi_{p_{3/2}} - \phi_{d_{3/2}}) - 0.2309\; d_{3/2}(E1) f_{5/2}(E2) \sin(\phi_{f_{5/2}} - \phi_{d_{3/2}})$$

$$\bar{B}_4 = -\,1.714\; p_{3/2}(E2) f_{5/2}(E2) \sin(\phi_{f_{5/2}} - \phi_{p_{3/2}})$$

It should be noted that $a_1(b_1)$ and $a_3(b_3)$ contain only E1 and E2 interference terms, while $a_2(b_2)$ contain only terms proportional to $(E1)^2$ or $(E2)^2$, and $a_4(b_4)$ contain only terms proportional to $(E2)^2$. Our analysis has neglected M1 capture.

The effective charges for ^{7}Li + p are e_1=1/2 for electric dipole radiation and e_2=0.813 for electric quadrupole radiation. In addition, the isospin Clebsch, I_c, is 1/2 for both final state isopins, T=0 and T=1.

The bound state wave function calculation for the 16.63 MeV state (binding energy 0.63 MeV) gave a well-depth, V_0, of 52.9 MeV for a $p_{3/2}$ proton about a ^{7}Li core. For a $p_{1/2}$ proton, the calculation gave V_0=64.6 MeV. These are reasonable well depths in comparison with Watson's optical model potential

(V_0 about 60 MeV).

The resulting E1-E2 direct capture calculation for $^7Li(p,\gamma_{16})$ shows quite remarkable agreement with the data. The solid curve in Fig.14 (chapt. 3), which is the result of the E1-E2 direct capture calculation, shows that there is very good agreement with the shape of the yield curve data. In particular, the position of the broad peak in the yield curve at about 8 MeV is described very well. Even more importantly, the calculation has been renormalized only by a factor of 1.27, indicating good agreement with the absolute magnitude of the data. These results are in marked contrast with measurements of nucleon capture reactions leading to ground or low-lying states. Typically for these cases, the direct calculations give absolute cross sections which are approximately an order of magnitude less than the data and often have the wrong shape as a function of energy. Two somewhat typical examples are the reactions $^7Li(p,\gamma_0)$ and $^7Li(p,\gamma_1)$, which will be discussed in some detail in Sec. D of this chapter.

Studies have been made to determine the dominant factors influencing the energy dependence of the calculated cross sections. The predominant matrix element was found to be $d_{5/2}$(E1) capture to the $p_{3/2}$ component of the bound state. This term accounted for approximately 80% of the total calculated cross section, and it has been analyzed as a function of energy. Shown in Fig.26 is the calculated total $d_{5/2}$ capture cross section as a function of energy. A possible explanation for the initial rise in the capture cross section is that the coulomb barrier is being crossed. The energy of the coulomb barrier is defined as: $E_c = \frac{1}{4\pi\varepsilon_o} zZe^2/R$, where R is the nuclear radius (given by $r_0A^{1/3}$), z·e is the projectile charge, and Z·e is the target charge. For protons on ^7Li, E_c=4.6 MeV, corresponding closely with the rise in the capture cross section. A more detailed study can be made by examining the

Figure 26. Calculated $d_{5/2}$(E1) direct capture cross sections for $^{7}Li(p,\gamma_{16})$.

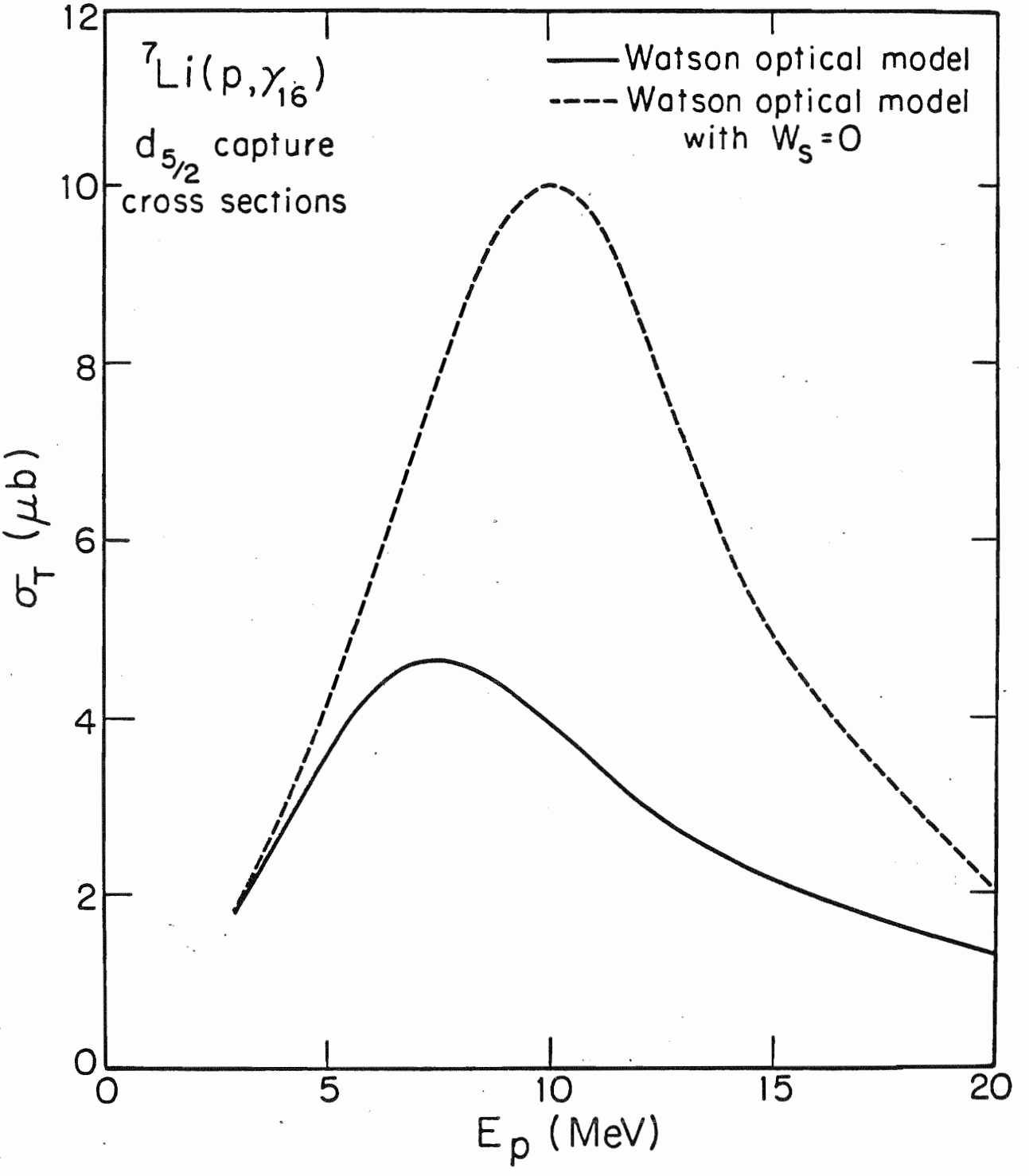
$^7Li(p,\gamma_{16})$
$d_{5/2}$ capture
cross sections
Watson optical model
Watson optical model
with $W_s=0$
σ_T (μb)
E_p (MeV)
0
2
4
6
8
10
12
0
5
10
15
20

Figure 27. d-wave proton penetrabilities for $^{7}Li + p$.

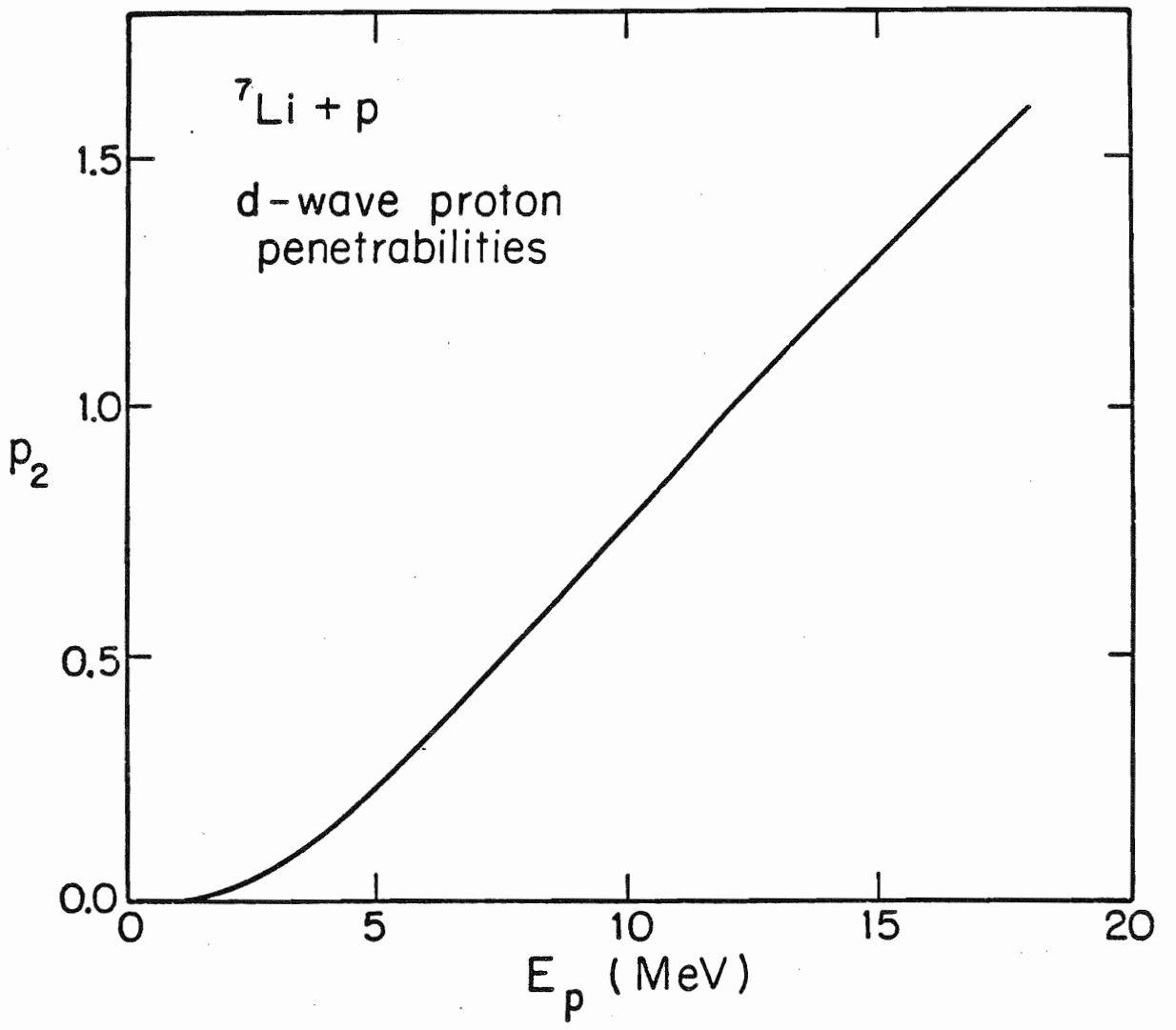
^{7}Li + p
d-wave proton
penetrabilities
1.5
1.0
0.5
0.0
p_2
0
5
10
15
20
E_p (MeV)

d-wave proton penetrabilities as a function of energy as shown in Fig.27. These do show a fast rise from 3 MeV and upwards, but in contrast with the data, they continue to rise above 10 MeV.

In an attempt to describe the peaking and subsequent decrease in the $d_{5/2}$ capture term, Fig.28 shows the 90° $d_{5/2}$ proton scattering cross section (nuclear part only) and the $d_{5/2}$ total reaction cross section, calculated with the optical model used in the direct calculation (Watson et al., 1969). The corresponding $d_{5/2}$ scattering phase shifts were investigated, and a plot of the $d_{5/2}$ real phase shifts (δ_R) and damping parameters (γ) is shown in Fig.29. Shown in Fig.30 are the corresponding complex scattering amplitudes ($C = (\gamma e^{2i\delta_R} - 1)/2i$). Although the phase shifts may correspond to some broad peaks in the scattering cross section, they do not exhibit any truly resonant behavior, since the scattering amplitudes do not show a loop in the complex plane. (For a more complete discussion of phase shifts, scattering amplitudes, and resonances, see, for example, Duval et al. (1967)).

From this phase shift investigation, and also from the fact that the $d_{5/2}$ capture yield peaks at a different energy than the $d_{5/2}$ scattering cross section, it is apparent that the peak in the capture yield is not due to resonances in the continuum channel.

The effect that the reaction cross section (represented by the imaginary surface potential W_s) has on the capture yield curve was investigated by setting W_s=0.0 in the calculations. The results on the $d_{5/2}$ capture yield are shown in Fig.26 as the dashed curve. Comparing with the "normal" direct calculation (solid curve) shows that the imaginary potential does indeed have a large effect. In particular, the absolute cross sections for W_s=0 are larger by a factor of about 2 throughout most of the calculated energy region, and the peak in the yield curve has been shifted up in energy by about 3 MeV.

Figure 28. Calculated $d_{5/2}$ scattering and reaction cross sections for $^{7}Li + p$.

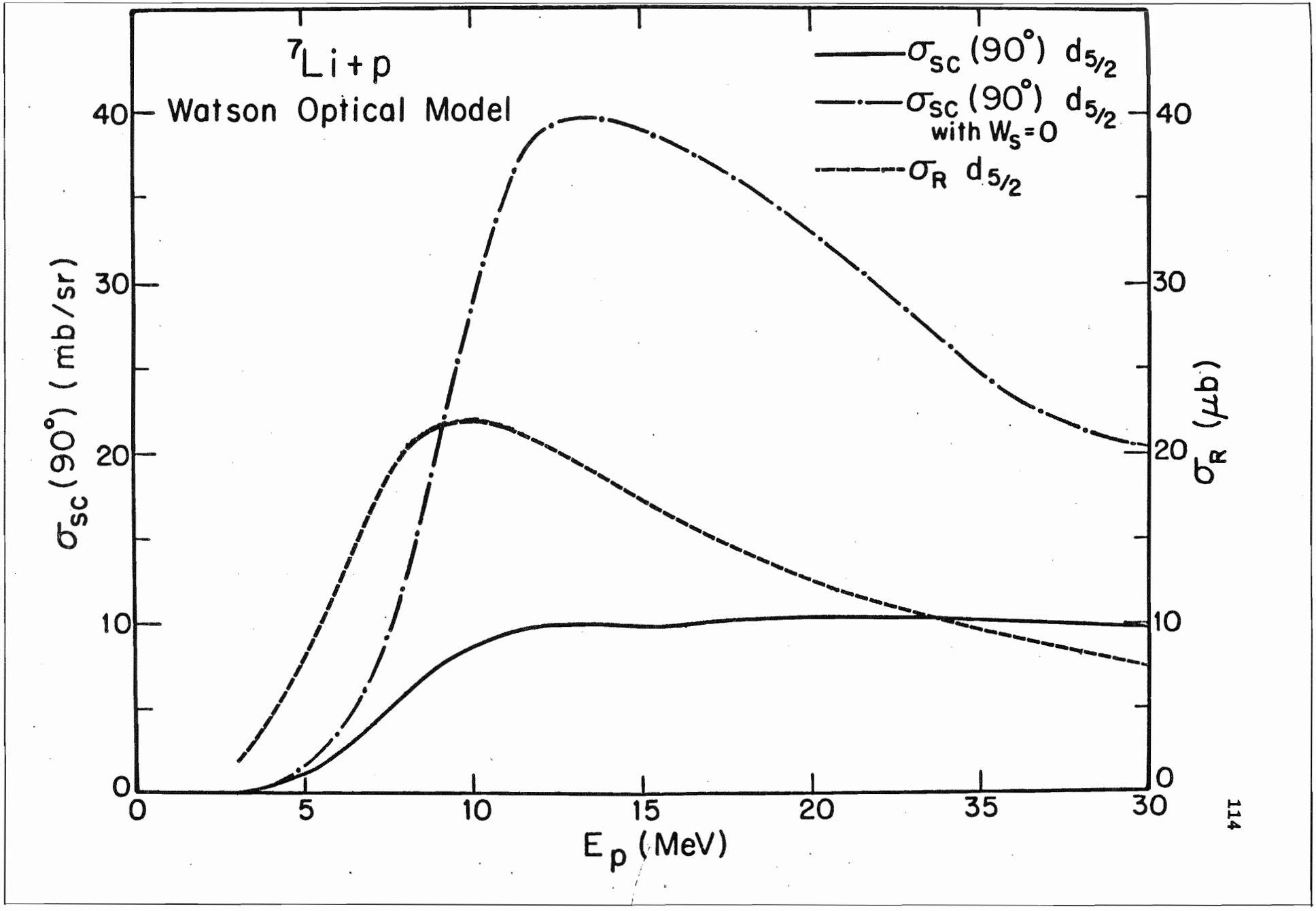
^{7}Li + p
Watson Optical Model
σ_{sc} (90°) $d_{5/2}$
σ_{sc} (90°) $d_{5/2}$ with W_s = 0
σ_R $d_{5/2}$
σ_{sc} (90°) (mb/sr)
σ_R (μb)
E_p (MeV)
0
5
10
15
20
35
30
40

Figure 29. Calculated $d_{5/2}$ real phase shift and damping parameter for $^{7}Li + p$.

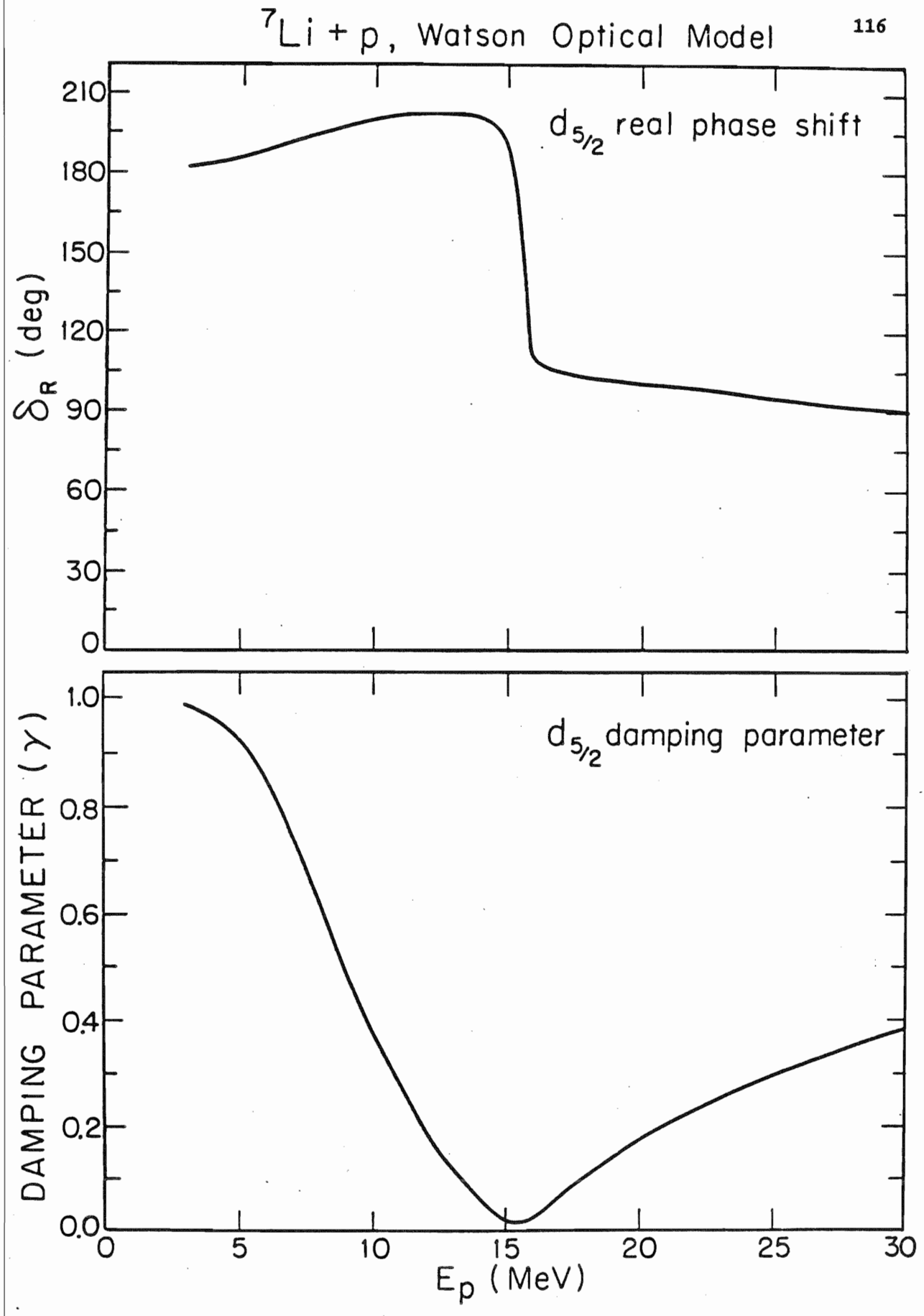
^{7}Li + p, Watson Optical Model
$d_{5/2}$ real phase shift
δ_R (deg)
210
180
150
120
90
60
30
0
$d_{5/2}$ damping parameter
DAMPING PARAMETER (γ)
1.0
0.8
0.6
0.4
0.2
0.0
0
5
10
15
20
25
30
E_p (MeV)

Figure 30. Calculated $d_{5/2}$ real and imaginary scattering amplitudes for $^{7}Li + p$.

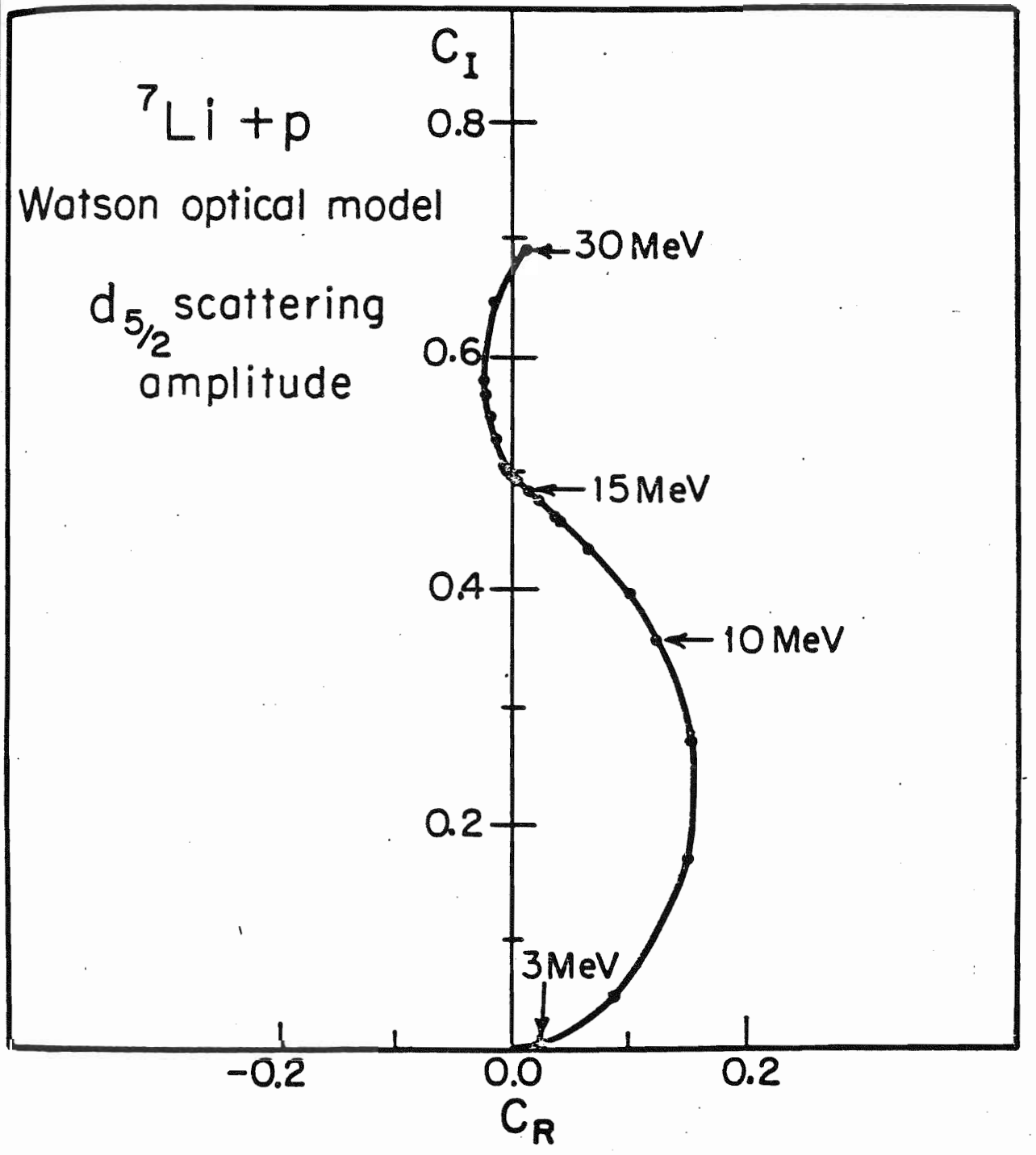
C_I
$^7Li + p$
Watson optical model
$d_{5/2}$ scattering amplitude
0.8
0.6
0.4
0.2
30 MeV
15 MeV
10 MeV
3 MeV
-0.2
0.0
0.2
C_R

(Fig.28 shows the effect that W_s=0.0 has on the scattering cross sections). It is apparent therefore that the absorption of protons in the incident continuum channel does affect the shape of the capture yield. However, even with W_s=0.0, the capture yield still shows a decrease at higher energies. It has thus been assumed that the decrease in the cross section for E_p above 8 MeV is due largely to the nature of the overlap of the incoming channel wave function with the state formed by the electromagnetic operator acting on the final state. In any case, the initial rise and peaking in the yield, followed by a gradual decrease, are typical characteristics of direct capture calculations.

Fig.16 in chapt. 3 shows a plot as a function of energy of the a_k coefficients obtained from the Legendre polynomial fits, along with the predictions of the E1-E2 direct capture model (shown as the solid curve). (The fact that the experimental data at 12 and 12.5 MeV may be affected by a contaminate has already been discussed in chapt. 3). From the figure, it is seen that the calculation predicts rather well the general trend of the data. In the a_1 coefficient, the calculation predicts a larger value than the data but does correctly describe the positive and increasing trend. For a_2, the agreement is quite good, showing the initial rise (up to 20 MeV) and the relatively constant region from 20 to 30 MeV. The calculated a_3 is somewhat larger in magnitude than the data but still predicts the correct sign and negatively increasing energy dependence. The agreement in a_4 is quite good, giving near zero from 12-16 MeV, and small and negative for 20-30 MeV. This non-zero value of a_4 at the higher energies is indicative of the increasing presence of E2 radiation.

The results for the angular distributions of analyzing power are somewhat in contrast with the unpolarized results. Fig.17 in chapt. 3 shows the angular distributions of $A(\theta)$, with the dashed curves representing the

direct E1-E2 capture calculation. There is clearly a disagreement between the data and calculation, which is quantized by looking at the b_k coefficients shown in Table VIII. Here it is seen that the b_2's in particular, and the b_1's to a lesser extent, are not well described. The data give values of b_2 between -0.05 and -0.10, while the calculation gives b_2 values which are very nearly zero.

The calculation was checked at the energy of 15 MeV to find the cause for b_2=0.0. (Since the b_k's are nearly constant from 13-16 MeV, any energy in this region should be typical). Separating the effects of the two different components of the final state, a b_2 of -0.033 was obtained for the $p_{3/2}$ component calculation, while a b_2 of +0.141 was obtained for the $p_{1/2}$ component calculation. These two numbers, when weighted properly for angular momentum and spectroscopic factors, combine to give the reported value near zero. The fact that the data give a larger, negative value of b_2 may suggest that the $p_{1/2}$ bound state component of the 16.63 MeV state is not as large as given by the shell model calculations reported by Sweeney and Marion (1969). Setting the $p_{1/2}$ component to zero gives: b_1=+0.071, b_2=-0.033 (as discussed above), b_3=-0.031, and b_4=-0.003. These values are in good agreement with the data for b_3 and b_4, and give better agreement in b_2 than the original calculation, but give worse agreement in b_1. The effects on the a_k coefficients of removing the $p_{1/2}$ component were also investigated and found to be negligible.

Since the assumption of no $p_{1/2}$ component was still unable to describe the data very well, the details of b_2 for the $p_{3/2}$ component calculation were investigated. Assuming only E1 radiation, the $\bar{B}_2$ equation used in the $p_{3/2}$ component calculation is written in terms of various matrix elements as

$$\bar{B}_2 = 0.3162\ s_{1/2}(E1)d_{3/2}(E1)\sin(\phi_{d_{3/2}} - \phi_{s_{1/2}})$$

Table VIII. $^{7}Li(p,\gamma_{16})$ b_k Coefficients Compared with Direct Capture Calculations

E_p	b_1	b_2	b_3	b_4	χ^2	Type
13.0	0.016±.011	−0.100±.008	−0.022±.006	−0.011±.005	1.64	Exp.
13.0	0.038	−0.003	−0.013	−0.001		Calc.
14.0	0.026±.010	−0.049±.006	−0.025±.005	−0.001±.004	4.18	Exp.
14.0	0.040	0.001	−0.017	−0.002		Calc.
16.0	−0.003±.009	−0.093±.006	−0.013±.005	0.009±.005	1.35	Exp.
16.0	0.040	0.001	−0.017	−0.002		Calc.

$$- 0.7746\ s_{1/2}(E1)d_{5/2}(E1)\sin(\phi_{d_{5/2}} - \phi_{s_{1/2}})$$
$$+ 1.225\ d_{3/2}(E1)d_{5/2}(E1)\sin(\phi_{d_{5/2}} - \phi_{d_{3/2}}).$$

Analyzing separate terms in this expression gives a b_2 (normalized) of 0.027 for the first term ($s_{1/2}$ and $d_{3/2}$ interference), -0.103 for the second term ($s_{1/2}$ and $d_{5/2}$ interference), and 0.043 for the third term ($d_{3/2}$ and $d_{5/2}$ interference). (Note that the sum of these numbers is equal to -0.033.) Without the $d_{3/2}$-$d_{5/2}$ interference term, this calculation would then give good agreement with the data for b_2. Since interference between $d_{3/2}$ and $d_{5/2}$ requires the presence of a finite spin-orbit potential, the sensitivity of b_2 to the spin-orbit potential (V_{so}) was investigated. The optical potential originally used in the direct calculation contained a V_{so} of 5.5 MeV. Since this potential was a global fit to many light nuclei, it is therefore likely to be reasonable. However, due to the lack of polarization data for ^{7}Li + p for E_p less than 50 MeV, the value of V_{so}=5.5 MeV has not been determined precisely. The potential V_{so} was adjusted in the $p_{3/2}$ component direct calculation, and the following values of b_2 were obtained: for V_{so}=5.5 MeV, b_2=-0.033; for V_{so}=0.0 MeV, b_2=-0.085; for V_{so}=2.7 MeV, b_2=-0.061; and for V_{so}=8.4 MeV, b_2=-0.012. Note that for V_{so} equal to or less than about 2.7 MeV, there is quantitative agreement with the data. The effects due to varying V_{so} on the other b_k and a_k coefficients was also investigated. There was a negligible effect on a_1-a_4 and only very small effects on b_1, b_3, and b_4.

These results show that at least a part of the difference between the experimental and calculated b_2 may be due to an incorrect spin-orbit potential. This effect, combined with the effect from varying the $p_{1/2}$ component of the bound state, may be sufficient to explain the data.

In conclusion, it has been shown for the reaction ^{7}Li(p,γ_{16}) that a

direct capture calculation including the effects of both E1 and E2 radiation provides good overall agreement with the yield curve, both in terms of shape and absolute cross section, and good agreement with the angular distributions. There is a disagreement with the analyzing power data, but this disagreement can be reduced by a reasonable adjustment of various parameters in the calculation.

D. Comparison with $^{7}Li(p,\gamma_0)$ and $^{7}Li(p,\gamma_1)$ Data

Direct E1-E2 capture calculations have been performed for the reactions $^{7}Li(p,\gamma_0)$ and $^{7}Li(p,\gamma_1)$ in an investigation of two aspects of these reactions: first, to show that the direct calculation is quite inadequate to describe the data in the region of the GDR (this is the typical case for a capture reaction); and secondly, to check the agreement of the calculation with the data at excitation energies above the GDR.

The coefficients of fractional parentage (cfp) of Cohen and Kurath (1967) have been used to describe the single-particle nature of the final states in ^{8}Be. They describe the ground state as a $p_{3/2}$ single-particle plus core state, with a spectroscopic factor of S=2.8981. The first excited state in ^{8}Be (at 2.94 MeV) is described as a mixed $p_{3/2}$ and $p_{1/2}$ single-particle state, with S=1.1188 for the $p_{3/2}$ component and S=0.7509 for the $p_{1/2}$ component. These two numbers give a total spectroscopic factor of S=1.869 for the first excited state. These calculated spectroscopic factors were compared to the experimental values of S=2.84 for the ground state and S=1.70 for the first excited state, as obtained from the stripping reactions (Azimov et al., 1976). The calculated values of Cohen and Kurath are therefore consistent with the data.

The optical model potential used in both cases was initially the same as that used for the $^{7}Li(p,\gamma_{16})$ calculation (Watson et al., 1969). However, in the use of this potential a problem occurred which is discussed in the following paragraphs.

For the bound state calculation for the ^{8}Be ground state, which has a binding energy of 17.255 MeV, the use of the Watson radius parameter of r_0=1.135 gave a well-depth, V_0, of 88.2 MeV. This is somewhat larger than the

value of about 60 MeV used by Watson for the continuum channel. Since the use of two significantly different well depths in the initial and final state calculations is not strictly valid (the average nuclear potential should not be time-dependent), it was believed that the results of the calculation might be unreliable. As a solution to this problem, the radius parameter was changed to r_o=1.45 fm, both in the incident channel and the bound state calculation. This value of r_o gave for the bound state a value of V_0=65.2 MeV, which is in much closer agreement with the real well-depth in Watson's potential. Of course, in this process the radius parameter has been forced to a value which does not agree with Watson's potential, but at least approximately the same potential is used for both the bound state and continuum calculations. Two calculations were then performed, one with the original unmodified potential (hereafter called the "unmodified" calculation) and the other with the modified potential (hereafter called the "symmetric" calculation).

The results of the two direct calculations were checked with the data at higher energies (20-30 MeV), since direct capture should be the dominant effect in the data at these energies. For the unmodified calculation, it was found that the calculated absolute cross section was approximately four times larger than the data at 30 MeV. However, for the symmetric calculation, very good agreement with the data was obtained for 25-30 MeV. The fact that these adjustments in the optical potential can cause such large changes in the absolute cross section suggests that the detailed results of our direct capture calculations are somewhat uncertain.

The details of the yield curve are shown in Fig.18 of chapt.4, along with the symmetric calculation (dashed line) and the unmodified calculation (dotted-and-dashed line). A clear difference is seen in the figure between the two calculations, with the symmetric calculation giving a good description

of the data for E_p=20-30 MeV. Whichever calculation is used, it is clear that neither calculation can correctly predict the shape or the magnitude of the data in the region of the GDR (E_p about 3-10 MeV). The small size of the calculation relative to the data (about 20% for the symmetric calculation) is typical of direct capture calculations in the region of the GDR built on the ground state.

Angular distributions were calculated for ^{7}Li(p,γ_0) assuming E1 and E2 radiation. The results of the calculations, in terms of the Legendre polynomial coefficients, a_k, are shown in Fig.21 of chapt.4, with the dashed line giving the symmetric calculation results, and the dotted-and-dashed line representing the unmodified calculation. The general trends of the two calculations as a function of energy are similar and agree with the general trend of the data. In the region of the GDR (up to at least 15 MeV), it might be expected that the direct model would not be completely adequate to describe the data, but there is, nonetheless, qualitative agreement. The Stanford data (Fisher et al., 1976), which include the region of the GDR, are shown as the solid curves in Fig.21, and the calculations give reasonable agreement with a_1, a_3, and a_4. However, there does appear to be a significant difference in terms of magnitude and energy dependence for a_2. This may indeed be a failure of the direct model in the GDR region, but, as discussed in chapt.4, the Stanford and the TUNL data for a_2 do not agree very well in the region of overlap, so it is possible that there are some problems in the data. Above the observed GDR, where we certainly expect the direct model to provide a good description of the reaction, there is reasonable agreement with the data, although neither calculation gives agreement within the error bars.

The angular distributions of analyzing power and the corresponding calculations for ^{7}Li(p,γ_0) are shown in Fig.22 in chapt.4, where the solid

curves give the fit to associated Legendre polynomials, the dashed curves show the symmetric calculation results, and the dotted-and-dashed curves show the unmodified calculation results. Shown in Table IX are the b_k coefficients from the data and the two calculations. The results indicate that the unmodified calculation is in reasonable agreement with the data, but the symmetric calculation does not provide very good agreement.

An investigation of the calculated b_k coefficients was undertaken to provide an indication of their sensitivity. For b_1, b_2, and b_3 it was discovered that there existed a large amount of cancellation between different terms in the expansions of the b_k's in terms of matrix elements. Specifically, for b_2 we can write:

$$b_2 = 0.3162\, s_{1/2}(E1)d_{3/2}(E1)\sin(\phi_{d_{3/2}} - \phi_{s_{1/2}}) - 0.7746\, s_{1/2}(E1)d_{5/2}(E1)\sin(\phi_{d_{5/2}} - \phi_{s_{1/2}}) + 1.225\, d_{3/2}(E1)d_{3/2}(E1)\sin(\phi_{d_{5/2}} - \phi_{d_{3/2}})$$

where the E2 terms have been neglected since they are considerably smaller. At 15 MeV, the unmodified calculation gives for the first term: b_2=+0.025, for the second term: b_2=-0.125, and for the third term: b_2=+0.065. (These do in fact add up to the total b_2 of -0.034). In this case, we see that all three terms have a significant effect on b_2, and because of cancellation, the final value is smaller in magnitude than the individual terms. This result is similarly true for b_1 and b_3 (although the expansion is more complicated due to many significant E1 and E2 mixing terms). It is therefore not surprising that the generally small calculated values of b_k are quite sensitive to the details of the calculation. This sensitivity is seen in the difference between the results of the unmodified and symmetric calculations.

For the direct calculation for capture to the first excited state of ^{8}Be (^{7}Li(p,γ_1)), a situation exists somewhat similar to that of the (p,γ_0)

Table IX. $^{7}Li(p,\gamma_0)$ b_k Coefficients Compared with Direct Capture Calculations

E_p	b_1	b_2	b_3	b_4	χ^2	Type
13.0	0.082±.011	−0.029±.008	−0.008±.006	0.000±.005	0.41	Exp.
13.0	0.081	−0.053	−0.022	−0.001		Unmod.
13.0	0.152	−0.021	−0.092	−0.013		Symm.
14.0	0.061±.012	−0.029±.008	−0.011±.006	0.000±.005	0.85	Exp.
14.0	0.089	−0.043	−0.025	−0.001		Unmod.
14.0	0.153	−0.022	−0.099	−0.015		Symm.
16.0	0.012±.011	−0.014±.007	−0.005±.006	0.013±.005	2.22	Exp.
16.0	0.102	−0.029	−0.029	−0.001		Unmod.
16.0	0.139	−0.023	−0.100	−0.016		Symm.

calculation. In detail, for the bound state wave function (consisting of both $p_{1/2}$ and $p_{3/2}$ single-particle components), the determined well-depth was V_0=99.5 MeV for the $p_{1/2}$ component, and V_0=82.9 MeV for the $p_{3/2}$ component, using the given well parameters r_o and a_o from Watson's potential. These values of V_0 are somewhat large, and it was again decided to perform a calculation with a "symmetric" potential. For this symmetric calculation, the radius parameter was changed to r_o=1.4, and the spin-orbit potential, V_{so}, in the bound state calculation was set to zero to give the same V_0 for both the $p_{1/2}$ and the $p_{3/2}$ states. This calculation then gave for the bound state well-depth V_0=65.9 MeV, in much better agreement with Watson's real well-depth.

The 90° yield curve for ^{7}Li(p,γ_1) along with the symmetric (dashed curve) and unmodified (dotted-and-dashed curve) direct calculations is shown in Fig.19 in chapt.4. As was true for the ^{7}Li(p,γ_0) reaction, a large absolute difference is seen between the two calculations. However, in contrast to the ^{7}Li(p,γ_0) case, the unmodified calculation gives better agreement with the data at higher energies (where we expect direct to be more nearly correct). A possible explanation of the situation is that, since the observed GDR built on the first excited state is centered at a higher excitation energy and is broader in energy, its high energy tail may still be significant for E_p=20-30 MeV. This would suggest that the symmetric calculation might in fact be correctly describing the direct capture, and that semidirect capture may provide the additional capture strength necessary to give agreement with the data at the higher energies. In order to test this suggestion, it would be necessary to extend the 90° yield curve to proton energies above 30 MeV.

Whichever calculation is used, it is true that both calculations fail to

describe the data in the GDR region.

Fig.24 in chapt.4 shows a plot of the a_k's obtained from the Legendre polynomial fits to the data, along with the results of the symmetric (dashed line) and the unmodified (dotted-and-dashed line) calculations. The a_k's appear to give a preference for the unmodified calculation, but the discussion given above concerning the location and width of the GDR also applies here. The important point, still, is that a direct calculation with reasonable parameters can provide a satisfactory description the data above the main strength of the GDR.

Also shown in Fig.24 in chapt.4 are the Stanford a_k's (Fisher et al., 1976) for $^7Li(p,\gamma_1)$. These data include the region of the GDR built on the first excited state. Interestingly, the direct calculations give good agreement for all coefficients a_1-a_4. For example, the initial positive value of a_2 (at about 5 MeV) followed by a fast decrease to a negative value (for 8-12 MeV) is described very well by the unmodified calculation.

It should be noted at this point that qualitative agreement between the measured a_k's and those calculated with a direct model is not surprising even in the region of the GDR. It has been shown (Mavis, 1977, and Weller and Roberson, 1980, and references therein) that the relative phases $\phi_{k a_{j_a}}$ and the a_k's do not change dramatically over the GDR and are in fact not much different from the off-resonance values. A partial explanation for the fact that the GDR appears to have little effect on the a_k's for the two capture reactions $^7Li(p,\gamma_0)$ and $^7Li(p,\gamma_1)$ may be that since the a_k's are all fairly small, large percent changes in any a_k would appear as only a small change in magnitude of the a_k. For example, if a given E1 matrix element were to double in value due to the presence of a GDR, the total cross section due to that matrix element would be increased by a factor of 4. However, the a_1

coefficient would only double, assuming that the relative phases and E2 matrix elements remained unchanged. If a_1 were small, for example about 0.05, then doubling to give 0.10 would probably not appear to be significant in comparison to our direct calculations.

The analyzing power results for $^7Li(p,\gamma_1)$ are shown in Fig.25 of chapt.4, along with the symmetric (dashed lines) and unmodified (dotted-and-dashed lines) calculations. Although neither calculation provides a precise fit to the data, the unmodified calculation does give reasonable agreement with the data, while the symmetric calculation gives considerably worse agreement. To quantize the level of agreement, the calculated and experimental b_k's are shown in Table X. The unmodified calculation gives good agreement for b_1, b_3, and b_4, although it is somewhat incorrect for b_2, especially at 16 MeV. The symmetric calculation fails somewhat for b_1, b_2, and b_3. It is true in this case, as for the $^7Li(p,\gamma_0)$ case, that the calculated b_k's are quite sensitive to the parameters in the calculation, so that it may be possible to fit the data better by adjusting these parameters.

In conclusion, a direct capture calculation with reasonable parameters can provide a satisfactory description of the $^7Li(p,\gamma_0)$ and $^7Li(p,\gamma_1)$ reactions, in terms of total cross sections and angular distributions of cross sections and analyzing powers, for the energy regions above the GDR. In the region of a GDR, the calculated angular distributions can still give qualitative agreement with the data, but the absolute cross sections are significantly too small.

Table X. $^{7}Li(p,\gamma_1)$ b_k Coefficients Compared with Direct Capture Calculations

E_p	b_1	b_2	b_3	b_4	χ^2	Type
13.0	0.021±.006	0.041±.004	0.013±.003	−0.013±.003	2.50	Exp.
13.0	0.015	0.052	0.006	0.001		Unmod.
13.0	−0.081	0.111	0.027	0.001		Symm.
14.0	0.023±.006	0.033±.004	0.015±.003	−0.002±.003	0.57	Exp.
14.0	0.014	0.061	0.007	0.001		Unmod.
14.0	−0.090	0.107	0.028	0.001		Symm.
16.0	0.018±.005	0.021±.003	0.010±.003	0.005±.002	4.67	Exp.
16.0	0.014	0.072	0.009	0.001		Unmod.
16.0	−0.109	0.099	0.033	0.002		Symm.

E. Direct-Semidirect Calculations

A brief introduction to the semidirect capture model was given in Sec. A of this chapter. The details of our calculations are discussed in this section.

For the DSD calculations performed for this thesis (Kitazawa, 1980), a real volume form factor was used of the type suggested by Potokar (1973). Specifically, the form factor was written:

$$4 \cdot V_1 f \alpha r \frac{1}{1+e^{\left(\frac{r-r_0}{a}\right)}},$$

where V_1 is the isospin symmetry potential well-depth, f is the fraction of the sum rule exhausted by the appropriate giant resonance, and α is the ground state correlation factor for the target nucleus. In one sense, V_1, f, and α, which all are constants affecting the total cross section, can be considered as parameters determinable from the fit of the DSD calculation to the data of the giant resonance. However, there are some restrictions on these parameters. V_1 can be obtained from (p,n) data. For example, the global fit of Watson *et al.* (1969) to light nuclei gives an isospin symmetry term of $27(\frac{N-Z}{A})$ MeV, so a number of near 27 MeV should be used for V_1. (It is customary when performing DSD calculations to report $4 \cdot V_1$, which is 108 MeV in this case). Typically, a giant dipole resonance exhausts about 100% of the sum rule (in all channels), so f should be about 1. (f is often somewhat less than 1 for light nuclei). The ground state correlation factor varies as a function of atomic mass A and approaches 1 for light nuclei (Leonardi, 1972). The calculations in this thesis have used α=1.0.

Other parameters needed for the calculation include an optical model potential for the incident nucleon plus target nucleus state (^{7}Li + p in this case). As for the direct capture calculations, the potential of Watson *et al.*

(1969) was used. Additionally, the bound final states in ^{8}Be were calculated with a Woods-Saxon well as described earlier in this chapter for the direct capture case.

For an initial check of the DSD calculation for a typical GDR, and to obtain some typical parameters for a GDR, a DSD calculation was performed for the reaction ^{7}Li(p,γ_0). Since the "symmetric" direct calculation (with r_o=1.45) gave better agreement with the data at higher energies than the "unmodified" calculation (see Sec. D), it was decided to use the symmetric potential for the DSD calculation. The result of the calculation is shown in Fig.31, along with the yield curve data at 90°. The calculation gives good overall agreement in the region of the GDR, although at higher energies, the calculated cross section is somewhat too large. To obtain this overall agreement, it was necessary to adjust some of the parameters for the semidirect term. The parameters used for the calculation shown in the figure were: V_1=50 MeV, f=0.60, α=1.0, Γ=4.5 MeV, and E_{res}=20.5 MeV. Of interest is the fact that the symmetry potential has been decreased by about a factor of 1/2, but it should be noted that V_1, f, and α have equivalent effects in terms of the calculation, so that any set of these parameters would fit the data equally well, provided that the product $V_1 \cdot f \cdot \alpha$ is kept constant. A value of f=0.60 is typical for light nuclei (Hayward, 1970).

As the next step, a DSD calculation for ^{7}Li(p,γ_{16}) was performed, using as a reasonable approximation the resonance parameters used in the ^{7}Li(p,γ_0) calculation, except of course for Γ and E_{res}. For simplicity, only the $p_{3/2}$ component of the bound state was included in the calculation (the effects of the $p_{1/2}$ component are small), but the other continuum and bound state parameters were the same as those used in the direct calculations of Sec. C.

Since there was no obvious GDR peak in the ^{7}Li(p,γ_{16}) data, it was

Figure 31. 90^{o} yield curve for $^{7}Li(p,\gamma_{0})$ including the results of the DSD calculations.

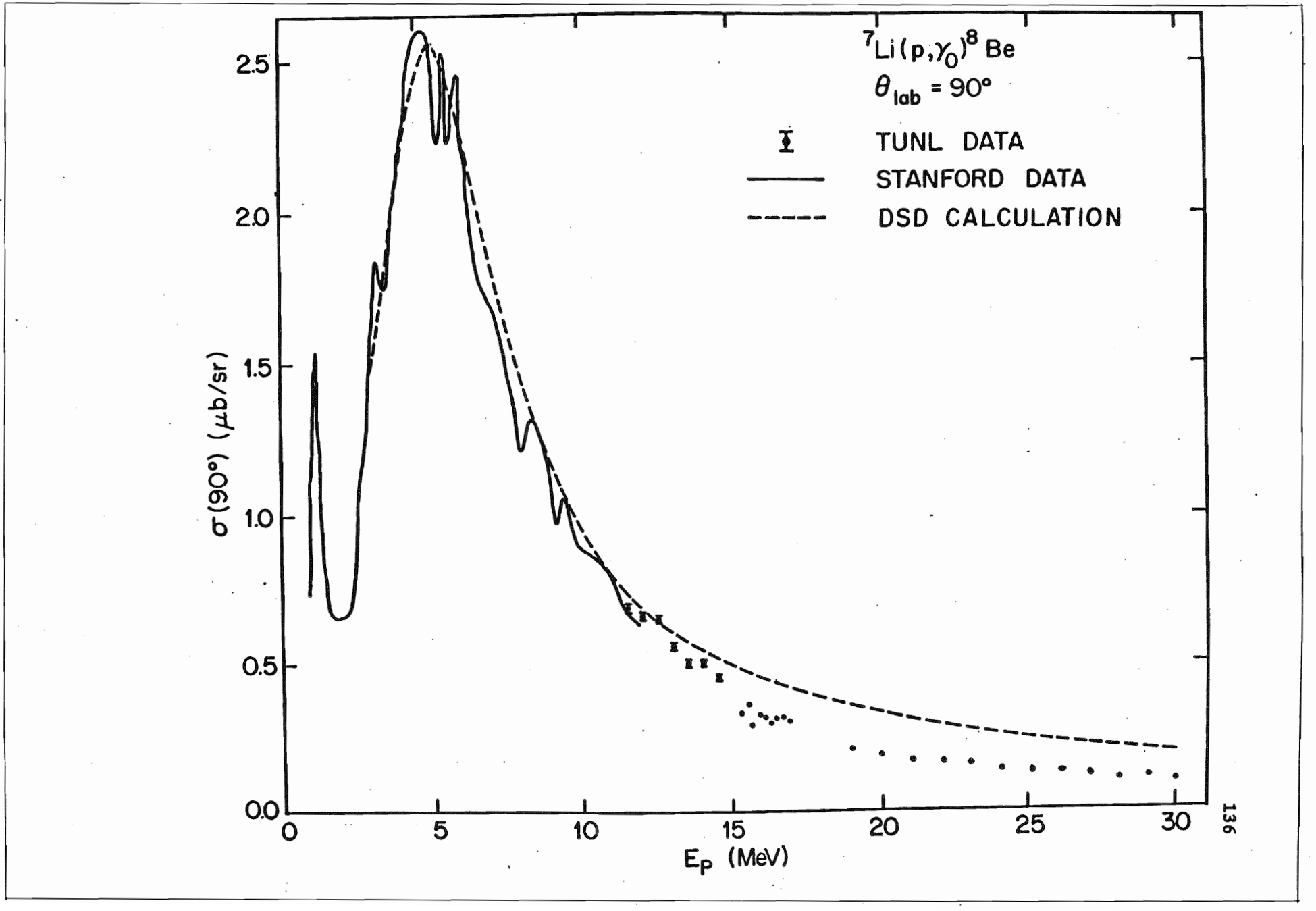
$^{7}Li(p,\gamma_0)^{8}Be$
$\theta_{lab} = 90°$
TUNL DATA
STANFORD DATA
DSD CALCULATION
$\sigma(90°)$ (μb/sr)
E_p (MeV)
0.0
0.5
1.0
1.5
2.0
2.5
0
5
10
15
20
25
30

necessary to predict, using some reasonable method, the resonance energy and width that might be expected for a GDR built on the isospin-mixed pair in ^{8}Be. The value of E_{res} was simply chosen to be 20 MeV above the final 16.6 MeV state (E_{res}=20+16.6=36.6 MeV), which is a typical value for light nuclei. The width, Γ, was less easy to predict precisely. In general, a giant resonance width is largely determined by two different mechanisms. One mechanism involves decay into a continuum nucleon plus core state (single-particle escape), where the process is governed in part by the barrier penetration. The width of the GDR determined from this mechanism is denoted as Γ_p in this thesis. The other important mechanism involves damping of the GDR into nearby multiple particle-hole configurations. The width from this mechanism is denoted as Γ_d. The effect of the γ-ray decay on the width is negligible. In medium weight and heavy nuclei, the damping process is dominate, while for light nuclei the single-particle escape process is almost totally dominate (Danos and Greiner, 1965). For proton capture to ^{8}Be the escape process is thus expected to give most of the observed 4.5 MeV width for the ground state GDR. The width of a GDR built on the 16.6 MeV state can then be estimated by extrapolating the width of the ground state GDR to higher energies.

To investigate the behavior of Γ_d as a function of energy, the expression of Danos and Greiner (1965) was used. Specifically, $\Gamma_d=\Gamma_0 E^g$, where Γ_0 is a constant and g is a number calculated by Danos and Greiner to be about 1.8. This energy dependence is due to the density of 2p-2h configurations as a function of energy. Assuming that Γ_d is about half of Γ for the γ_0 GDR (2.25 MeV) would give Γ_d=6.4 MeV for a GDR at 36.6 MeV. This value of Γ_d for the γ_{16} GDR is probably a considerable overestimate since Γ_d for the γ_0 GDR is probably much less than 2.25 MeV.

The situation for Γ_p is considerably different. This width can be written for a given partial wave L as $2P_L\gamma^2$, where P_L is the penetrability and γ^2 is the reduced width, giving the overlap of the GDR with the continuum state. Assuming that d-wave capture is predominate for both $^7Li(p,\gamma_0)$ and $^7Li(p,\gamma_{16})$ (as is often true in light nuclei (Snover et al., 1980)), and that γ^2 is roughly the same for both reactions, we may write, approximately, $\Gamma_p(E) \propto P_2(E)$. Since the d-wave proton penetrability is almost 10 times larger at the expected position of a γ_{16} GDR (E_p=20-25 MeV) than at the position of the γ_0 GDR (E_p=5 MeV), Γ_p should be about 40 MeV for a γ_{16} GDR. From these arguments, we would expect $\Gamma \simeq \Gamma_p \simeq 40$ MeV.

DSD calculations have been performed for $^7Li(p,\gamma_{16})$ using various widths, and the results are shown in Fig.32. All the calculations shown have been normalized by the factor of 1.27 to give better absolute cross section agreement in the low energy region. The results for Γ=10 MeV clearly do not describe the experimental results. For Γ=20 MeV, a curve is obtained which does not actually fit the data, but gives the shape of a small broad resonance between 20 and 30 MeV that may be present in the data. These results indicate that if a GDR is present, it must have a width of at least 20 MeV or be significantly reduced in strength. Also shown in the figure are the results for the predicted width, Γ=40 MeV. Since the effect of this resonance on the calculation is not very dramatic, it is difficult to conclude whether or not the yield curve data suggest such a resonance. The data is reproduced fairly well either with a pure direct calculation or with a calculation which adds a broad resonance (DSD).

The effects on the angular distributions of adding a semidirect term were checked. The a_k's obtained for various calculations are shown in Table XI. at 15 and 25 MeV. The first row gives the a_k's obtained from a direct

Figure 32. 90^{o} yield curve for $^{7}Li(p,\gamma_{16})$ including the results of the DSD calculations.

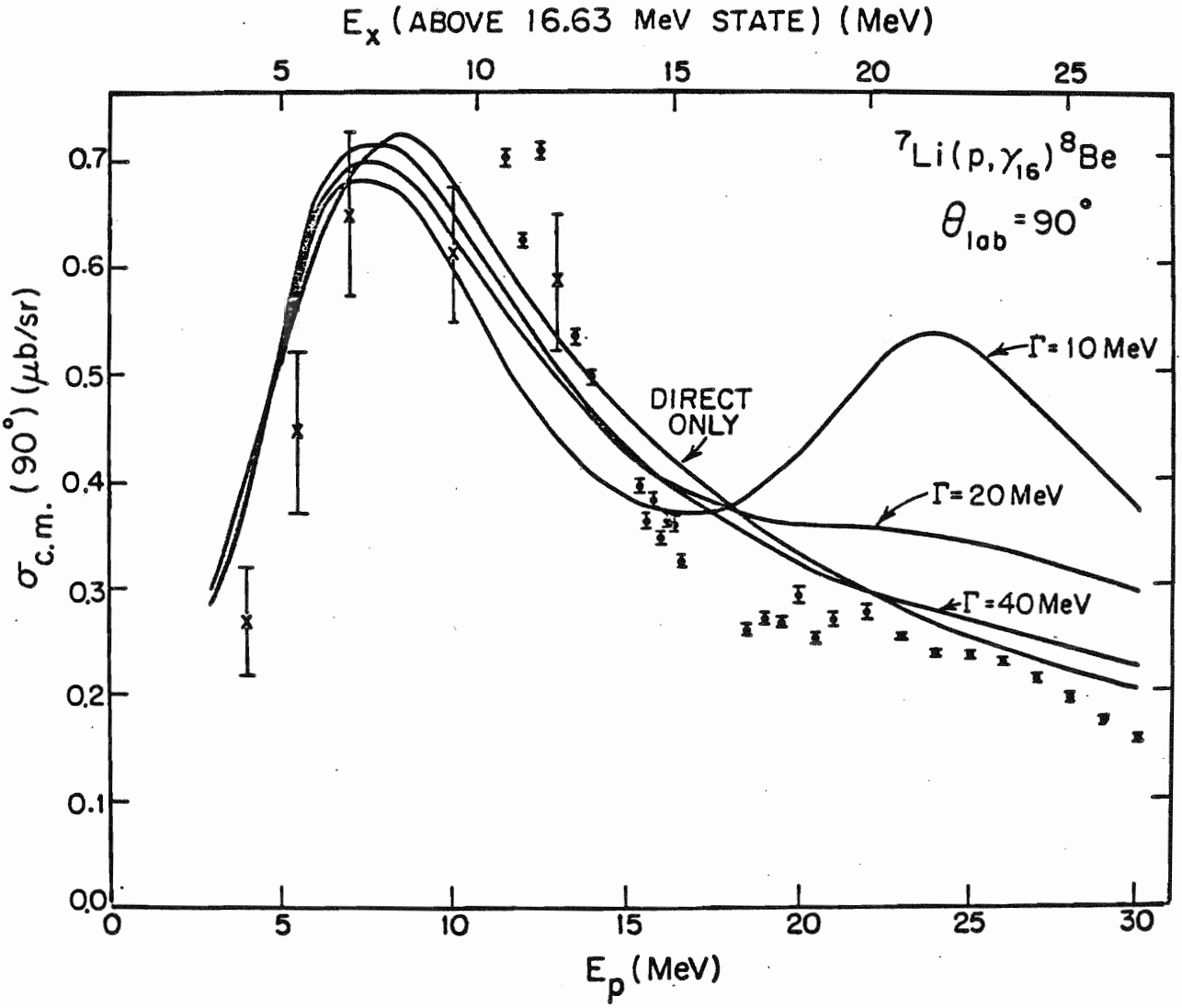
E_x (ABOVE 16.63 MeV STATE) (MeV)
5
10
15
20
25
$^7Li(p,\gamma_{16})^8Be$
$\theta_{lab} = 90°$
Γ= 10 MeV
DIRECT ONLY
Γ= 20 MeV
Γ= 40 MeV
$\sigma_{c.m.}$ (90°) (μb/sr)
0.0
0.1
0.2
0.3
0.4
0.5
0.6
0.7
0
5
10
15
20
25
30
E_p (MeV)

Table XI. $^{7}Li(p,\gamma_{16})$ a_k Coefficients from DSD

E_p	a_1	a_2	a_3	a_4	Type
15.0	0.450	-0.503	-0.167	-0.011	$p_{3/2}$ only, direct
15.0	0.451	-0.502	-0.169	-0.010	DSD, Γ=40
15.0	0.462	-0.497	-0.173	-0.011	DSD, Γ=20
25.0	0.863	-0.478	-0.499	-0.092	$p_{3/2}$ only, direct
25.0	0.800	-0.523	-0.462	-0.073	DSD, Γ=40
25.0	0.725	-0.563	-0.420	-0.058	DSD, Γ=20

calculation which neglected the $p_{1/2}$ component of the bound state. Shown in the next two rows are two DSD calculations, with Γ=40 and Γ=20 MeV. Both assume for simplicity only the $p_{3/2}$ component of the bound state. A comparison of these a_k's indicates that the angular distributions are not very sensitive to the addition of the semidirect term.

Similarly, Table XII shows the results of the calculations for the b_k coefficient. The first row gives the results of the direct calculation with the $p_{3/2}$ component only, and the second and third row give the two DSD calculation results. Again, the results are rather insensitive to the addition of the semidirect term.

The results of these direct-semidirect calculations indicate that it is difficult in this reaction to establish the presence of a GDR which has a width greater than about 20 MeV. The difficulty is due to the limited sensitivity of the a_k's, b_k's, and 90^o yield curve to the addition of such a broad semidirect term.

Table XII. $^{7}Li(p,\gamma_{16})$ b_k Coefficients from DSD

E_p	b_1	b_2	b_3	b_4	Type
15.0	0.070	-0.034	-0.032	-0.003	$p_{3/2}$ only, direct
15.0	0.061	-0.040	-0.030	-0.003	DSD, Γ=40
15.0	0.054	-0.046	-0.030	-0.003	DSD, Γ=20

Chapter 6 Summary and Conclusions

The 90^{o} yield curve has been measured from E_p=4 to 30 MeV for the reaction $^{7}Li(p,\gamma_{16})^{8}Be^{*}$, where the final state is the region of the isospin-mixed pair of levels in ^{8}Be. Angular distributions of cross sections for this reaction have been measured at nine beam energies from 12 to 30 MeV. Angular distributions of analyzing power have been measured at 3 energies. The yield curve data for this reaction do not exhibit any pronounced peaking at the expected energy for a giant dipole resonance built on the 16 MeV states. Furthermore, a simple direct capture model calculation, including E1 and E2 radiation, is sufficient to give a good description of the data. In particular, the peaking in the yield curve at about E_p=8 MeV and the absolute cross section are described very well by the direct calculation.

To investigate the possibility of a GDR built on the isospin-mixed pair, DSD calculations were performed for the reaction $^{7}Li(p,\gamma_{16})$. Although no obvious GDR is suggested by the yield curve data, the DSD calculations indicate that a GDR could be consistent with the data if it were at least 20 MeV wide. The energy dependence of the d-wave proton penetrabilities indicates that the width for a GDR built on the isospin-mixed pair of states might be about 40 MeV. The DSD calculations show that it would be very difficult to determine the existence of a GDR with such a large width. Therefore, there would seem to be little utility in calling such a resonance a

"giant resonance".

These results are in contrast with the two capture reactions, $^{7}Li(p,\gamma_0)$ and $^{7}Li(p,\gamma_1)$. The 90^{o} yield curves for these two reactions have been measured at beam energies from 11.5 to 30 MeV. Our results combine with results from other work (Fisher et al., 1976) to provide 90^{o} yield curves for E_p=2 to 30 MeV. Additionally, angular distributions of cross sections and analyzing powers have been measured at various energies from 12 to 30 MeV. In the region of the observed GDR's (about 5 MeV for γ_0 and about 8 MeV for γ_1), the direct capture model is not sufficient to describe the data for either reaction. In particular, the calculated cross sections are too small and do not have the correct energy dependence. Above the regions of the GDR's, the direct model can provide a reasonable description of the data. Direct-semidirect (DSD) calculations have been performed for the reaction $^{7}Li(p,\gamma_0)$. The inclusion of an E1 semidirect term provides a good description of the overall shape and magnitude of the yield curve.

References

F.Ajzenberg-Selove, Nucl.Phys. A230, 1 (1979).

L.G.Arnold, Phys.Rev.Lett. 42, 1253 (1979).

S.A.Azimov et al., Sov.J.Nucl.Phys. 22, 115 (1975).

F.C.Barker, Nucl.Phys. 83, 418 (1966).

S.Baskin and R.R.Carlson, Phys.Rev. 97, 1245 (1955).

D.Berghofer, M.D.Hasinoff, R.Helmer, S.T.Lim, D.F.Measday, and K.Ebisawa, Nucl.Phys. A263, 109 (1976).

S.L.Blatt, et al., to be published, 1981.

D.M.Brink, Ph.D. Thesis (Oxford University, 1955) (unpublished).

G.E.Brown, Nucl.Phys. 57, 339 (1964).

B.Buck and A.A.Pilt, Nucl.Phys. A280, 133 (1977).

T.B.Clegg, G.A.Bissenger, W.Haeberli, and P.A.Quin, Polarization Phenomena in Nuclear Reactions, ed. H.H.Barschall and W.Haeberli, (University of Wisconsin Press, Madison, Wis., 1970).

C.F.Clement, A.M.Lane, and J.R.Rook, Nucl.Phys. 66, 273 (1965).

S.Cohen and D.Kurath, Nucl.Phys. A101, 1 (1967).

S.R.Cotanch, North Carolina State University, private communication, 1978.

C.F.Cvelbar and S.L.Whetstone, in Charged-Particle-Induced Radiative Capture, (International Atomic Energy Agency, Vienna), p.271, (1974).

P.J.Daly, J.R.Rook, and P.E.Hodgson, Nucl.Phys. 56, 331 (1964).

M.Danos and W.Greiner, Phys.Rev. 138, B876 (1965).

J.S.Duval,Jr., A.C.L.Barnard, and J.B.Swint, Nucl.Phys. A93, 164 (1967).

J.M.Eisenberg and W.Greiner, Excitation Mechanisms of the Nucleus (Amsterdam, 1970).

G.A.Fisher, P.Paul, F.Riess, and S.S.Hanna, Phys.Rev. C 14, 28 (1976).

R.Gleyvod, N.P.Heydenburg, and I.M.Naqib, Nucl.Phys. 63, 650 (1965).

Dean Halderson and R.J.Philpott, Phys.Rev.Lett. 46, 100 (1981).

S.S.Hanna, Aust.J.Phys. 29, 511 (1976).

M.N.Harakeh, P.Paul, and Ph.Gorodetzky, Phys.Rev. C 11, 1008 (1975).

E.Hayward, Nat. Bur. of Stand., Washington, D.C., private communication.

E.Hayward, Nat.Bur.Stand.U.S.Monogr. 118 (1970).

D.L.Johnson, Ph.D. Thesis (University of Washington, 1974) (unpublished).

S.E.King, Duke University, private communication, 1980.

H.Kitazawa, Tokyo Institute of Technology, Tokyo, Japan, private communication, 1980.

M.A.Kovash et al., Phys.Rev.Lett. 42, 700 (1979).

A.M.Lane, Nucl.Phys. 11, 625 (1959).

R.Leonardi, Phys.Rev.Lett. 28, 836 (1972).

J.B.Marion, P.H.Nettles, C.L.Cocke, and G.J.Stephenson, Jr., Phys.Rev. 157, 847 (1967).

J.B.Marion and M.Wilson, Nucl.Phys. 77, 129 (1966).

R.E.Marrs, E.G.Adelburger, K.A.Snover, and M.D.Cooper, Phys.Rev.Lett. 35, 202 (1975).

D.G.Mavis, Ph.D. Thesis (Stanford University, 1977) (unpublished).

G.Mitev, Duke University, private communication, 1980.

H.W.Newson, E.G.Bilpuch, F.O.Purser, J.R.Boyce, and T.B.Clegg, Nucl.Inst.Meth. 122, 99 (1974).

R.W.Peelle, Phys.Rev. 105, 1311 (1957).

M.Potokar, Phys.Lett. B 46, 346 (1973).

C.Rolfs, Nucl.Phys. A217, 29 (1973).

B.M.Skwiersky, C.M.Baglin, and P.D.Parker, Phys.Rev. C 9, 910 (1974).

K.A.Snover, P.G.Ikossi, E.G.Adelberger, and K.T.Lesko, Phys.Rev.Lett.

44, 927 (1980).

M.Suffert, W.Feldman, J.Mahieux, and S.S.Hanna, Nucl.Inst.Meth. 63, 1 (1968).

W.E.Sweeney, Jr., Phys.Rev. 182, 1022 (1969).

W.E.Sweeney, Jr., and J.B.Marion, Phys.Rev. 182, 1007 (1969).

S.-F.Tsai and J.T.Londergan, Phys.Rev.Lett. 43, 576 (1979).

T.A.Trainor, T.B.Clegg, and P.W.Lisowski, Nucl.Phys. A220, 533 (1974).

B.A.Watson, P.P.Singh, and R.E.Segel, Phys.Rev. 182, 977 (1969).

H.R.Weller and N.R.Roberson, Rev.Mod.Phys. 52, 699 (1980).

H.R.Weller and N.R.Roberson, IEEE Transactions on Nuclear Science NS-28, 1268 (1981).

H.R.Weller et al., Phys.Rev. C 13, 922 (1976).

S.A.Wender, C.E.Floyd, T.B.Clegg, and W.R.Wylie, Nucl.Inst.Meth. 174, 341 (1980).

S.A.Wender, H.R.Weller, N.R.Roberson, D.R.Tilley, and R.G.Seyler, to be published, 1981.

BIOGRAPHY

STEPHEN HART MANGLOS

PERSONAL: Born August 23, 1955, Detroit, Michigan

EDUCATION: B.S. in Physics and Math, Alma College (1976)

POSITIONS: National Science Foundation Fellow, Duke University (1977-1980)
Research Assistant, Duke University (1980-1981)

PUBLICATIONS:

1. Inelastic α Cross Sections in the Region of the Giant Quadrupole Resonance for Nuclei Near Mass 60 (with H.R.Weller, S.A.Wender, N.R.Roberson, M.Potokar, and D.R.Tilley) Phys.Rev. C 20, 1589 (1979).

2. Evidence for a 2^+ Resonance in ^{4}He at 40 MeV (with R.C.McBroom, H.R.Weller, N.R.Roberson, S.A.Wender, D.R.Tilley, D.M.Skopik, L.G.Arnold, and R.G.Seyler) Phys.Rev.Lett. 45, 243 (1980).

3. Proton Capture to Excited States of ^{8}Be and ^{14}N (with H.R.Weller, N.R.Roberson, D.R.Tilley, S.A.Wender, and S.L.Blatt) Bull.Am.Phys.Soc. 25, 603 (1980).